GROWTH OPTIMISATION AND LASER PROCESSING OF THIN FILM PHOSPHORS FOR ELECTROLUMINESCENT DISPLAYS

GABRIEL BOUTAUD

A thesis submitted in partial fulfilment of the

requirements of Nottingham Trent University

for the degree of Doctor of Philosophy

February 2010

COPYRIGHT STATEMENT

ABSTRACT

This thesis presents results of a study of ZnS:Mn thin film phosphors used in Thin Film ELectroluminescent (TFEL) and Laterally Emitting TFEL (LETFEL) devices, examining techniques for phosphor growth optimisation and post deposition processing in order to strengthen development of novel TFEL devices. To achieve this, thin films of phosphor were deposited using RF magnetron sputtering to investigate the use of co-sputtering in order to optimise dopant concentration. 800 nm films of ZnS:Mn were simultaneously co-sputtered from ZnS and ZnS:Mn (1 wt.%) solid targets. The thin films were deposited at different manganese concentrations by varying the relative RF power applied to each target. The films were deposited directly onto 100 mm diameter (100) n-type silicon substrates, or onto a layer of 300 nm of Y_2O_3 to fabricate electroluminescent test devices. Luminescence from the phosphor films was characterised via photoluminescent excitation using a 337 nm pulsed N_2 laser, with the photoluminescence (PL) optimum obtained at 0.38 ZnS:Mn power ratio. Electroluminescence (EL) from TFEL devices were excited by applying a sinusoidal waveform voltage at a frequency of 1 kHz with maximum luminance obtained at 0.36 ZnS:Mn power ratio. Two monitoring techniques were investigated for the control of the Mn concentration necessary to ensure optimised batch to batch film deposition reproducibility. Both techniques relate to the specific relationships with Mn concentration which was identified to be linearly proportional to the logarithmic of both luminescent decay constant and ratio of red over yellow photoluminescence emissions. In addition, different laser processing techniques were used to further increase the emission from both phosphor thin films and TFEL devices. First, the PL and EL results, obtained after the combined effect of varying Mn concentration and laser annealing, demonstrated that laser annealing was more beneficial to the ZnS:Mn layer with higher Mn concentrations, suggesting a higher optimum Mn concentration if combined with laser annealing. The second technique was to deposit ZnS:Mn films 200nm at a time, with growth interrupted to undertake laser processing. The results have shown gradual improvements on both PL and EL emissions from 1 to 4 layers successively laser annealed and have demonstrated the feasibility of a novel processing technique for enhanced TFEL devices. Finally, novel TFEL fabrication techniques were investigated via industrial collaboration projects.

ACKNOWLEDGEMENTS

This research programme was financially supported by a Vice-Chancellor's Bursary from Nottingham Trent University.

There are several people to whom I owe a great debt for their effort and help towards the completion this thesis.

Firstly, I would like to express most sincerely my gratitude towards my Director of studies, Prof. Wayne Cranton, who has not only given me the opportunity to do this research but also who has been a great mentor and to whom I will be eternally respectful.

I must thank especially Dr. Demosthenes Koutsogeorgis for his supervision and continuous support towards RF magnetron sputtering and laser processing. Also I am grateful to Dr. Robert Ranson for his supervision and for his useful advice and guidelines. I should thank Emeritus Prof. Clive Thomas for his very challenging but exciting projects ideas. Thank you to Dr. Costas Tsakonas for all the team work we have done together. Thank you to Dr. Steve Wakeham (from PQL Ltd) who I worked in collaboration for a joint research project.

Thank you also to my immediate colleagues in the Display Research Group of NTU, like Dr. Sharron Wilson, Dr. Sook Voon Yap, Thomas Miller and Carly Farrow who contributed to the dynamism and the lab organisation.

Finally, I would like to thank my family for encouraging me throughout my studies and especially my wife Millie for her continuous love and support and for giving birth to our newborn baby - little princess Anaïs.

LIST OF PUBLICATIONS

Articles

G. Boutaud, W. M. Cranton, D. C. Koutsogeorgis, R. M. Ranson, C. Tsakonas and C. B. Thomas, "*Growth optimisation of ZnS:Mn thin film phosphors for high intensity miniature electroluminescent displays"*, Materials Science and Engineering: B, vol. 165, pp. 202-206, 2009.

S. Wakeham, M. Thwaites, W. Cranton, C. Tsakonas, D. Koutsogeorgis and G. Boutaud, Journal of the Society for Information Display, vol. Selected papers from Eurodisplay 2009, "*A new technique for the high rate deposition of EL devices onto plastic substrates"*, June 2010.

S. Wakeham, M. Thwaites, C. Tsakonas, W. M. Cranton, R. M. Ranson, G. Boutaud and D. Koutsogeorgis, *"A new reactive sputtering technique for the low temperature deposition of transparent light emitting ZnS:Mn thin films"*, Physica Status Solidi (a), accepted for publication.

From MSc Project: S. L. Wilson, W. M. Cranton, R. Ranson, D. C. Koutsogeorgis, A. Mosley, C. B. Thomas, G. Boutaud, S. Wagland, E. A. Mastio, S. Lipiec, A. Spiller, J. Scott and S. Stoute, *"Optimization of the electrical and optical properties of ink-jet-printed SnO(2):Sb using thermal annealing and excimer-laser processing"*, Society for Information Display, Digest of Technical Papers SID International Symposium, pp. 530, 2005.

Conferences:

Oral presentation at 5th International Conference on Nanosciences & Nanotechnologies NN08, Thessaloniki, "*Growth optimisation of ZnS:Mn thin film phosphors for high intensity miniature electroluminescent displays*", G. Boutaud, Nottingham Trent University, 14-16 July 2008.

From MSc Project: Poster presentation at EuroDisplay 2005, Edinburgh, *"An Investigation into the Use of Ink-Jet Printed Transparent Conductors for Electroluminescent Displays",* G. Boutaud, Nottingham Trent University, The ELJET Consortium and DisplayMasters, 19-22 September 2005.

CONTENTS

LIST OF ABBREVIATIONS AND SYMBOLS

3D	3 dimensions
α	Absorption coefficient
Å	Angstroms (1×10^{-10} metres)
AC	Alternating current
Ag	Silver
Al	Aluminium
Ar	Argon
ArF	Argon fluoride
$ArO_2^{5\%}$	Argon with 5% oxygen content
ATD	Atomic layer deposition
at%	Atomic percentage
c	Speed of light in a vaccum
cd	Candela
CDT	Cambridge Display Technology
Cu	Copper
CVD	Chemical vapour deposition
cm	Centimetre
Cp	Specific heat
CRT	Cathode ray tube
e	Exponential
˚C	Degree Celsius
d_{hkl}	Distance between two adjacent planes of miller indices (hkl)
E_G	Band gap
E_F	Fermi level
FOV	Field of view
GaAsP	Gallium arsenide phosphide
GaP	Gallium Phosphide
GPIB	General Purpose Interface Bus
EL	Electroluminescent
ETL	Electron-transporting layer
FED	Field emission display
eV	Electron volt
h	Planck constant
H_2S	Hydrogen sulphide
HCl	Hydrogen chloride

HiTUS	High target utilisation sputtering
HTL	Hole-transporting organic layer
Hz	Hertz
θ	Angle between the incident beam and the atomic plane
I	Photoluminescent intensity
I_0	PL intensity at the laser irradiation pulse cut off time
I_r	PL intensity of red emission
I_y	PL intensity of red emission
In_2O_3	Tin oxide
ITO	Indium tin oxide
J	Joule
K	Boltzmann constant
KrF	Krypton fluoride
kV	Kilovolt
λ	Wavelength
L-V	Luminance versus voltage
LCD	Liquid crystal display
LED	Light emitting diode
LETFEL	Laterally emitting thin film electroluminescent
MBE	Molecule beam epitaxy
MHz	Megahertz
Mn	Manganese
ms	Millisecond
mTorr	MilliTorr
µm	Micrometre (1×10^{-6} metres)
µs	Microsecond (1×10^{-6} second)
mW	Milliwatt
OLED	Organic light emitting diode
Pa	Pascal
PEN	Planarised polyethylene naphathalate
PET	Polyethylene terephthalate
PL	Photoluminescence
PLS	Plasma launch system
PQL	Plasma Quest Ltd
psi	Pound per square inch
PVD	Physical vapour deposition
mbar	Millibar
n-type	Negative type (semiconductor)
N_2	Nitrogen

NTU	Nottingham Trent University
nm	Nanometre ($1 \times 10–^{9}$ metre)
n	Refractive index
ns	Nanosecond
p-type	Positive type (semiconductor)
PDP	Plasma display panel
PL	Photoluminescence
PMT	Photomultiplier tube
PSI	Phase-shifting interferometry
polyOLED	Polymeric organic light emitting diode
R	Reflectivity
RGB	Red green blue
RF	Radio frequency
R_S	Protector resistor
SiC	Silicon carbide
SiO_2	Silicon dioxide
SMOLED	Small molecules organic light emitting diode
SnO_2	Tin oxide
SRELD	Sunlight readable electroluminescent device
τ	Decay constant
TFEL	Thin film electroluminescent
TV	Television
UV	Ultraviolet
VFD	Vacuum fluorescent display
Vppk	Peak to peak voltage
Vrms	Root mean squared voltage
W	Watt
wt.%	Weight percentage
XeCl	Xenon chloride
XRD	X-ray diffraction
Y_2O_3	Yttrium oxide
Zn	Zinc
$ZnCl_2$	Zinc chloride
ZnS	Zinc sulphide
ZnS:Mn	Zinc sulphide doped with manganese
Ω	Ohm

LIST OF FIGURES

LIST OF TABLES

Chapter 1 Introduction

1.1 Overview

Due to great advances in technology, displays are now used in a variety of applications such as consumer appliances, watches, mobile phones, automobile dashboards, computers and TVs. Display Technologies include CRTs (cathode ray tubes), LCDs (liquid crystal displays), plasmas, OLEDs (organic light emitting diodes), LEDs (Light emitting diodes), electroluminescent, FEDs (field emission displays), VFDs (vacuum fluorescent displays) and others. The LCD display technology sector holds the highest market size because of more efficient manufacturing methods and higher sales volume. However, the demand for OLED and electroluminescent displays are increasing due to their potential to provide enhanced visual characteristics at reduced power consumptions.

While Thin film Electroluminescence (TFEL) occupies only a small segment of the flat panel display market, this technology dominates niche applications where its advantages are important. The combination of wide viewing angle, high contrast, very good ruggedness, and reliability, makes this solid state technology an ideal candidate for medical, military and instrumentation applications.

The conventional device structure consists of a central light emitting phosphor layer sandwiched between two dielectric layers and front transparent and rear opaque electrodes. In an alternative device configuration, reflected lateral emission from this phosphor layer using micromirrors has been shown to demonstrate the feasibility of high intensity luminous emission from fixed legend miniature displays [1]. These

laterally emitting thin film electroluminescent (LETFEL) displays have potential application for see-through head mounted systems, where luminances in excess of 3000 cd/m^2 are required, but without the need for a full graphics display. One of the most important considerations to realise these high luminances relies upon increasing the light emission of TFEL devices.

To achieve this, it is therefore imperative to optimise the phosphor growth used for the active light emitting layer, by enhancing its luminescent properties. In addition, issues with volume production reproducibility have highlighted the need to ensure using suitable monitoring techniques for batch to batch deposition reproducibility.

The TFEL process relies on electron emission from the interface trapping states between the dielectric and a phosphor film such as ZnS:Mn. In high electric fields, electron energy is transferred to manganese ions. Excitation and deexcitation of such ions results in visible emission at 580 nm.

Necessary for emission is post deposition annealing of the phosphor film. This can be achieved by either conventional thermal or laser annealing – the latter process has demonstrated higher efficiency [2-6].

Numerous deposition techniques are available for the fabrication of TFEL devices, Radio Frequency (RF) sputtering is one that has been used in research and volume production due its simplicity of use. However, other deposition methods may enhance film quality and luminescent properties such as Atomic Layer Deposition [7, 8] or other novel sputtering deposition such as HiTUS technology [9, 10].

This thesis presents the results of a study of ZnS:Mn thin film phosphors used in TFEL and LETFEL devices, examining techniques for phosphor growth optimisation

and post deposition processing in order to underpin development of novel TFEL devices.

1.2 Aim and Objectives

This project aims to investigate the optimisation and the physical processes involved in excimer laser processing of phosphor thin films to increase the efficiency of thin film electroluminescent display devices, with a target application of sunlight readable indicator display systems.

The specific objectives of this project were to:

- Investigate the optimisation of the growth quality and the dopant concentrations of thin films of zinc sulphide doped with manganese (ZnS:Mn) by co-sputtering from appropriate targets.
- Determine the viability of non-destructive monitoring techniques for enhanced repeatability and dopant concentration determination
- Laser anneal phosphor thin films with different dopant concentration using various irradiation conditions to investigate the effect on phosphor performance and to determine optimum processing parameters
- Investigate the feasibility of combining laser processing and sputter deposition to produce optimised thin film electroluminescent devices via the application of a progressive optimised layer processing.
- Liaise with industrial partners and carry out collaborative projects to investigate alternative thin film electroluminescent devices fabrications towards performance enhancement.

1.3 Structure of thesis

The background knowledge needed for this project is discussed in Chapter 2. This study reviews the electroluminescent (EL) devices physics and also the annealing and laser processing of thin phosphor films use for these devices.

The third chapter presents details of the experimental systems and techniques used to undertake this research - including the growth of thin film, EL device fabrication, laser processing and characterisation systems.

The fourth chapter presents and analyses results obtained with the luminescent behaviour of the films as a function of deposition optimisation, in order to demonstrate the feasibility of co-sputtering as a deposition technique – combined with luminescent decay time and monitoring of the red/yellow emissions that would facilitate the in-situ characterisation of Mn concentration variations and hence could provide a mechanism for positive process control.

Due to the requirement of high temperature post deposition, laser annealing was employed to enhance luminescent properties and results from novel processing techniques are presented in the fifth chapter. For the work presented here, the first laser processing technique has been applied to investigate the combined effect of laser processing and varying dopant concentration. The second technique was the introduction of a novel process of successive layer processing to investigate the potential improvement of electroluminescence efficiency.

The main objective of the sixth chapter is to present an evaluation of TFEL devices fabricated using RF magnetron sputtering compared to devices produced using alternative industrial techniques.

The last chapter is the conclusion of this chapter and summarises the achievements obtained during this research and suggests some potential future work to this research.

Other work undertaken during this research programme could not be presented in the main body of this thesis. The appendices present two examples, first a project on an original EL structure and then a study on laser processing of ZnS:Mn deposited on glass substrates. Finally, the third appendix is the publication of a paper to Material Science & Engineering: B.

Chapter 2 Literature Review

2.1 *Introduction*

As introduced in Chapter 1, this research is aimed at enhancing the light output efficiency of thin film electroluminescent devices by optimising phosphor thin film growth and laser processing techniques. In this chapter, a review of electroluminescent devices is first presented detailing the important phosphor characteristics. This is followed by a description of the LETFEL technology developed by NTU Display Research Group which is used as the basis for the device applications investigated. The most widely used fabrication techniques for ACTFEL devices are presented and compared. Finally a review on laser processing of polycrystalline thin films is presented. However, it is first essential to discuss EL technology in the context of emissive displays and how the technologies compare to each other in terms of physics and performance.

2.2 Emissive display technologies

Emissive displays can be defined as those that emit their own radiation (active devices). They can be classified in two types with their major materials used: organic displays with polymers and small molecules and inorganic displays with phosphors and semiconductors. All the materials have the property that they can produce visible photon emission from electron transitions due to energy transfers. The most important examples of organic and inorganic technologies are presented showing

their structure, operation and present State of the Art. Finally, the technology specifications are compared.

2.2.1 Luminescence

Both organic and inorganic materials use luminescence to produce light as illustrated in Figure 2-1.

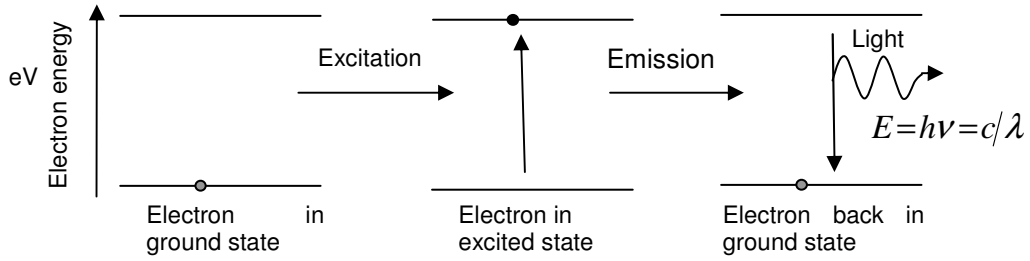

Figure 2-1: Schematic diagram showing the principle of the luminescence with the excitation and de-excitation of an electron via emission of a photon (producing light) [11]

2.2.2 Organic emissive displays

These displays are essentially Organic Light Emitting Diodes. OLEDs are electronic devices which are made by placing a series of organic thin films between two conductors. Small molecules and polymers are the two major types of material that are used. Both small molecules OLEDs (SMOLEDs) and polymeric OLEDs (polyLEDs) (see Figure 2-2) operate by accepting charge carriers of opposite polarities, electrons and holes, from the cathode and anode contacts, respectively. An externally applied voltage drives these carriers into the recombination region where they form a neutral bound state, or exciton. There are two types of excitons formed, called singlets and triplets. On average one singlet and three triplets are formed for each four electron-hole pairs injected into the exciton formation region of the OLED.

Quantum mechanics allows de-excitation (or recombination) of the singlet within a few nanoseconds of formation. This leads to a photon emission and is called fluorescence. Recombination of the triplet exciton is slow (taking about 1 ms to 1 second) and when it does occur, usually results in heat rather than light. But if a heavy-metal atom such as iridium or platinum is placed in an otherwise organic molecule, the characteristics of singlet and triplet excitons mix, speeding the emission of light to within 100 ns - 100 µs. This kind of emission is called phosphorescence.

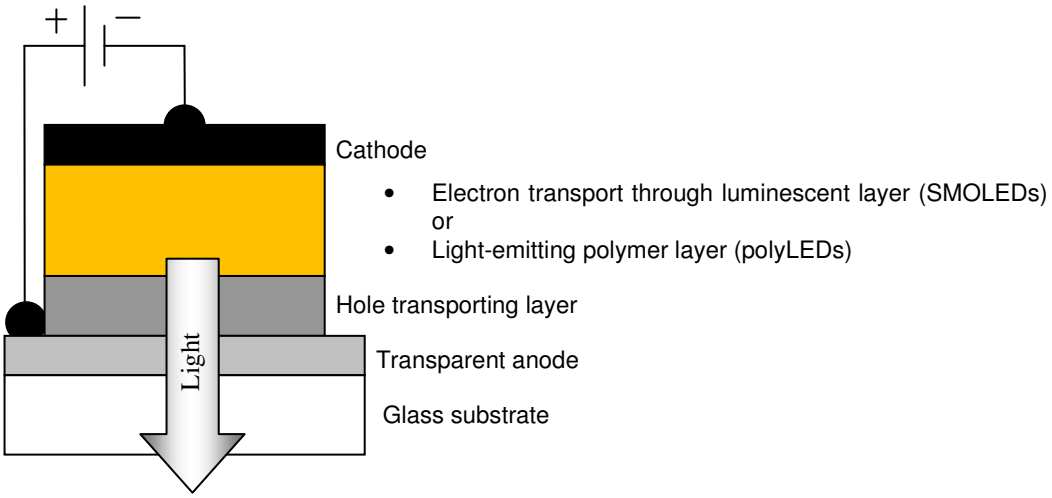

Figure 2-2: Schematic diagram showing the general structure of organic emissive displays

Small molecules OLEDS

Figure 2-2 shows a schematic diagram of typical organic light-emitting device. Luminescent molecular excited states are generated in the electron transport and luminescent layer near its interface with the hole transport layer. Small molecules OLEDs are deposited on a glass or plastic substrate to form a multi-layer structure about 100 nm thick. The substrate is first coated with a conducting transparent electrode such as indium tin oxide (ITO) or polyaniline, which serves as the anode. This is followed by a thin, hole-transporting organic layer (HTL) typically made

from chemicals called diamines. An organic light-emitting layer of comparable thickness is then deposited onto the HTL surface. This latter layer often doubles as the electron-transporting layer (ETL). Finally, the device is completed by depositing a cathode consisting of a metal with a low work function such as calcium or an alloy such as magnesium-silver onto the ETL surface. A low work function is necessary to ensure efficient, low-resistance injection of electrons from the cathode into the ETL [12].

Polymer LEDS

A display based on polymer light-emitting diode (polyLED) technology consists of the same basis structure as shown on Figure 2-2. The entire device is encapsulated with a metal (or glass) seal. The centerpiece of a polyLED is the light-emitting polymer layer. This layer as well as the hole transporting layer can be applied by spin coating or an ink jet process. The former process can be used for the preparation of monochrome displays, while the latter should be used for full-colour devices. Applying a small voltage across the device results in the injection of charge carriers that drift through the light-emitting polymer layer under the influence of the applied electric field. At some point, the charge carriers can recombine and release energy in the form of photons which are emitted through the transparent anode. This process occurs millions of times per second and gives the device its high brightness [13].

The first polymer LED, fashioned in 1990, was made from the hydrocarbon polymer poly(p-phenylene vinylene), which emits only in the yellow part of the spectrum. Conducting polymers have since been devised that glow right across the visible range, so that full color displays are now possible in principle from polymer LEDs and full-color polymer LED displays are commercially available [14]. Cambridge

Display Technology (CDT) has developed a hybrid system based on light-emitting polymers and dendrimers, which combines the advantages of small molecules (high efficiency) with polymers (less expensive to manufacture) [15].

2.2.3 Inorganic emissive displays

2.2.3.1 Using semiconductors

The basis of a light-emitting semiconductor device is the pn junction diode. This is produced by creating a junction between a p-type semiconductor and an n-type semiconductor as illustrated on Figure 2-3.

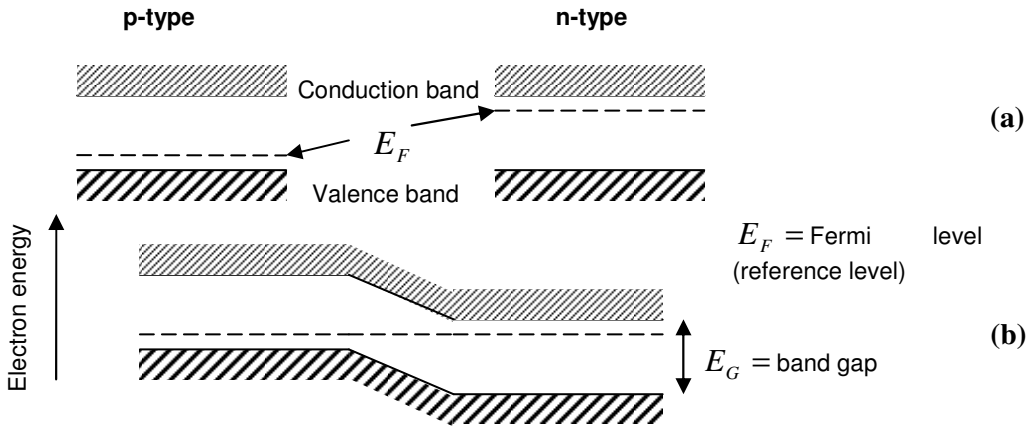

Figure 2-3: Schematic representation of the formation of a p-n junction: (a) initially separated p-type and n-type materials; and (b) the energy band distribution after the junction is formed [12]

When the two types of semiconductor are formed as adjacent layers, the mobile electrons in the n-type region are attracted by the holes in the p-type region and so move across the junction to fill a hole. The boundary region thus becomes depleted of majority charge carriers and an energy barrier is formed. The application of a forward bias (n side cathode) reduces the barrier and allows electrons and holes to flow across the junction – where electrons fill 'holes'. This process is called

recombination, and releases an amount of energy equal to the band gap energy, E_G. For optical devices, if semiconductors are indirect bandgap materials, an electron recombines with a hole and then loses some momentum. This process involves an electron, a photon, and a lattice vibration. It is much simplier for a lattice vibration to take away all the energy and momentum of the electron on its own. So, to have an efficient device in terms of light emission, the semiconductor must have electrons which have only energy to lose. This semiconductor is called direct bandgap material.

LED

LEDs (Light Emitting Diodes) are photon emitting semiconductors which emit light due to the injection electroluminescence effect (see in next section). Their structure is represented on Figure 2-4.

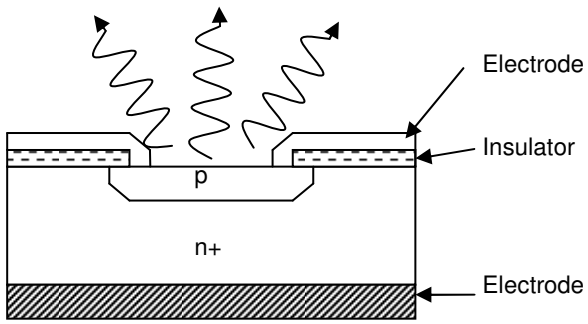

Figure 2-4: Schematic diagram of an LED

The wavelength of the emitted light varies primarily due to the choice of semiconductor materials used, and is commonly in visible spectrum or infrared.

Now, new LED devices using materials such as GaAsP/GaP have an efficiency factor of 0.76 which means only 24% of the light emitted is absorbed by the substrate (against 85% for a GaAsP/GaAs device). Moreover by adding a domed surface to the

LED chip the critical angle has increased from 17 degrees to 26 degrees and more light can be emitted.

2.2.3.2 Using phosphors

Phosphors are materials that emit light (infrared to ultraviolet) under external energy excitation. These materials absorb incident energy and then re-emit that energy in the form of electromagnetic radiation over and above thermal radiation. Phosphors that emit light in the visual range of the electromagnetic spectrum are of the most concern for practical applications, such as indicators and displays. To produce a colour display, the majority of the light emission from phosphors must be within the visual range (of wavelengths). Phosphors use a process, by which light (or radiation) is produced when energy is applied to a material, called luminescence (see Figure 2-1) which has three main categories for display technology.

- If the carriers are excited by photon absorption, the radiation resulting from the recombination of the excited carriers is called photoluminescence (plasma panels).
- If the excited carriers are created by high energy electron bombardment of the material, the mechanism is called cathadoluminescence (cathode ray tubes - CRT).
- If the excitation occurs by the introduction of current, the resulting luminescence is called electroluminescence [16].

When the excitation mechanism is switched off, if the luminescence persists for a time equal to the lifetime of the excited state, then this process is called fluorescence. If, however, the luminescence persists for much longer than expected, then it is called phosphorescence. Materials exhibiting phosphorescence are called phosphors.

Phosphor materials depend for their action on the presence within the material of impurity ions called activators [17].

Incident energy arrives on the surface of the material and travels through the material until it is absorbed by an activator, denoted by the dark circle in Figure 2-5. The energy of the activator ion is raised to an excited state by promoting one or more electrons from their ground state to higher energy levels (see Figure 2-1). As the electron returns to the ground state a photon can be radiatively emitted. The photon energy is proportional to the energy difference between the excited and ground states of the electron. Nonradiative emissions can occur when the activator emits phonons, which are lattice vibrations that transport energy in the form of heat.

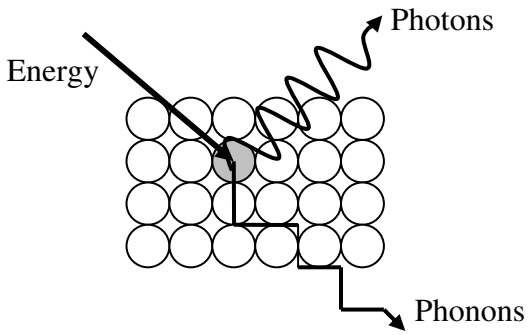

Figure 2-5: An illustration of how a phosphor emits light. The dark circle denotes an activator ion which is surrounding by a host lattice.

The three major inorganic emissive technologies are CRT, Plasma and electroluminescent displays. The CRT display is a mature technology and is becoming less and less popular due to many reasons (heavy, bulky, power hungry, potentially harmful, flickering and spherical effect on edges). Plasma display panel is mainly restricted to large TV displays. Electroluminescent displays are typically monochromatic, but can be an ideal solution for the most challenging and demanding applications where other technologies are simply inadequate, such as embedded

displays for extreme conditions, and also where ruggedness, reliability, high contrast, and high viewing angles are required.

Plasma

PDP (Plasma Display Panels) contain xenon and neon gas in hundreds of thousands of tiny cells positioned between two plates of glass. Long electrodes are sandwiched between the glass plates, on both sides of the cells. The address electrodes sit behind the cells, along the rear glass plate. The transparent display electrodes are surrounded by an insulating dielectric material and are covered by a magnesium oxide protective layer. These electrodes are mounted above the cell, along the front glass plate. An addressable display is produced by building the electrodes as a matrix of intersecting rows and columns [15]. When the intersecting electrodes are charged (with a voltage difference between them), an electric current flows through the gas in the cell. The current creates a rapid flow of charged particles, which stimulates the gas atoms to release ultraviolet photons as shown in Figure 2-6.

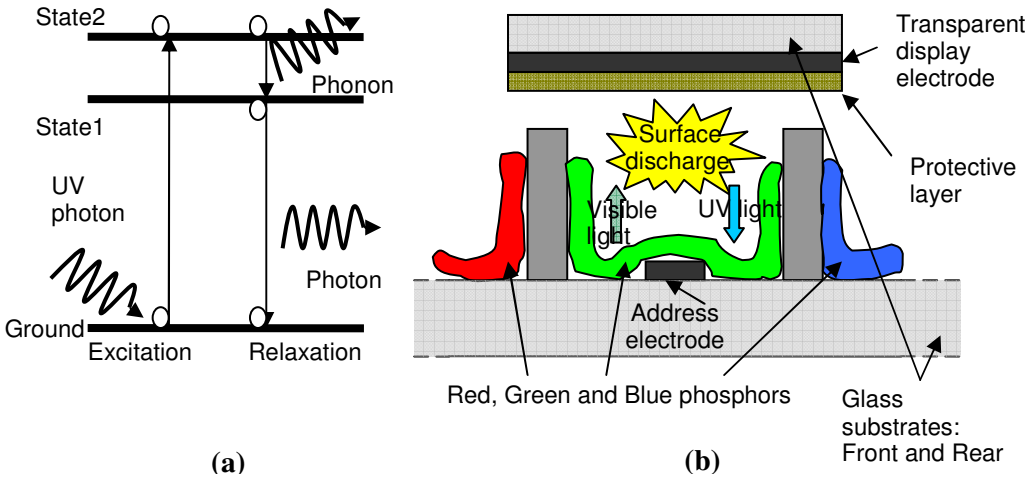

Figure 2-6: Schematic representations of the photon excitation (a) and a cell structure for PDPs (b)

The excitation method for a plasma display is via photoluminescence. When ultraviolet photons are incident on the phosphor in the cell, lower energy visible luminescence is produced by the energy transfer process.

When RGB phosphors are excited the plasma display gives off red, green and blue light. Every pixel is made up of three separate subpixel cells, each with different coloured phosphors. One subpixel has a red light phosphor, one subpixel has a green light phosphor and one subpixel has a blue light phosphor. These colours are mixed to create the overall colour of the pixel, using pulse width modulation of the addressing of each subpixel [18, 19].

Plasma displays have now sizes that can be over 100 inch in diagonal screen. Panasonic has recently developed the world largest (152 inch or 3.9 m) 3D capable high definition plasma television.

2.3 Electroluminescent devices

2.3.1 Brief history

Electroluminescence (or EL) is the phenomenon in which electrical energy is converted to luminous energy without thermal energy generation. It was first observed in silicon carbide (SiC) by Captain Round in 1907. In 1936, Destriau [20] was the first to publish a report on EL in which a high voltage is applied to a luminescent material (ZnS compound).Various devices of this type have been developed in the 50s and early 60s, but because the phosphor was in powder form, these devices were unreliable and inefficient [21]. In 1974, with the advancement of thin film process technology, the first reliable and efficient Thin film EL device was successfully fabricated by Inoguchi [22]; with lifetimes of more than 10000 hours

using the double insulating layer structure reported (refer to Figures 2-7 and 2-8 for structure and operation).

2.3.2 Types of EL devices

There are two major classes of EL devices. The first class of devices is injection luminescence in which light is generated by electron-hole pair recombination at a p-n junction. Light emitting diodes (including OLEDS) fall into the first class of devices; the second class of devices are the ones in which light is generated by impact excitation of a light emitting centre by high-energy electrons. This work is focused on the second class of EL. In these devices, a high electric field (of the order of 10^6 $V.m^{-1}$) is applied across the phosphor layer. The electrons derive very high energies from the applied electric fields and excite the light-generating (or luminescent) centre by impact excitation. The excited luminescent centres generate light. This type of EL is called *high-field electroluminescence.* [23]

The high field EL devices are classified based on the configuration of the phosphor layer and the drive voltage waveforms as

- AC (alternate current) thin-film EL device
- AC powder EL device
- DC (direct current) thin-film EL device
- DC powder EL device

Powder devices have the phosphor layer in powdered form while in thin-film devices the phosphor layer is deposited using thin-film deposition techniques. Powder EL devices typically have short lifetimes (~ 2500 hours [24]) and are not suitable for the majority of consumer applications. However, there is a resurgence of interest in these

devices for industrial applications such as advertising where relatively shorter lifetime is not an issue [25] and for substrate flexibility [26].

With the improvements in thin-film deposition technologies, interest has shifted to AC and DC thin-film devices. But it has been observed that DC-TFEL devices suffer from reliability problems. Hence ac thin-film EL devices have been the most consistently studied of the TFEL devices. This work will focus on ac-TFEL devices because of the advantages of these devices over the powder devices.

Thin-film EL devices are all solid state, and can exhibit ruggedness, high contrast, and a wide viewing angle which makes them particularly useful for applications such as military, medical, transport, and instrumentation.

2.3.3 Structure and operation of ACTFEL devices

A TFEL device can be fabricated by sandwiching a phosphor layer between two electrodes (one of which is transparent) and applying high voltage waveform (typically ~ 200 V_{rms}) between the two electrodes. However in such a structure with high voltages, any imperfection in the phosphor layer that leads to a short circuit would cause a destructive amount of energy to be dissipated in the device. To remedy this problem, a double insulating device structure was proposed by Russ and Kennedy [27]. This structure has gained wide acceptance and popularity ever since Inoguchi [22] reported devices with very long lifetimes using this structure. A schematic of this device structure is shown in Figure 2-7. In this device, the insulating layers protect the device from short circuiting the two electrodes even if there is a short in the phosphor layer (provided that the insulating layers are of very good quality and free of pinhole defects).

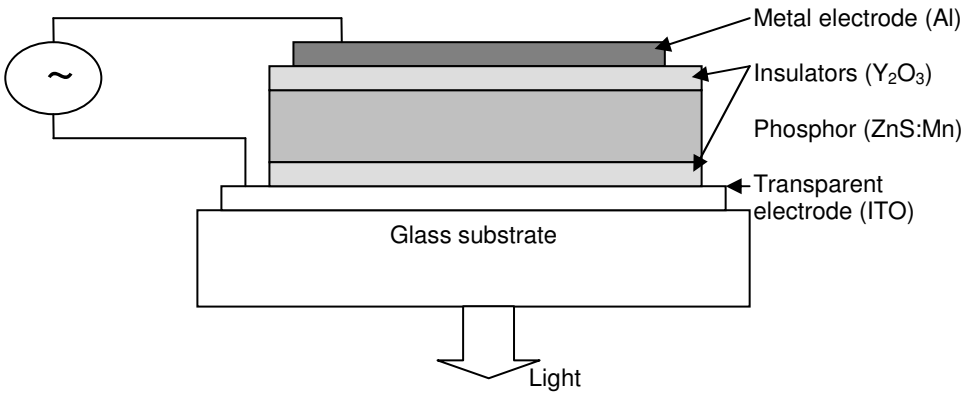

Figure 2-7: Schematic of a double insulating TFEL device

The operation of a double-insulating layer TFEL device works as follows and is illustrated on Figure 2-8. As the voltage between the electrodes is increased beyond the threshold voltage, electrons are injected from the interface states between the phosphor layer and the insulating layer due to high-field assisted tunnelling (1). The injected electrons are accelerated and gain kinetic energy large enough to excite luminescent centres in the host lattice (2). These high-energy electrons (or hot electrons) excite luminescent centres through an impact-excitation mechanism. Light is generated when these electrons in the excited states of the luminescent centres transition radiatively to the ground state (3). The hot electrons are finally trapped at the opposing interface states (4) [23], and the process starts again at the opposite polarity cycle.

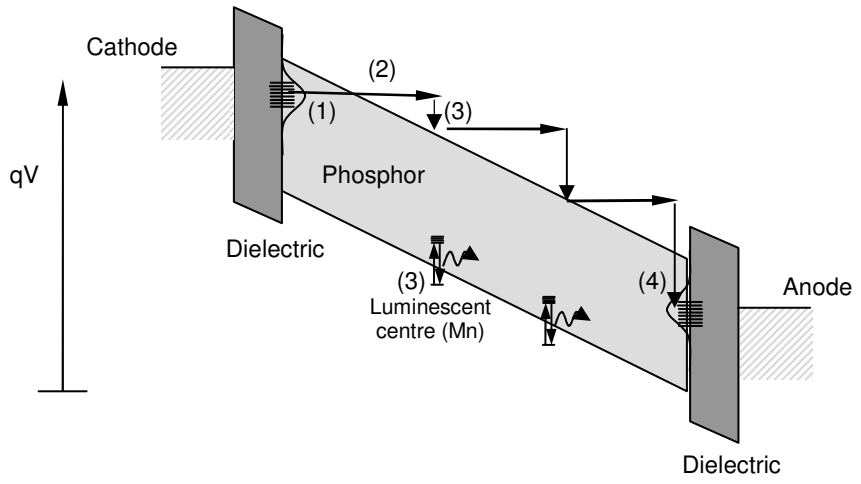

Figure 2-8: Energy band diagram of TFEL process [28].

2.3.4 Phosphor requirements

The phosphor layer in a Thin Film Electroluminescent (TFEL) device consists of a host lattice with a luminescent centre incorporated into it. The requirements of the host material, the luminescent centre and the phosphor layer are summarized from reference [23].

Host material

- As these are polycrystalline films, grain boundaries and defects are electron scattering centres and are minimised by annealing - related to enhancements in crystallinity as observed by XRD.
- It must be able to incorporate the luminescent centre in a substitutional lattice site; otherwise the excited centre will lose its energy non radiatively to a nearby lattice defect.
- The typical doping level of the host material is of the order of 1%. In order to maintain the required good crystallinity at these dopant levels, it is important to match both the geometric size and the valence of the host cation with that of the

dopant. If there are fewer mismatches, the dopant atoms will fit in the substitutional site. If not, they will sit in the interstitial site.

Luminescent centre

- The luminescent centre should be properly incorporated into the host materials and emit visible radiation.
- It should have a large cross-section for impact excitation.
- It should be stable in the high E-field of the order of 10^6 $V.m^{-1}$. Phosphors based on the recombination of electron-hole pairs at shallow donor-acceptor states are not efficient under TFEL operation because these states tend to remain ionized in the electric field. For this reason CRT phosphors such as ZnS:Cu,Al and ZnS:Ag are not efficient phosphors for TFEL devices. For example, Cu acts a poor luminescent centre in ZnS TFEL devices, but is an excellent candidate for CRT based devices. This is due to the fact that the shallow donor and acceptor levels in Cu are unstable in high electric fields because electrons can tunnel out of these levels. On the other hand Mn is an excellent luminescent centre for TFEL devices because Mn levels are very deep. To date, all efficient TFEL luminescent centres are atomic in nature with deep energy levels, i.e. isolated luminescent centres.
- The luminescence must not be quenched by the high electric field (greater than or equal to 10^8 $V.m^{-1}$).

Phosphor layer

- The phosphor layer must have large enough band gap to emit visible light without significant absorption

- It must hold high E-field of the order of 10^8 V.m^{-1}without electric breakdown and it must have insulating characteristics below threshold voltage; and it must not be degraded by the high electric field.
- It must be able to sustain a current of hot electrons through the film.

TFEL device optimisation is thus concerned with maximising these various parameters which the premise of the work presented here - where new combinations of co-sputtering and laser processing are used to investigate optimisation and reproducibility.

2.3.5 LETFEL technology

In an alternative device configuration, reflected lateral emission from TFEL devices has been shown to demonstrate the feasibility of high intensity luminous emission from fixed legend miniature displays [1]. The light intensity emitted at the edge of a TFEL thin film display is much greater than that emitted directly though the surface [29]. This occurs because the refractive index of the phosphor thin film is generally higher than that of the dielectric layers resulting to up to 90% light loss for the surface emission due to internal reflections. This novel technology makes use of the laterally transmitted and internally reflected high intensity light of a TFEL device by including micro-mirrors capable of redirecting the light towards the surface of the device and resulting with considerably enhanced light output from more effective emitting regions [30] as represented in Figure 2-9. This structure using a different process emission can produce a typical four-fold increase compared to conventional emission [31].

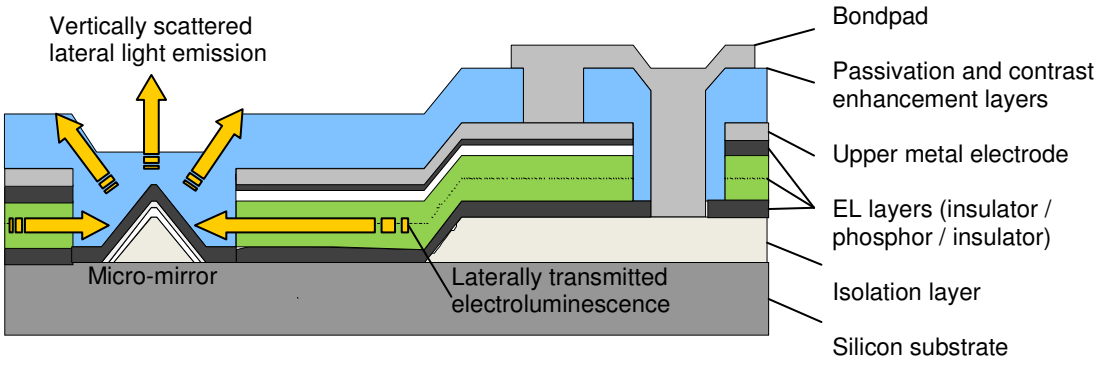

Figure 2-9: Cross section of a LETFEL device [32]

2.4 EL devices fabrication

This research focuses on the growth optimisation of the phosphor layer to be used in electroluminescent devices. However, the fabrication of EL devices requires also the development of other layers and their successful integration. It is important to mention that there is no standard thin film deposition technique for the fabrication of the phosphor layer, therefore a range of viable deposition methods will be discussed. However, the insulators used in TFEL devices are predominantly deposited by R.F. sputtering techniques. [33]. High quality ITO films are usually also obtained by R.F. magnetron sputtering and with control of oxygen partial during deposition [23]. R.F. sputtering is therefore the preferred technique for commercial TFEL deposition and particularly for this research purpose, due to its simplicity and as it requires only one type of deposition system, reducing layer contamination. On the other hand, the intrinsic characteristic of the sputtering process generates a relatively poor crystallinity for the as-deposited films. Hence, thermal processing techniques are typically exploited to improve the overall film quality. These techniques are also presented.

2.4.1 Thin film deposition methods

The manufacturing of ACTFEL devices is highly dependent upon the ability to produce thin films in a controlled manner. The films must meet certain criteria in a repeatable fashion with control over parameters such as thickness uniformity, roughness, purity and crystallinity. These deposition techniques are generally categorised into two categories - PVD and CVD. Physical vapour deposition (PVD) occurs when a vapour is generated from the source material by a physical process, transported through a vacuum, and deposited on the substrate surface to grow a film. Chemical vapour deposition (CVD) is a process whereby the growing film is the result of a chemical reaction from suitable gas-phase reactants introduced to a chamber and allowed to react at the surface of the substrate. The most important deposition methods for the fabrication of EL devices, such as thermal evaporation and sputtering for PVD methods, and atomic layer deposition for CVD methods, are briefly reviewed.

2.4.1.1 Evaporation

Evaporation occurs when a material is heated to its equilibrium vapour pressure. Equilibrium vapour pressure can be defined as the pressure reached when a condensed phase is in equilibrium with its own vapour. If the pressure level is low enough, the evaporated atoms travel at high velocity without collision with other particles and then condense on the inside of vacuum chamber and the substrate. The two most common techniques are thermal evaporation and electron beam evaporation. For thermal evaporation, the material to be evaporated is placed in a resistance heating or ‘boat’ where current is passed through it [34] with material melting point temperature of less than 1400°C. Electron beam evaporation employs a

focussed electron beam of high energy (~10 keV) to vaporise source materials from a crucible at temperatures below 2200°C [23]. The phosphor layer may be deposited by electron beam evaporation as, for example, the melting point of ZnS is 1800 to 1900°C [23]. An important consideration with the evaporation process is the production of very stoichiometric films. This can be achieved by adjusting the substrate temperature. With the example of ZnS, with a vapour pressure high enough and a substrate temperature above 200°C [23], the atoms of Zn and S will not adhere to other similar atoms forming alternate layers of Zn and S as indicated in Figure 2-10. However, strains are often produced and need to be removed by post-thermal annealing.

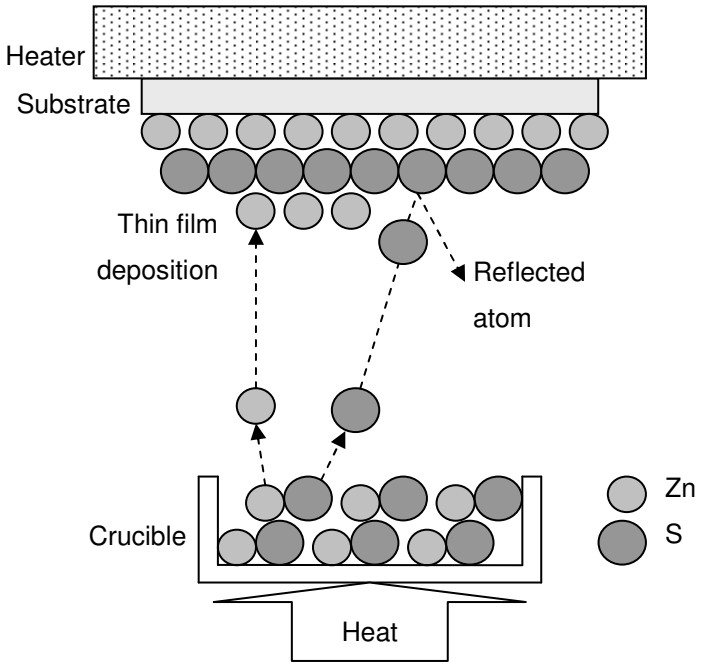

Figure 2-10: ZnS evaporation process with formation of alternate layers of Zn and S atoms [23]

2.4.1.2 Sputtering

Sputtering is the primary alternative to evaporation for thin film deposition. This process involves the physical (and not thermal) vaporisation of atoms from a surface by momentum transfer from bombarding energetic particles to the target material to be sputtered [35]. These energetic particles are ions accelerated to the negatively charged cathode in a plasma initiated by applying a large voltage across a gap containing a low-pressure gas. With sufficient energy to be ejected, the sputtered atoms travel trough space and eventually coat the anode (substrate). This energy should be enough for the incident particle to adsorb to the surface of the wafer and not bounce off, but also not too high to penetrate and damage the substrate. Figure 2-11 illustrates some of the processes that may occur during sputtering of an energetic particle.

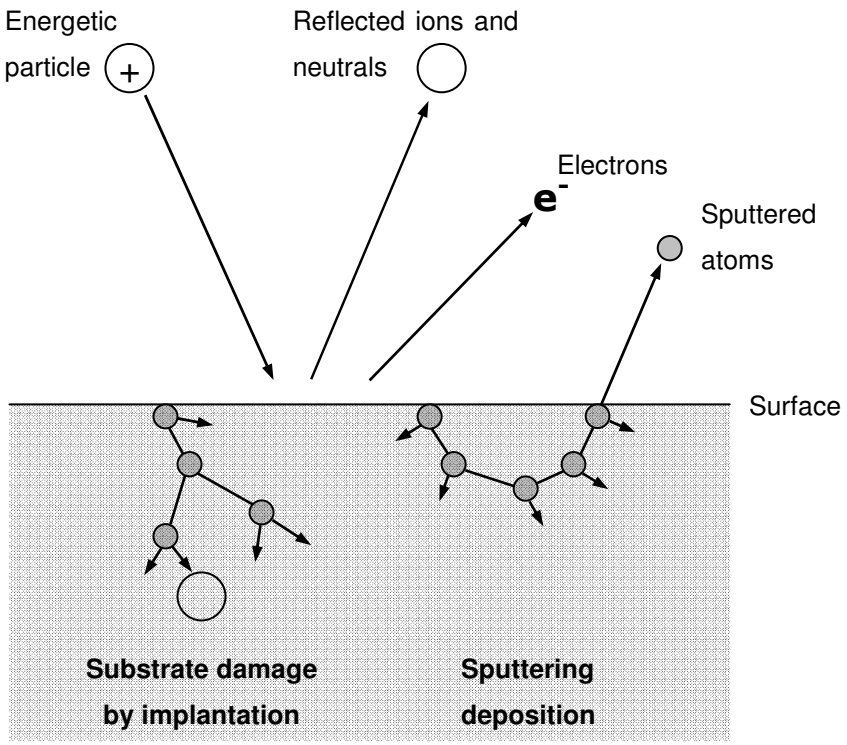

Figure 2-11: Main effects of sputtering process [35]

Since the chemical composition of the substrate is usually the same as the target material, sputter deposition is better than evaporation process at producing films of alloys (e.g. phosphor compounds used in ACTFEL devices). Most importantly, sputtering systems are suitable for in-line processes as both the insulators, the phosphor layer and the electrodes can be grown using this deposition method [23].

To enhance the thin film phosphor crystallinity, it can be necessary to use reactive sputtering [36]. Reactive sputtering is a process in which the inert sputter gas (Ar) is replaced by a inert/reactive mixture (e.g. Ar/H_2S). The chemical composition of the deposited film can be varied by varying the partial pressure of the reactive species in the plasma. The typical problem in reactive sputter deposition is to prevent poisoning of the sputtering target by the formation of a layer on its surface. Therefore, high deposition rates are required with control of reactive gas and monitoring of partial pressure.

2.4.1.3 Atomic layer deposition

Atomic layer deposition (ALD), also referred to formerly as atomic layer epitaxy, was first used specifically as a technique to make electroluminescent displays [37]. ALD can produce high quality films with accurate thickness control and good reproducibility. The major disadvantage is the very slow deposition rate. As a CVD method, ALD uses reactant gases to deposit films on the substrate in a reaction chamber. However, reactants are introduced sequentially and not at the same time to form a monolayer as illustrated in figure 2-12 for the deposition of ZnS.

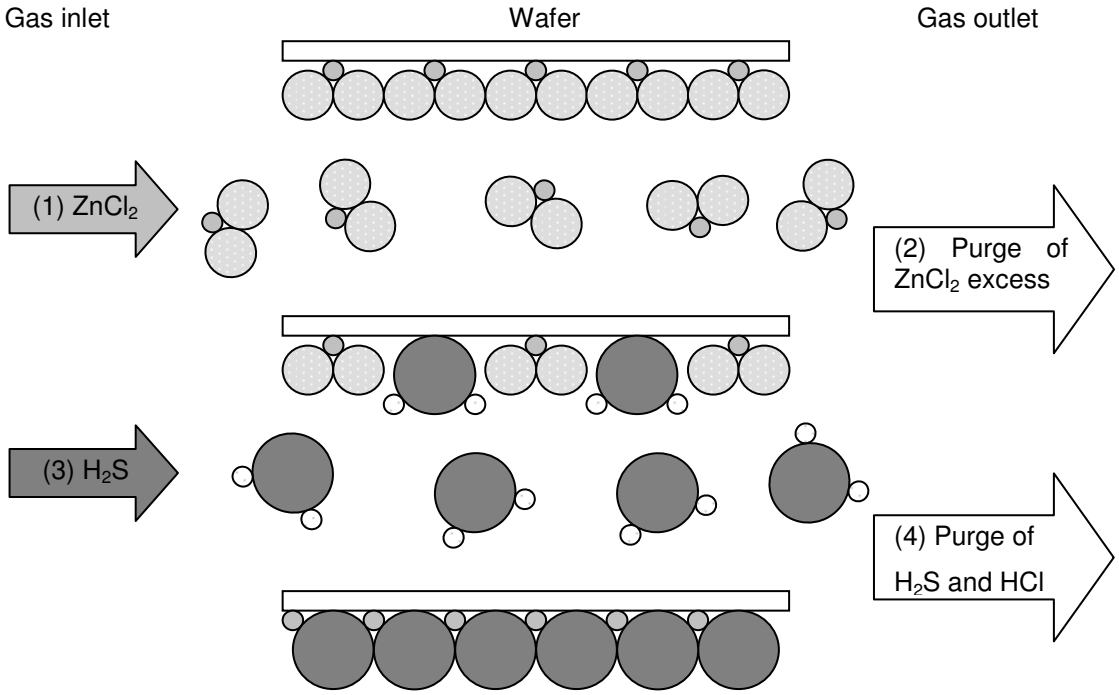

Figure 2-12: Atomic layer deposition of one monolayer of ZnS [23] **The substrate (wafer) is typically held at high temperature (400°C-500°C) during deposition**

The ALD process for one monolayer of ZnS depends on the following reaction:

$$ZnCl_2 + H_2S \rightarrow ZnS + 2HCl$$

The cycle starts by introducing $ZnCl_2$ vapor in the gaseous phase which adheres to the heated substrate. The excess of $ZnCl_2$ vapor is purged with an inert gas to be replaced with H_2S vapour. The desired ZnS compound is then formed, and the by-product HCl is liberated from the deposited film as vapour. The excess of H_2S and the produced HCl are purged to complete the cycle. [23].

Contrary to evaporation and sputtering methods, the deposition is not influenced by pressure but growth temperature can be highly important and low temperature variation can greatly affect the grain size and the luminous efficiency of the devices fabricated using this technique [38].

2.4.1.4 Deposition methods comparison

Table 2-1 summarises the deposition methods described previously with their conditions and characteristics of ZnS:Mn based ACTFEL devices.

	Evaporation	Sputtering	ALD
Deposition rate (Å/min)	>1000	>100	10-50
Substrate temperature (°C)	200	200	500
Crystal structure	Zinc blende	Zinc blende	Wurtzite
Luminance (cd/m^2)	>3000	>1500	>3000
Luminous efficiency (lm/W)	~3	~2	~3

Table 2-1: Emissive displays specifications comparison from Ref. [39]

2.4.2 Post-deposition annealing

The performance of EL devices is greatly influenced by the crystallinity of the phosphor layer. Post-deposition annealing enhances this phosphor layer by improving crystallinity, removing strain and increasing impurity diffusion.

2.4.2.1 Thermal annealing

The crystalline quality of the film grown depends heavily on the substrate temperature. At lower temperatures, the atoms on the surface do not have enough energy and velocity to diffuse and only a few can form crystallites. At higher temperatures, the energy and the mean free path of diffusion of the atoms is high, hence they can diffuse to the right crystallographic sites thereby increasing quality of the film. For ZnS:Mn, it was found that the critical temperature for which the resultant film quality was acceptable was 190°C [40-42]. Post deposition thermal annealing is typically required for the fabrication of ACTFEL [43] and it improves furthermore the crystallinity and dopant distribution of the as deposited films and

hence the overall film quality [41, 44]. Photoluminescence intensity increases with annealing temperature which results from the diffusion of Mn^{2+} into Zn vacancies, moreover 500°C was found to be the optimum annealing temperature for the EL intensity [28].

Annealing improves the phosphor but due to mechanism of high field EL, a reduction of interface state density by annealing can limit the performance – hence the interest in highly localised annealing, using laser processing.

2.4.2.2 Laser annealing

Laser annealing of the thin polycrystalline thin films is typically an epitaxial regrowth or laser-induced recrystallisation [45]. In the case of silicon (very well known and widely used in thin film transistor technology), `laser annealing' refers to the transformation of small grain polycrystalline into large grain crystalline material. But in the case of phosphors (and particularly for ZnS), it is believed that laser annealing induces an in depth solid state phase transition without melting and promotes dopant diffusion. Instead of a recrystallisation, as with silicon, in sputtered ZnS the original cubic phase appears to change to a mixed phase: hexagonal and cubic which suggests a re-ordering and probable removal of defects. The advantages of laser processing over standard or traditional thermal (heater used in this research) annealing are related to the short processing cycles that can be achieved with lasers. With short pulsed laser beam dwell time (20 ns for KrF), the precipitation of dopants (Mn) can be widely suppressed, generating high concentration of active dopants [45]. In the case of this study, the main advantage is the localisation of the annealing effect, hence retaining the electrical properties of the lower dielectric surface without reducing the interface state density.

2.5 Laser processing of polycrystalline thin films

2.5.1 Physics of laser processing

Laser processing has been used extensively for the last 25 years. The use of high-power pulsed laser beams in the nanosecond regime allows the transfer of a large amount of energy in short time into the near-surface region [46]. Under suitable conditions, the irradiation can lead to the melting of the surface to a depth not exceeding a few thousand of angstroms. The melting threshold, melt depth and melting duration depend on a complicated fashion on the different parameters involved in the interaction between the incident laser beam and sample, including the wavelength, duration and shape of the pulse and the optical and thermal characteristics of the irradiated surface [47].

The immediate effect of irradiating a material by an intense laser beam results in the modification of some properties of this material. Indeed, the parameters k (thermal conductivity), C_P (specific heat), α (absorption coefficient) and R (reflectivity), can be modified following a heating of the material.

For any type of material, the laser irradiation can modify and even destructively modify the irradiated surface. The threshold and the degree of destruction depend on several factors:

- the wavelength and the fluence of the beam laser;
- the nature of the irradiated material, the absorption coefficient and the melting temperature of the materials vary;
- the surface roughness of the irradiated surface – the absorption coefficient of a rough surface is amplified by multiple reflections on the surface, resulting in the diminution of destruction threshold;

- the cleanness of the surface – the presence of very absorbent impurities drops the destruction threshold;
- the operation mode of the laser – continuous or pulsed mode [48].

The destruction of the irradiated surface is related to the augmentation of the material temperature: over the melting temperature in the region of the incident beam, some deformations appear onto the surface.

2.5.2 ZnS:Mn thin films laser processed review

Laser processing has been successfully used since the 1970s to convert amorphous silicon to polysilicon for the purposes of TFTs in display applications. Excimer lasers are usually the laser of choice because of their high energy UV output. This includes lasers such as XeCl (308nm), KrF (248nm) and ArF (193nm).

In terms of thin film phosphor applications, there has been a recent growth in interest in methods of improving the characteristics of phosphors without traditional thermal annealing. The wavelengths associated with the KrF and ArF excimer systems are compatible with the absorption spectrum of ZnS:Mn and the absorption coefficient prevents the laser radiation from reaching and damaging the substrate.

Laser annealing of ZnS:Mn films were first reported in 1983 [49]. Mn was implanted into RF sputtered ZnS films to form ZnS:Mn (0.3 at%) which was laser processed by a XeCl laser (λ = 308 nm). Under a pressure of 90 psi and at a fluence of 2.5 J/cm^2 , the PL would become about twice as bright as the PL achieved only by thermal annealing (500°C). But EL was not improved and laser annealed thin films were unsuccessful in EL devices [50].

More recently, an extensive programme of work of laser annealing at 248 nm commenced in 1997 with the awards of two doctorates (Mastio [42] and Koutsogeorgis [51]) from NTU. Some of this work [51] has been realised based on novel light emitting device technology developed by the NTU Display Group. The work covered research into novel high intensity laterally emitting thin film electroluminescent (LETFEL) displays, enhancement of performance in commercial thin film EL displays, and the development of laser processing techniques for enhancing thin film phosphors. Using a KrF excimer laser, NTU has shown a four-fold increase electroluminescent emission [52] of ZnS:Mn TFEL commercial devices from a combination of laser plus thermal annealing compared with thermal annealing only (at 450°C) (see Figure 2-6).

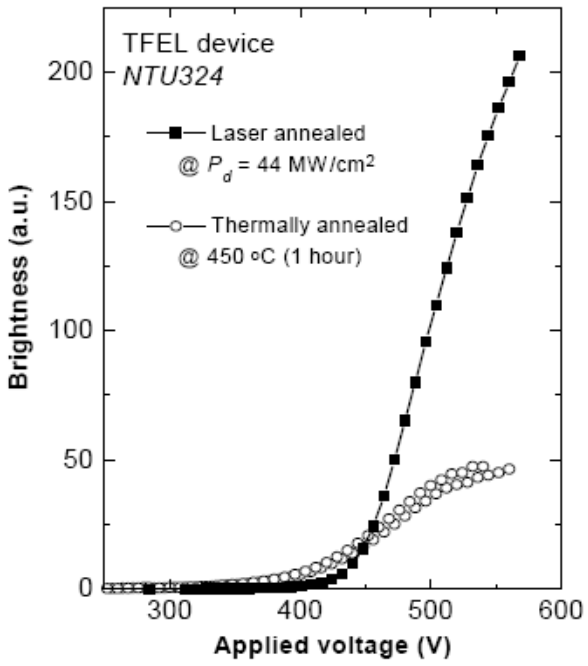

Figure 2-13: Brightness vs applied voltage for a TFEL device showing that laser annealing improves device output (after reference [28]**).**

Indications from both X-ray diffraction [42] and ellipsometry [53] showed that a phase change occurs in the upper 200 nm of film. This was confirmed with thermal simulations indicating that under solid state conditions the sphalerite (cubic) to wurtzite (hexagonal) should be confined within the first 250nm of the ZnS thin film. Also, exploratory comparison with a laser annealing model suggested substantial temperatures rises in the films during a laser annealing pulse, the maximum temperature occurs after a short time (25ms) for a 20ns pulsed KrF excimer at various fluences [2].

A research group from the University of Hull has concentrated on the laser ablation of ZnS:Mn thin films for patterning [54, 55] and has worked in collaboration with NTU group [56]. The objective of laser ablation is to remove material but for laser annealing material removal can be detrimental. These studies have shown the importance of using pressurised environment whilst irradiating the thin films with UV lasers. But more importantly, this represents a base for a future thermal model necessary for this project. Indeed, characterisation of the ablation properties could lead to establish the optimum regime for processing. Because, the depth removal is related to thermal removal, it is important to determine the thermal properties of thin film phosphor combined with laser characteristics such as pulse length and fluence to create a theoretical depth profile [57].

2.6 Conclusion

While various techniques for deposition and processing of TFEL devices have been presented in the literature, and indeed resulted in commercial devices, there is still a need to optimise phosphor deposition, particularly for viable in-line processing using

RF magnetron sputtering. This deposition method has presented, in some cases, problems with batch to batch depositions; therefore monitoring techniques such as control of dopant concentration can be essential. Some companies such as Lite Array have ran into difficulty facing these problems, only ALD (Planar) consistently provided the consistency for commercial devices, but at low deposition rates, and with high temperature processing. Therefore, by optimising RF sputtering and combining with laser processing, this research here will investigate whether a reliable and reproducible technique to produce high quality films can be realised, potentially with low temperature deposition and processing that could be applied to flexible substrates. Also, for the first time, the use of successive layer laser processing is investigated.

Chapter 3 Experimental Techniques

3.1 Introduction

This chapter describes the experimental systems and techniques used throughout the research project. This includes the deposition, processing and characterisation of thin films, the fabrication and characterisation of devices.

To enhance the efficiency of TFEL devices, it is first necessary to optimise each individual layer composing this structure. This work concentrates specifically on optimising the phosphor layer. Therefore phosphor thin films were first deposited on a semiconductor substrate to investigate the material and photoluminescence properties. Following optimisation, the fabrication of TFEL devices was undertaken using photolithographic techniques of NTU [58].The deposition technique chosen for this work was RF magnetron sputtering as the sputter technique is able to deposit compounds (such as ZnS:Mn and Y_2O_3) and is used extensively in silicon technologies [59] – hence is a viable technique. Also, sputtering is suitable for in line processes, because both the insulating layer and the phosphor layer can be grown by the same deposition method [60-62]. In the case of ZnS:Mn, however, the crystallinity of the deposited films is usually relatively poor. Post deposition annealing is generally employed to improve the overall film quality [63] . Both thermal annealing (in-situ) and laser annealing of ZnS:Mn layer were investigated for the optimisation studies presented here.

It is also important to mention that during the project, the entire experimental facility was decommisssioned and moved from NTU city campus to a new location on the

Clifton campus. This facilitated a complete re-commissioning by the author of the systems utilised in the investigation.

In this chapter, the device fabrication technique used for this work is detailed. This includes the process conditions for the phosphor, dielectrics and electrode depositions. The experimental arrangement for laser annealing of the phosphor is outlined. Both photoluminescence and electroluminescence measurements were the major methods used for the characterisation of each obtained device as a function of fabrication parameters in order to reach optimum conditions; therefore, both methods with design details are presented in depth. Surface roughness and X-ray diffraction examinations were also carried out.

3.2 Growth of thin films

The fabrication of an ACTFEL device involves sequential deposition of the individual layers onto the surface of a substrate. The common techniques used are sputtering, molecule beam epitaxy (MBE) and atomic layer deposition (ALD) (see Chapter 2). The thin films of insulator and phosphor were deposited here using the radio frequency (RF) magnetron sputtering technique. Thermal evaporation, which can produce good stoichiometry for elements and simple compounds (such as Al), was used for the deposition of the aluminum upper electrodes. For the majority of devices studied, an n-type single crystal silicon wafer was used as a substrate and as the base electrode. ITO was later chosen as an alternate but more common material as an upper-transparent electrode. Magnetron sputtering was also used as the standard deposition method for high-quality ITO films [64, 65].

3.2.1 RF magnetron sputtering

An intrinsic characteristic of the sputtering process is that the composition of the substrate film will be the same as the target material unless using reactive sputtering. This is the reason why complex materials, such as ZnS:Mn, are excellent candidates for sputtering deposition. The sputtered material deposits on a substrate that is placed facing the target.

Another unique characteristic of sputtering is control of the thickness. After a calibration run has been made, thickness control can be undertaken by deposition time control (see later Thickness monitor). Moreover, the lifetime of a sputtering target may be as long as hundreds of runs compared to 10 runs for evaporation.

Thereby, the films are produced by sputtering because this method of deposition gives high quality films and it can be controlled to give high purity, good adhesion strength, and good homogeneity.

The high vacuum chamber used in the present work for the RF magnetron deposition of Y_2O_3 and ZnS:Mn thin films is illustrated in Figures 3-1 and 3-2. A schematic diagram of the typical Radio-frequency (RF) sputtering system is depicted in Figure 3-3.

In order to preserve cleanliness of the films, the substrate (n-type silicon single crystal) is loaded from a clean room (class 100) via a pumped load lock, with a magnetically coupled loading arm used to position the substrate into the substrate holder without exposing the deposition chamber to air. The reason for this is to prevent the out gassing of water vapour from the chamber walls during deposition. Appropriate heating elements (heating tape) were also used to bake the chamber,

usually after opening it to the atmosphere when changing targets, or undertaking maintenance.

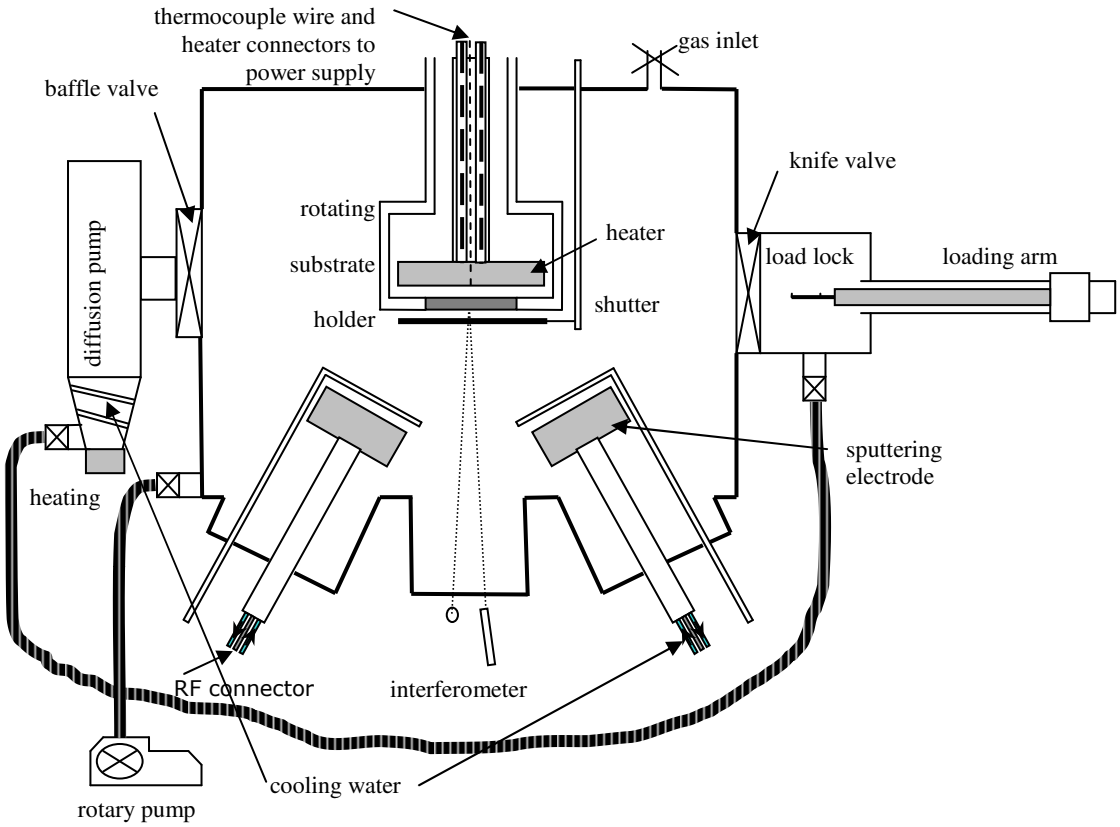

Figure 3-1: Cross section of the high vacuum deposition chamber used for RF magnetron deposition of thin films

Figure 3-2: Photograph of the high vacuum deposition chamber

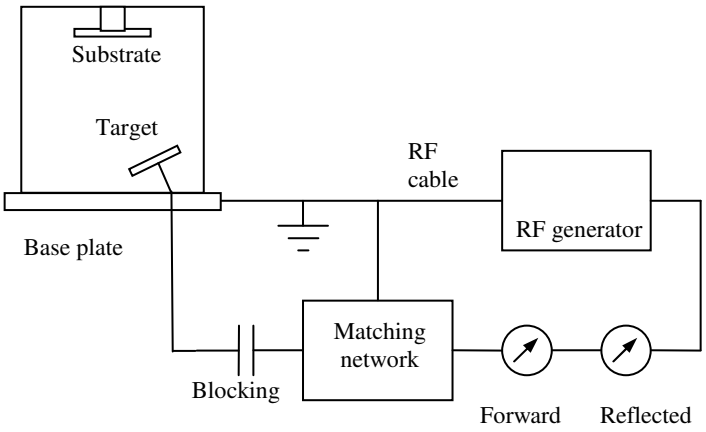

Figure 3-3: Schematic diagram of a radio-frequency magnetron sputtering system. The blocking capacitor is used to prevent shorting the target to ground through the matching network for sputtering conductors. The RF generator is designed to have an output impedance of 50 Ω to match the available transmission cable and must feed into a load impedance of 50 Ω.

The deposition chamber is initially pumped down to very low pressures of less than 10^{-6} mbar (1×10^{-4} Pa); this high vacuum is obtained using an oil diffusion pump backed up by a rotary pump. Prior to deposition, the substrate is prebaked at 550°C for typically one hour to remove any moisture from the surface of the wafer. Argon gas is injected into the chamber as the sputtering gas and the initial plasma is obtained by increasing the relative pressure of the chamber to 25 mTorr while an RF power electric field with a frequency of 13.56 MHz is applied to the magnetron target and set to 40 W. The two adjustments controls of the matching network are tuned to give zero reflected power. The pressure is then gradually reduced to the deposition value of 3 mTorr (0.4 Pa) using a baffle valve, while the power is

gradually increased. Subsequent steps of increasing the power level and retuning the matching network are needed to bring the power up to the desired operating level.

The argon (Ar) gas turns into a plasma made of positive Ar^+ ions and electrons. The target is an insulator but which is on top of the RF electrode and which accumulates a net negative charge, becoming the cathode. This then attracts the accelerated positive ions which eject or sputter off the surface atoms. These material particles are then deposited onto a rotating (~ 10 rpm) substrate (i.e. anode) for uniform deposition. A heater is situated behind it to control temperature during deposition.

3.2.2 Thermal calibration

The deposition temperature plays an important role in growth of thin films. For the Y_2O_3 deposition, the substrate temperature was maintained at 190°C, based on results of previous investigations demonstrating that this temperature gives the best dielectric properties [41, 66]. It has been also found for the ZnS:Mn deposition that the best deposition temperature is 190-200°C which produces a good crystalline ZnS film [41, 42] and good luminescence properties [40]. This temperature depends on the heater controller settings. For this work, the heater needed refurbishing and a new calibration following relocation of the facility. Thermal labels were placed on the wafer for temperature monitoring, these labels have five temperature ratings which turn black at the rated temperature. The results of this calibration verified the previous calibrations done on this heater (see Figure 3-4).

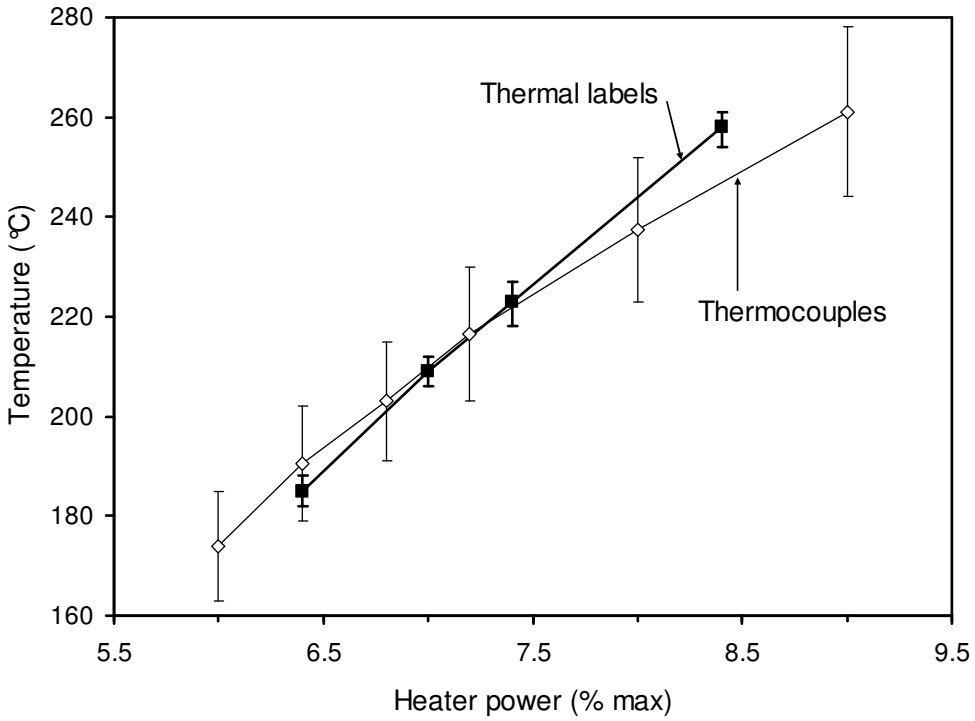

Figure 3-4: Heater calibration for deposition temperature (with previous thermocouples calibrations)

This method of using thermal dots for calibration has the advantage to use the heater in rotation (as with normal conditions of deposition), and is quick for verifying one temperature, but it revealed also that it was time consuming and does not allow temperature calibration above 260°C, and the post annealing for ZnS:Mn is required to be at 500°C. A previous direct calibration of the substrate temperature vs. heater controller settings was done using the average temperature given by two thermocouples connected to the centre (upper error bar limit) and edge (lower error bar limit) of the substrate, via vacuum feed-throughs. This represents a more accurate and a much quicker method with no need to unload and reload the wafer into the chamber. Nevertheless, these results confirmed that the heater was calibrated for the required temperature deposition of 190°C.

3.2.3 Sputtering targets

In this study, four types of target (all 3 inches diameter and 5mm thick discs) were mounted into four Kurt Lesker Torus electrodes:

- Zinc sulphide target ZnS (Testbourne Ltd Z1-9006-D), Purity 99.99%.
- Zinc sulphide doped with manganese target ZnS:Mn 1 wt% (Testbourne Ltd Z1-9017-M), Purity 99.95%.
- Zinc sulphide doped with manganese powder target 0.43 wt% which is a previously determined value [67] for a powder phosphor source prepared at NTU using a target press system.
- Yttrium oxide target Y_2O_3 (Testbourne Ltd Y2-9004-D1), Purity 99.99%.

Previous works used optimisation of powder phosphor material, but batch to batch reproducibility problems were experienced. Therefore there was a need to use alternative but more reliable sputtering techniques, i.e. co-sputtering from solid targets and also examination of reactive sputtering (with Plasma Quest Ltd).

The targets of ZnS and ZnS:Mn are used for co-sputtering.

Before the ZnS:Mn targets are placed in the sputtering system it was verified by photoluminescence test that the emission peak of the phosphor is at 585nm using a Nitrogen laser (337nm) excitation source. After cleaning the inside of the chamber, these four targets were mounted on the sputtering electrodes in the following arrangement:

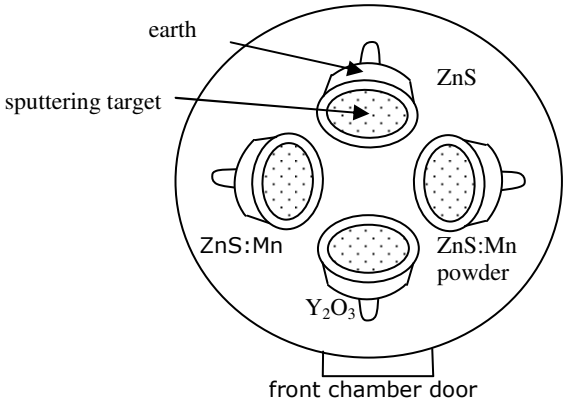

Figure 3-5: Plan view of the four sputtering electrodes inside the chamber

The ZnS:Mn Powder targets are made using a hydraulic press system represented on Figure 3-6.

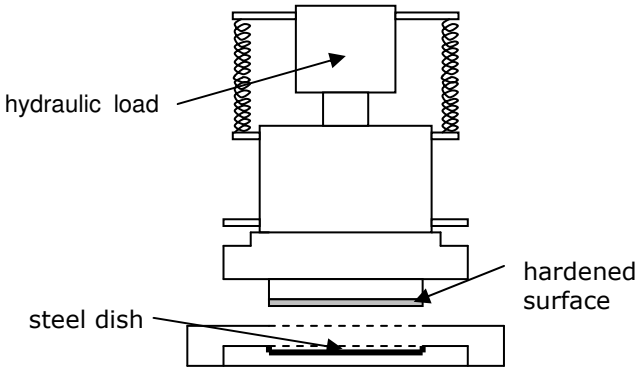

Figure 3-6: Cross section of the powder target press

The powder is placed into the steel dish and compressed initially by hand using a plastic ruler, this is repeated until the dish is completely full. The powder has to be evenly distributed and smoothed. A hydraulic pump is used to press the powder which is compressed to a pressure of 280 bar. The pressure is maintained for 8 minutes, with further pumping when necessary. After this time, the hydraulic press is dismantled and the powder target carefully removed.

Depositions from ZnS:Mn and Y_2O_3 targets were completed to test and optimise the system. Two main problems were faced. Firstly, the powder target sputtered through (rendering the target useless), this could be due to imperfections created from when the target was made with the press target. Secondly, the first depositions from solid targets created a film surface which was non uniform and subject to "crazing" (i.e. fine cracks on the surface), this was probably due to contamination of the top layer of the target; thereby a pre-sputtering process was needed for each new target for a minimum of 5 hours at high power (120-180 W).

3.2.4 Thickness monitior

The thickness of the deposited thin films is determined during growth using a simple in-situ interferometer system using a laser beam directed towards the deposited thin film (see sputter system in Figure 3-1). A part of the beam is reflected off the film surface depending on angle of incidence to the sample, refractive index of the material used and thickness of the film; the rest is transmitted to the substrate before it is reflected again from the substrate. The optical path difference and phase change upon reflection cause interference between the two beams which changes depending upon film thickness, and which can then be monitored using a photodiode and monitoring software (Picolog Data Acquisition). The measurement set up is shown in Figure 3-7.

Constructive interference of the two reflected beams occurs when the thickness of the film satisfies: $m\lambda = 2nd$, where λ is the wavelength of the incident laser light (625 nm), m is an integer, n is the refractive index of the film and d is the thickness of the film.

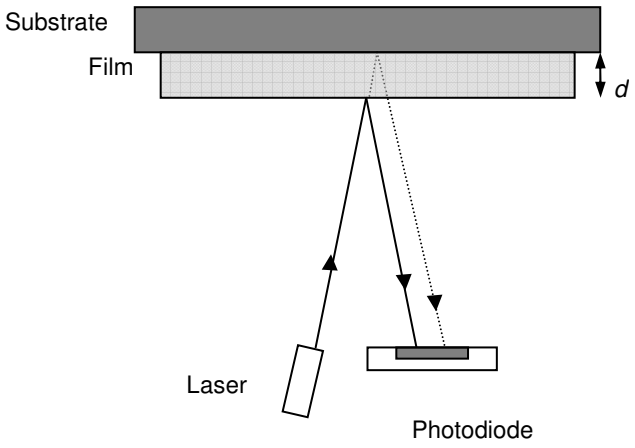

Figure 3-7: Thickness monitoring using a simple interferometer

The resultant intensity is recorded graphically against time and shows a series of cycles. The corresponding thickness for one cycle depends on the refractive index of the sputtered material. The two main materials deposited and monitored were zinc sulphide and yttrium oxide and their deposition characteristics are shown in Table 3-1.

Material (sphalerite structure)	*n* (at λ = 625 nm)	*d* (nm)	Number of cycles needed
ZnS	2.368 [68]	800	≈ 6.0
Y_2O_3	1.931 [68]	300	≈ 1.8

Table 3-1: Index of refraction, typical thickness and number of cycles of deposited zinc sulphide and yttrium oxide thin films

In order to check the thickness of these films an optical reflectance spectrometer F20 from Filmetrics was used in reflectance mode. Figure 3-8 shows an example of ZnS:Mn film thickness profile following deposition.

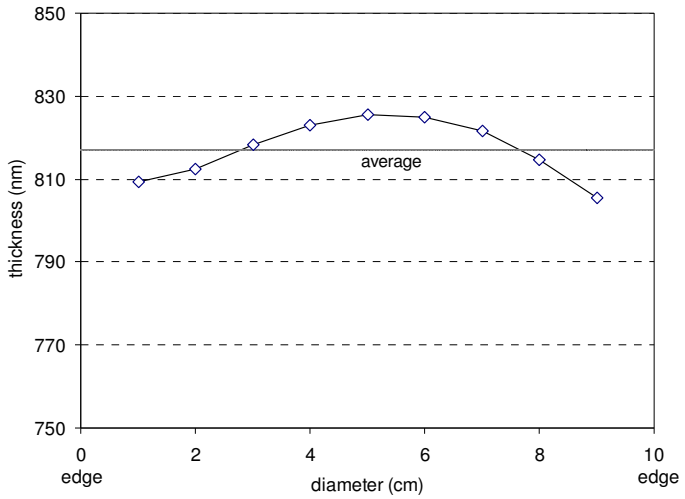

Figure 3-8: Typical thickness profile obtained for co-sputtered ZnS:Mn thin film on a 100 mm diameter silicon substrate

An average of ± 3% thickness variation across the wafer was measured for 100 mm diameter deposited thin films.

3.2.5 Deposition of EL devices electrodes

3.2.5.1 Al dots by evaporation

Unlike sputtering, evaporation is the result of energy delivered to a solid to raise its temperature to the point where atoms obtain enough energy to leave the surface of the solid [69].

For this project, aluminium (Al) electrodes were first deposited using the vacuum evaporator shown in Figures 3-9 and 3-10. The aluminium filament is placed in a tungsten basket which is heated by passing a current. The current is then raised until the aluminium starts to evaporate at a significant rate and condenses onto the wafer forming an Al film.

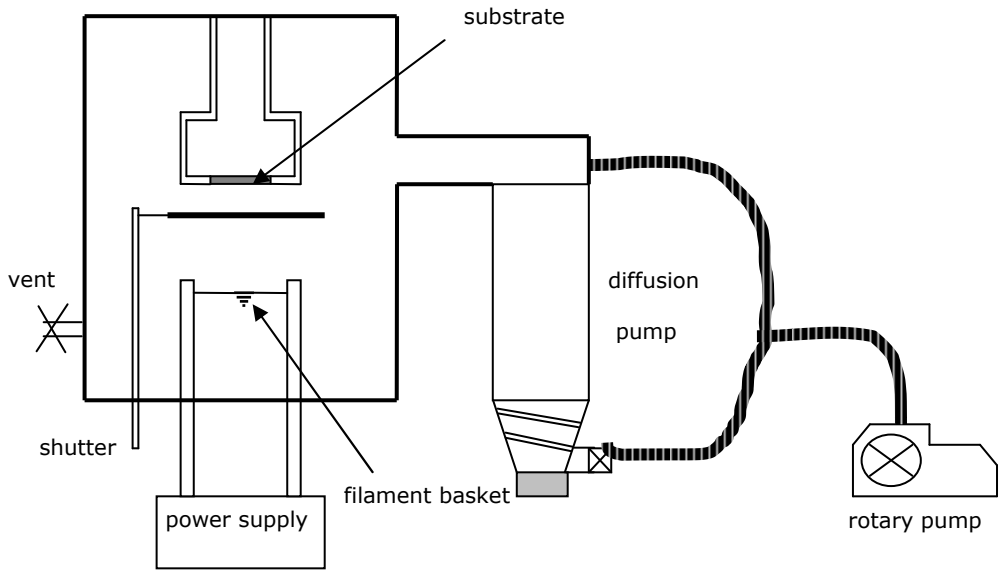

Figure 3-9: Cross section of the thermal evaporator system

Figure 3-10: Photograph of the thermal evaporator

By placing an evaporation mask in front of the substrate, the geometry of the evaporated film can be controlled. 1 mm diameter dots mask was used to deposit the Al top electrode of the EL test devices.

3.2.5.2 ITO dots by RF magnetron sputtering

An alternative, but more effective TFEL top electrode of ITO (Indium Tin Oxide), the display industry standard transparent conducting oxide, was later chosen as the preferred material because of its optical properties. Control of oxygen partial pressure during deposition is important for the deposition of this material. Another RF magnetron system similar to the one represented in Figure 3-1 was used to deposit thin films of ITO through a 1 mm diameter dot shadow mask. The ITO solid target with the following composition was used for the sputtered films:

- 90% Indium Oxide (In_2O_3)
- 10% Tin Oxide (SnO_2)
- Purity 99.99% (Testbourne SuperVac)

The depositions were made under a 2 mTorr total pressure of Argon with 0.2 % Oxygen concentration at a substrate temperature of 180°C. The electrode power was set to 90 W with a distance target – substrate of 10 cm. The ITO films resistivity was $(1.8 \pm 0.1)\times10^{-4}$ Ω.cm in average.

3.3 Laser annealing

Laser annealing has been demonstrated by the NTU Display group to be beneficial to the phosphor material for TFEL devices over thermal conventional annealing method in terms of photoluminescence [2, 4, 5, 42] and electroluminescence [3, 51, 70].

The laser utilised for this investigation was a Lambda Physik LPX 305i excimer laser charged with Krypton Fluoride (KrF), emitting pulses of 20 ns at 248 nm (5.13 eV photon energy).

3.3.1 Beam alignment and homogenisation

The beam line from the KrF laser was designed to allow laser processing with high fluences (above 1 J/cm^2) and with a homogenous laser beam profile as shown in Figures 3-11 and 3-12.

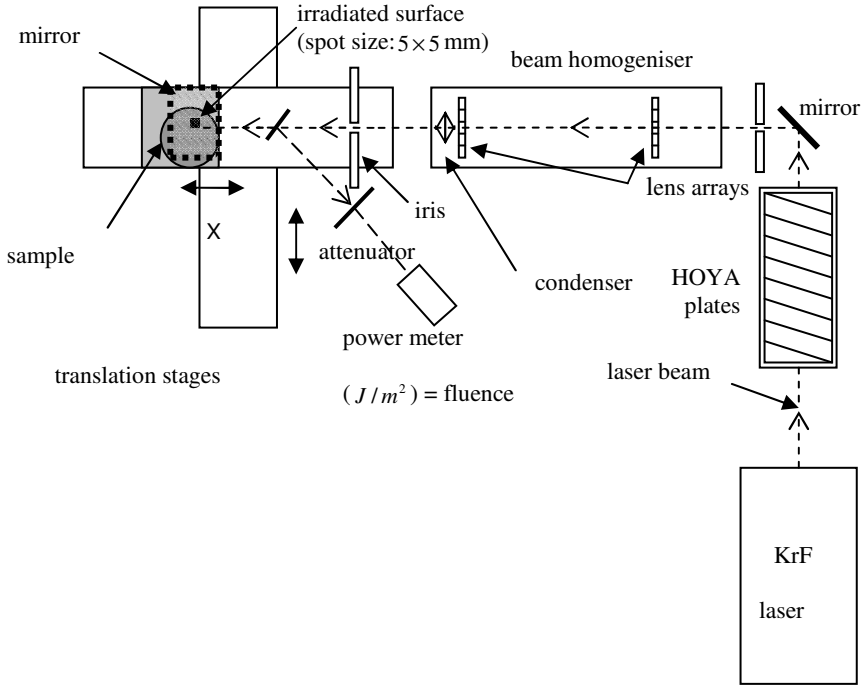

Figure 3-11: Plan view of experimental set up for KrF laser beam with translation stages

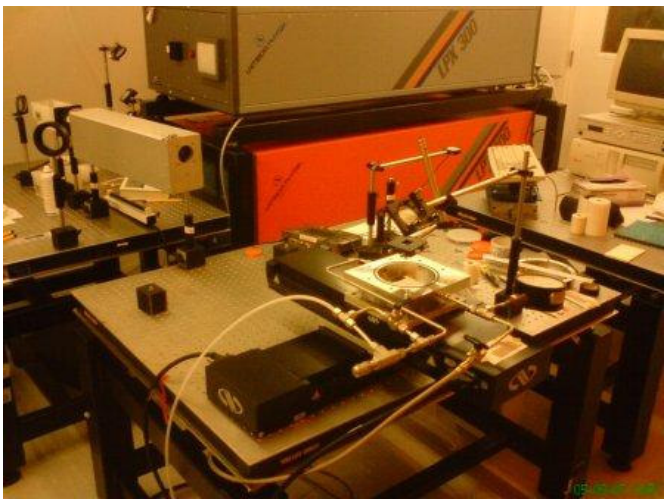

Figure 3-12: Photograph of the KrF laser (at the back), homogeniser (on the left), and pressure cell mounted on translation stages (in front)

An Excitech homogeniser EX-HS-700D is used here to convert the non-uniform rectangular beam into the top hat profile required for a uniform density profile. On-line energy measurements of the 20 ns pulsed KrF (248 nm) laser beam is achieved using quartz plates or an iris to attenuate the beam. Translation stages were installed by the author and programmed (controlled from a PC via RS232 interface) to allow accurate automation of laser processing – step and repeat sample positioning.

The beam line from the KrF laser was adjusted for homogeneity and focal length lens was used in the homogeniser to obtain an irradiated square surface of 5 by 5 mm which is necessary to attain a fluence superior to 1 J/cm^2.

The sample was also situated in a pressure cell (with UV grade window) mounted on two automated translation stages. The use of the pressure cell is to minimise ablation [54, 56], which results in material loss.

3.3.2 Laser processing conditions

The energy delivered by the laser beam was measured at the sample position, and at the same time, at another position where a part (10%) of the beam was deflected to be monitored. This energy was converted into fluence:

$f = E / A$ where f is expressed in mJ/cm^2 and A is the irradiated area (0.25 or 0.1 cm^2).

The fluence could be calibrated as a function of the laser voltage, plotted on Figure 3-13.

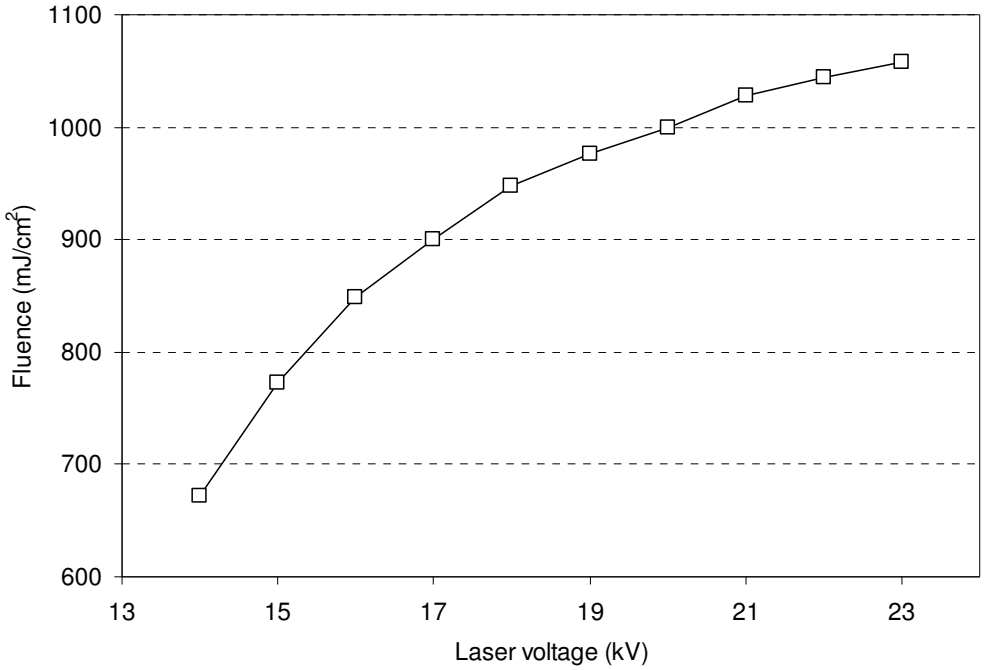

Figure 3-13: Calibration curve of fluence applied at the surface of the sample vs KrF laser voltage

14 kV being the lowest voltage, if lower fluences were needed, HOYA fused silica plates could be used to attenuate the energy of the laser beam (each reducing it by 8%), alternatively an iris diameter would be used to reduce the global beam energy delivered. The pulse frequency could be varied from 1 to 25 Hz, 1 Hz was chosen because of the low numbers of pulses needed (1, 2 or 3 pulses). If non atmospheric pressure was needed, argon gas was injected into the pressure cell to achieve a 150 psi pressure (~10 bars).

The laser setup shown in Figure 3-10 was later improved and its dimensions were considerably reduced. Moreover, it provided a fixed distance between the sample and the exit of the homogeniser by using an appropriate set of lenses, and also proved to be a better measurement control.

The required fluence needs to be adjusted using the following calibration curve in Figure 3-14.

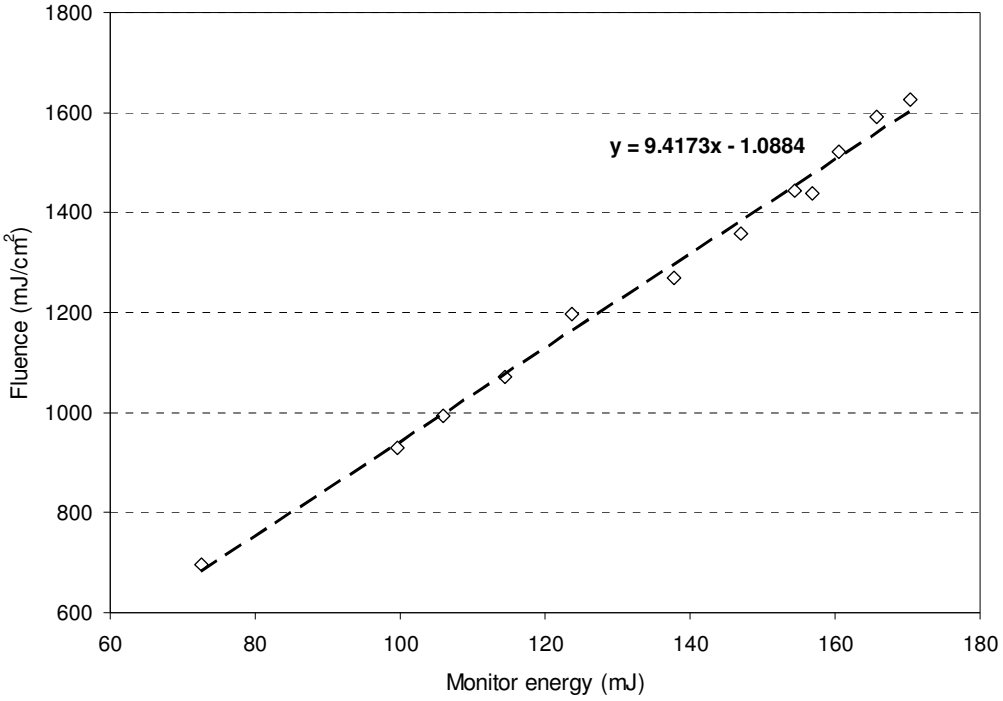

Figure 3-14: Calibration curve of fluence applied at the surface of the sample vs monitor energy

3.4 Electroluminescent device fabrication

3.4.1 TFEL fabrication process

In this project, simple TFEL devices were produced for electrical and optical characterisations. The major process steps used for this fabrication are explained below and illustrated on Figure 3-15.

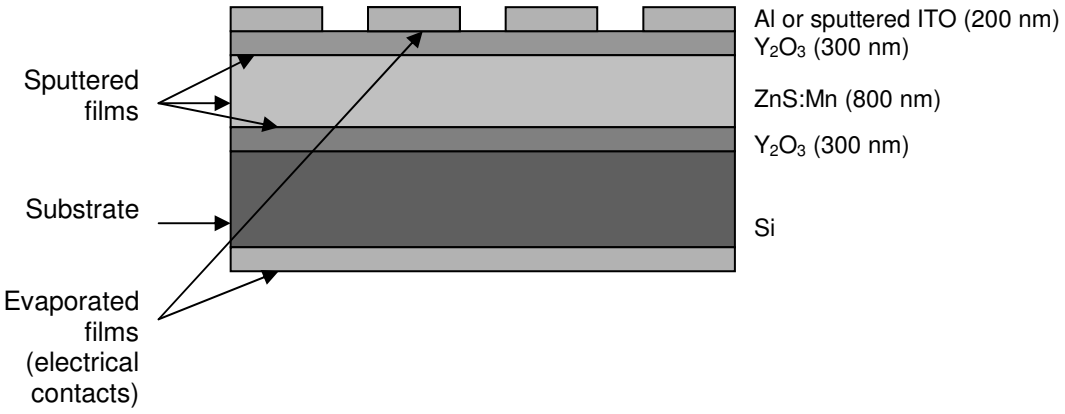

Figure 3-15: Main steps for production of TFEL devices

The growth deposition parameters were set to about 10^{-6} mbar base pressure. The Si substrate used for the devices - n-type (100) 100 mm diameter silicon wafer with thin layer of SiO_2 at the top) was prebaked for a duration of 1 hour at 550°C.

3.4.1.1 Deposition of phosphor

8000 Å of RF magnetron co-sputtered ZnS:Mn (ZnS and ZnS:Mn targets) thin films were deposited at a rate of 30 to 50 Å/min (depending on magnetron electrode powers), with a substrate temperature maintained at 190°C. Thin films made from powder pressed targets were also deposited with the same parameters but at a higher rate of 100 Å/min which is obtained at 80W (higher power was deteriorating the target – "sputtering through"). Different laser annealing parameters can be applied on the top of the ZnS:Mn surface (see the next section of this chapter and the Results chapter). This can be followed by thermal annealing at 500°C for 1 hour.

3.4.1.2 Deposition of insulators

3000 Å of RF magnetron sputtered Y_2O_3 thin films were deposited at a rate of 8 Å/min at 120 W with a substrate temperature maintained at 190°C.

3.4.1.3 Electrodes fabrication

About 2000 Å of evaporated Al was deposited as the top electrode through a contact mask with circular openings or to be patterned by photolithography. Aluminium is also deposited in the same way (but not using mask) on the back of the Si wafer and heated during the evaporation to improve the contact. For some devices, an alternative top contact was formed by depositing 2000 Å of ITO using RF magnetron sputtering at a rate of ~ 60 Å/min at 180°C in $ArO_2^{5\%}$.

3.4.2 Patterning

The most common technique used for transferring patterns is photolithography. This technique uses ultraviolet light to transfer a geometric pattern from a photomask to a light-sensitive layer (photoresist) on the substrate. A series of chemical (or physical) treatments then transfers the exposure pattern into the material underneath the photoresist. It is important to place the wafer in a clean room which is illuminated by yellow light since photoresists are not sensitive to wavelengths greater than 0.5 μm [71]. The process of EL device patterning used for this study is described below and illustrated on Figure 3-16, and an example for EL device patterned with aluminum is illustrated in Figure 3-17.

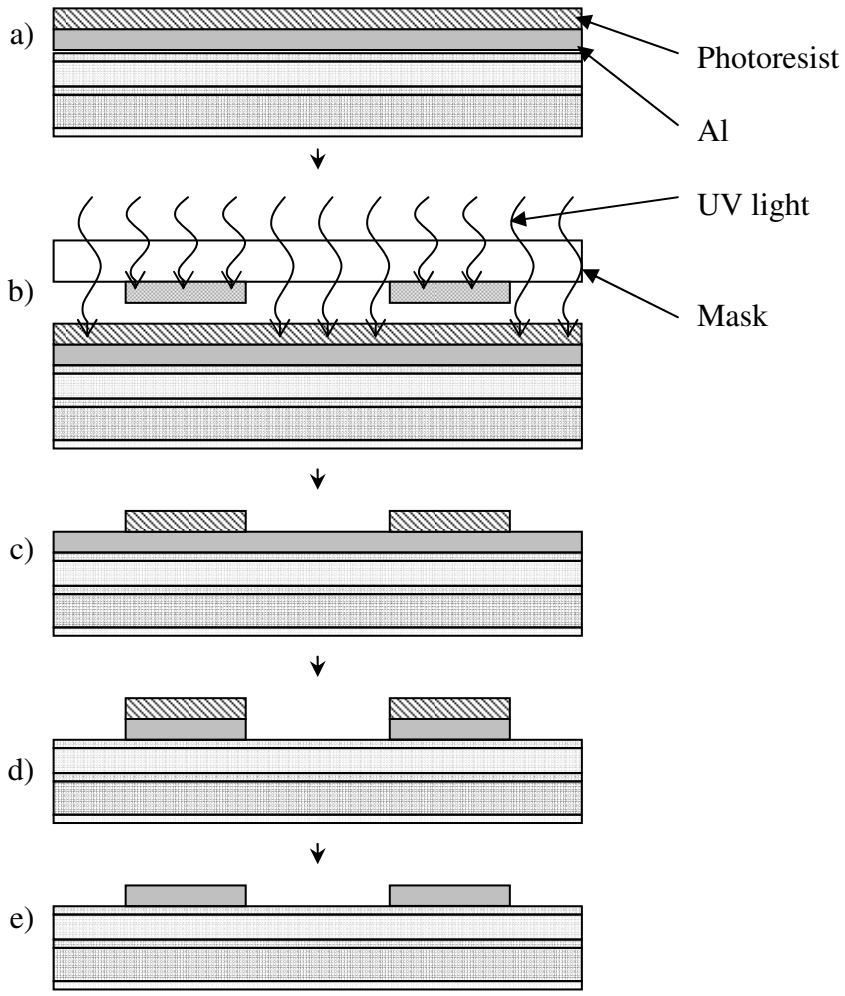

Figure 3-16: Process sequence for the positive photolithography applied on Al film: a) spin-coating with photoresist; b) mask placed in "soft contact" and exposure occurs; c) photoresist developed; d) Al etch; e) Photoresist removed

a) The EL sample with Al on top is spinned-coated using a U.V. light sensitive photoresist coating (S813). The wafer is held on a vacuum spindle, and 2 to 3 cm^3 of the liquid photoresist is applied to the centre of the wafer. The wafer is then rapidly accelerated to a constant speed (spinned at 500 rpm for 5s to spread the photoresist and then at 4000 rpm for 30 s to coat evenly the whole wafer). The wafer is then "soft baked" (105^oC for 75 s) to remove the solvent from the photoresist film and to increase resist adhesion to the wafer.

b) The quartz mask containing the pattern is brought into "soft contact" (or proximity) with the wafer with Karl-Zeiss mask aligner. The photoresist is then exposed to an exposure time of 1.7s.

c) A positive photoresist is used and the exposed resist is dissolved in the developer (Microdeposit Developer concentrate diluted at 50% with deionised water). A post baking (105°C for 10 min) is then used to increase the adhesion of the resist of the substrate.

d) An aluminium etchant (phosphoric acid) is used which will remove Al but will not attack the photoresist or the underlying Y_2O_3.

e) The photoresist is finally removed with acetone followed by isopropanol and nitrogen to dry the sample.

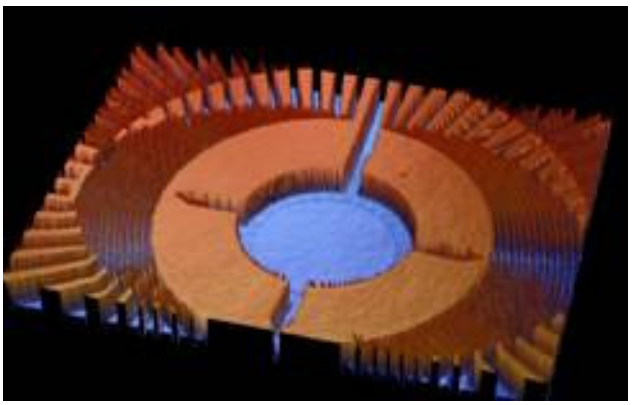

Figure 3-17: Optical profilometer image of an Al pattern on EL device

3.5 Characterisation systems

Characterising can be defined as determining some characteristic or some properties of a material in a defined and reproducible way. Physical, optical and morphological properties of the analysed samples were determined in this investigation.

3.5.1 Photoluminescence and luminescent decay

Photoluminescence (PL) is a non destructive technique for the detection of certain impurities in a host material [72]. To produce photoluminescence, the photons must have enough energy to excite the phosphor material. This occurs if the energy produced by the exciting source is superior to the band gap of the material ($h\nu > E_g$). The phosphor material used is ZnS and its band gap is 3.6 eV [73]. To convert energy to wavelength, one simply can use the equation:

$E(eV) = \frac{hc}{\lambda}$ where h is the Planck constant ($h = 4.136 \times 10^{-15}$ eV s) and c is speed of light in a vacuum ($c = 3 \times 10^8$ m/s), therefore $\lambda < 345$ nm. A UV nitrogen laser with $\lambda = 337$ nm is a potential candidate as an exciting source for the ZnS phosphor. This laser was subsequently used for the PL measurements of the ZnS:Mn used in this investigation.

The PL was obtained by exciting the surface of the films with the nitrogen laser. The light emitted was then collected by an optical fibre and measured with a spectrometer as shown in Figure 3-18; this required an arrangement which would allow measurements with reproducible results. The system consisting of the spectrometer and the optical fibre was calibrated using a calibrated tungsten halogen light source with known absolute intensity values at wavelength from 300-1050 nm. The integration time for collection was varied depending upon the PL intensity of the luminescent output; the intensity of the profiles was later normalised to negate this effect. Due to UV light scattering from the sample, a visible cut-on filter was used to allow only wavelengths above 385 nm to be collected by the fibre [51]. In addition,

the reflected laser power from the sample was monitored in an attempt to evaluate the relative efficiency of the films.

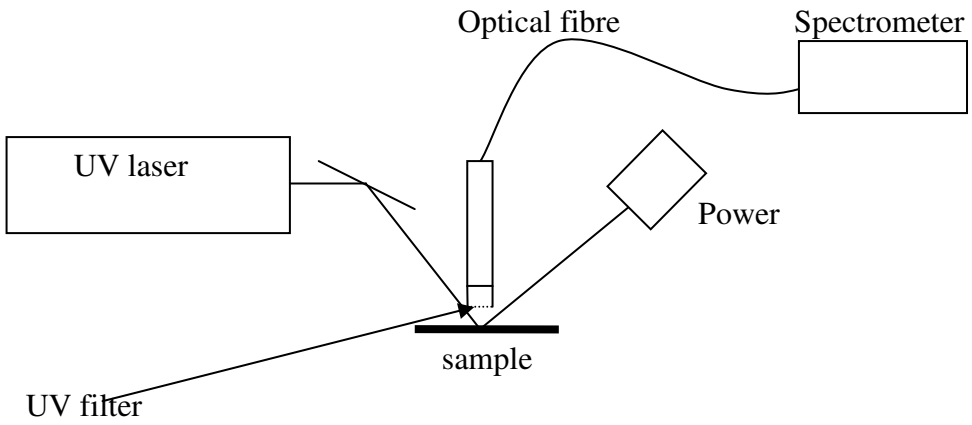

Figure 3-18: Schematic of PL set up

Using the pulsed laser irradiation from the N_2 laser to excite the phosphor, the transient photoluminescence emission from the sample was collected through a UV filter and a monochromator, and measured via an Electrons Tube 9558QB photomultiplier connected to a Gould DSO 4072 digital storage oscilloscope as illustrated on Figure 3-19. The decay constant was measured by fitting a single exponential decay over the specific measurement period to avoid laser interference effects.

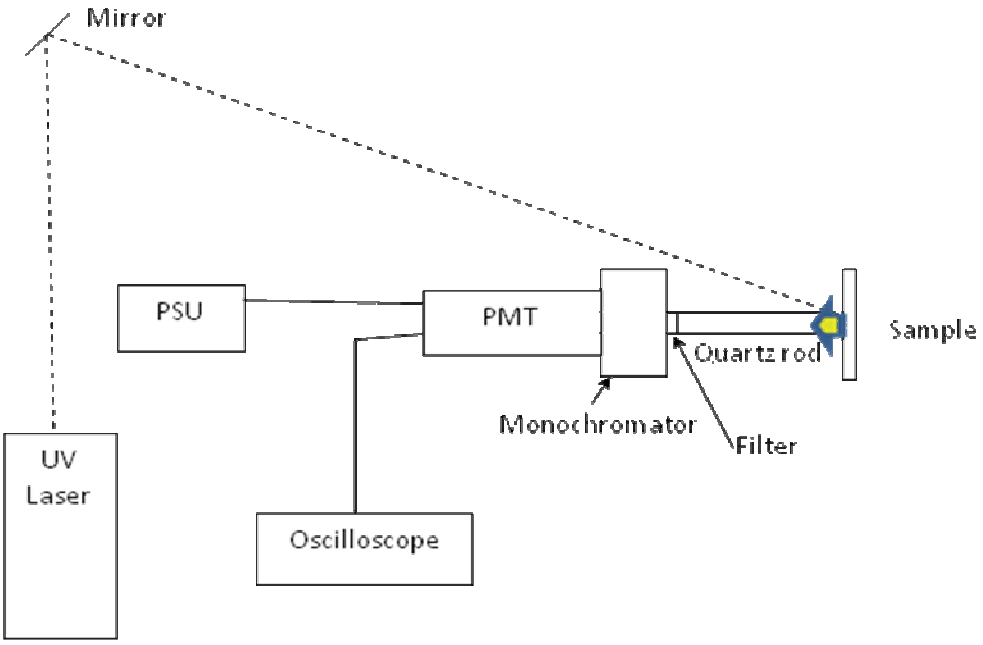

Figure 3-19: Schematic of the decay set up

A value of decay time constant τ was determined by fitting the transient luminescent data to a single exponential decay $I = I_0 e^{\frac{-t}{\tau}}$ where I_0 is the photoluminescence intensity at the laser irradiation pulse cut off time as shown in Figure 3-20 and 3-21.

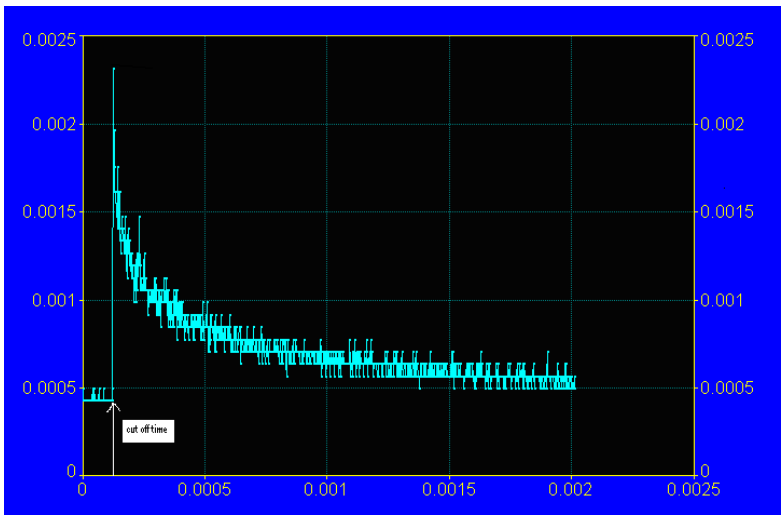

Figure 3-20: Example of decay signal from a Zns:Mn thin film

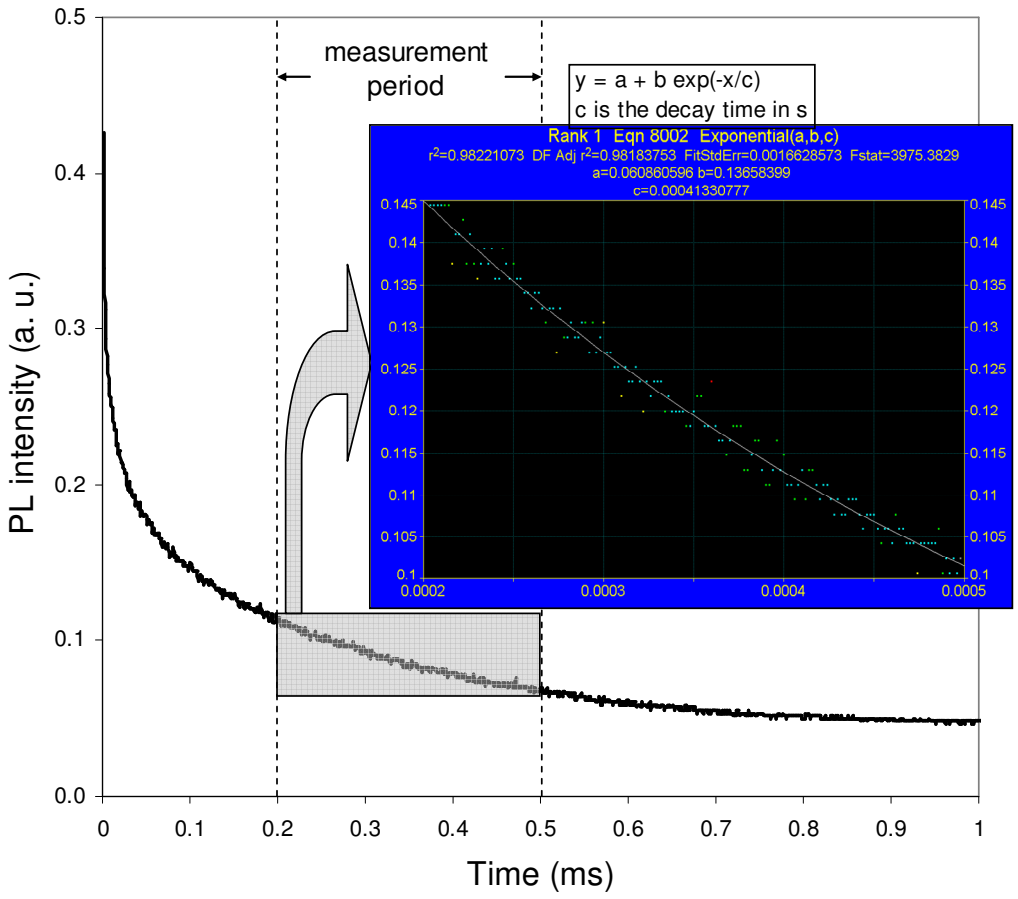

Figure 3-21: Example of decay time calculation using TableCurve 2D v5.01

3.5.2 X-ray diffraction

X-ray Diffraction (XRD) is a noncontact and nondestructive technique used to identify the crystalline phases present in materials and to measure the structural properties of these phases. When x-rays are scattered by the periodic arrangement of planes of atoms in a crystal structure, the angle of diffraction from a crystal (the angles at which the scattered rays interfere constructively) is given by Bragg's law [74]:

$$\lambda = d_{hkl} \sin\theta_{hkl}$$

Where λ is the wavelength of x-rays, d_{hkl} is the distance between two adjacent planes of miller indices (*hkl*), and θ_{hkl} is the angle between the incident beam and the atomic plane.

In a single crystal, for every (*hkl*) plane, there is a unique angle of orientation of the sample relative to the incident x-ray beam for which the Bragg's condition is satisfied. Epitaxial thin films behave similar to single crystals, on the other hand non-epitaxial thin films, in general, consist of many grains or crystallites that are oriented in different directions. The crystallites could be completely randomly oriented where the diffracted x-rays create a "powder" diffraction pattern. Or the crystallite could have a fibre texture where all the crystallites in the film have the same atomic planes parallel to the substrate surface, but are otherwise randomly distributed. Thin films usually fall in between these two classes.

The mechanical assembly that makes up the sample holder, detector arm and associated gearing is referred to as goniometer. For polycrystalline films used for this study, the Bragg-Brentano goniometer is used and represented in Figure 3-20. In this setup, the x-ray source is kept fixed, and after collimation by slits is focused on to the sample. The diffracted x-rays from the sample are focused on the detector using the receiving slits. The diffraction system was a Phillips, PANalytical X'Pert PRO with a monochromated Cu-$K_{\alpha 1}$ radiation source, λ = 1.54056 Å. The bracket flat stage was used for attaching thin film materials. All parameters for both stages such as scanning angle and step size are programmable via the software X-Pert Data Collector.

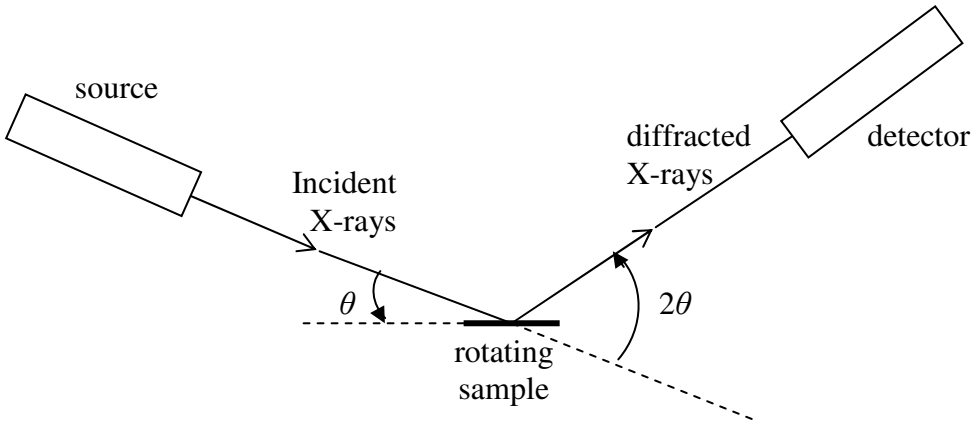

Figure 3-22: Schematic of XRD goniometer

The measured XRD patterns can be displayed individually or combined using the X'Pert Data Viewer. The phases present in the thin films can be identified by comparing the angles of the peaks of the measured angles in the diffraction pattern with known standards.

3.5.3 Surface morphology

The surface morphology of the samples made were analysed using an optical profilometer (Wyko NT110) as illustrated in Figure 3-21. Before any set of measurement this device needs to be calibrated and each measurement must be repeatable, following a specific method.

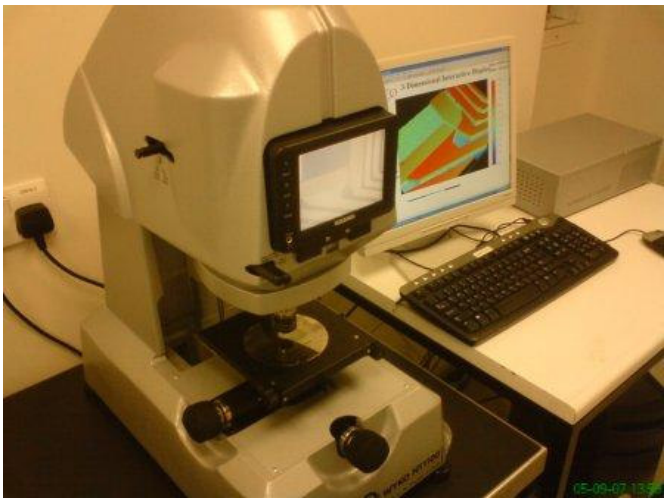

Figure 3-23: Photograph of the optical profilometer used for the surface morphology analysis

This profilometer (Wyko Surface Profiler) is a non-contact profilometer, which uses two technologies: Phase-Shifting Interferometry (PSI), which allows measurements of smooth surfaces and small steps; and Vertical Scanning Interferometry, which allows measurements of rough surfaces and steps up to several millimetres high. The samples used are expected to have a very smooth surface, hence the PSI mode is used to analyse surface morphology. In PSI mode, a white-light beam is filtered and passed through an interferometer objective to the test surface. The interferometer beamsplitter reflects half of the incident beam to the interference surface within the interferometer. The beams reflected from the test surface and the reference surface recombine to form interference fringes, which can be seen when the surface is in focus. Then the system converts the intensity of these fringes to wavefront (phase) data and the relative surface height can be calculated [75].

When using the PSI function, a calibration is undertaken by focusing two or three fringes on the benchmark and setting the objective and FOV (field of view) used on the profiler. Afterwards, the focus is adjusted on the sample until the fringes can be

seen [76], the highest contrast fringe corresponding to the position of best focus, for that the tilt (X) and the tip (Y) are used with the focus. It was found that the best way to have good results was to use the high PSI with an objective of 10X and a FOV of 1.0. The repeatability must be respected; thereby the conditions of measurement are always the same (intensity, contrast, position and cleanness of the sample).

3.5.4 Electroluminescence

In order to test the effect of manganese concentration and laser annealing on electroluminescence performance, TFEL samples were first tested 'manually' using a simple arrangement to measure the luminance emitted at different applied AC voltages from the excited ACTFEL devices. However this method did not show consistent results and was time consuming. The setup was therefore improved by the author to become fully automatised; Figure 3-24 illustrates this setup.

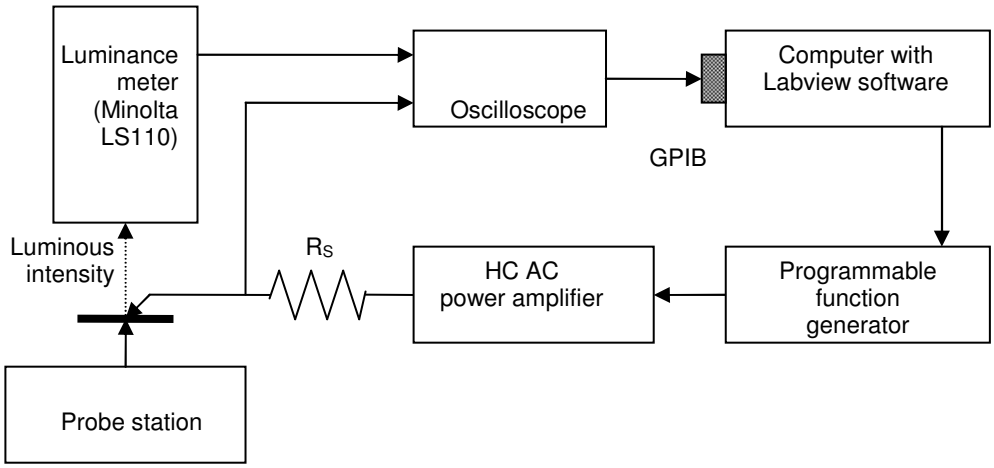

Figure 3-24: Schematic diagram of computerised setup for ACTFEL device characterisation

The probe station is capable to move accurately a probe to test small test devices (1.5 by 1.7 mm or 1 mm diameter dot). To align the probe with the aluminium pixel electrode or ITO dot, a microscope is used. The device can be then probed accurately. The output of the power amplifier drives the ACTFEL device via a protection resistor (R_S = 100 kΩ). The microscope is then moved away and replaced with a Minolta LS-110 luminance meter which is positioned at 20 cm vertically away from the wafer to measure the electroluminescent light from a small circular (1.1 mm diameter) area of the surface-emitting region of the device. This luminance meter has an internal lens system of a 1/3° angle acceptance cone so only light emitted within this solid angle is detected. A Tektronix TDS220 oscilloscope is used to monitor this luminance from the ACTFEL device. The computer communicates with the oscilloscope and the function generator via a General Purpose Interface Bus (GPIB) port. A program was accomplished using National Instruments LabVIEW Version 5.0 software, a graphical programming to record the luminance obtained from the devices. The following parameters were also controlled using LabView programming on the same program:

- Waveform (sinusoidal, triangle or square)
- Drive frequency (1 to 5 kHz typically)
- Drive voltage (below threshold up to breakdown voltages)
- Drive voltage step (voltage increment in between each measurements)
- Step duration

Aluminium dots were first used as the top electrode. However a definite degradation was observed when the device would undergo identical successive series of ramped up voltages most probably due to the deterioration of the top aluminium electrode

(during tests, sparks can be observed). This degradation can be increased by having longer test durations which is associated with the lifetime of the device.

The aluminium top electrode was then replaced with ITO dots for an easier process of fabrication and lower sample failure and degradation.

3.6 Conclusion

This chapter has provided a general overview of the equipment and the methods used in this project for the fabrication of thin film phosphors and full TFEL devices. The specific setup for the treatment of thin film phosphors by KrF laser was also described. Finally the equipment used for the analysis of the samples was also overviewed. As a result, a study of the thin film phosphor of ZnS:Mn and TFEL devices has been performed in the next chapter.

Chapter 4 Growth optimisation of co-sputtered ZnS:Mn thin films for EL devices

4.1 Introduction

One of the negative issues highlighted during the work in the 1990s on electroluminescent displays was the difficulty in controlling the luminescent quality of phosphor films deposited by volume production techniques, such as sputtering. More recently, rare-earth doped ACTFEL devices using co-sputtering have been reported [77-79]. The part of the research programme presented here investigates co-sputtering of the transition metal ion doped ZnS:Mn thin film phosphor. The work specifically examines the importance of controlling the luminescent quality and identifies a mechanism to ensure that monitoring of phosphor quality could be performed in-situ, utilising the inherent luminescent properties of the phosphor thin films.

One of the primary factors which governs the efficiency of a ZnS:Mn active layer is the Mn dopant concentration. The optimum concentration reported in the literature varies with deposition technique and methods used to characterise, but is typically around 0.5 wt.% [80-82]. However some reports have indicated `optimums' as high as 3 Mn mol% (1.5 wt.%) [83] or as low as 0.2 wt.% [84]. Part of the issue related to this inconsistency is the nature of the materials characterisation used – which is often not detailed, and the fact that from the work undertaken by the NTU Display Research Group, a variation was observed in optimum performance with the age of the sputtering source used, the target supplier, and the annealing temperatures

utilised. With volume production in particular, it is the batch to batch deposition variation which is a major concern.

For this study, therefore, the luminescent behaviour of the films was examined as a function of deposition optimisation, in order to demonstrate the feasibility of co-sputtering as a deposition technique – combined with luminescent decay time and monitoring of the red/yellow emissions that would facilitate the in-situ characterisation of Mn concentration variations and hence could provide a mechanism for positive process control.

4.2 Thin film preparation

Thin films of ZnS:Mn (800 nm) were co-sputtered via the simultaneous sputtering of ZnS and ZnS:Mn (1wt%) solid targets onto a rotating 100 mm diameter (100) n-type Si wafer substrate using a custom built Kurt Lesker Torus four-electrode magnetron system represented in Figure 3-1. The substrate temperature was maintained at 190°C (± 10 °C) during deposition in 0.40 Pa of Ar. The vacuum deposition chamber had a base pressure of 1 x 10^{-4} Pa and the deposition was followed by an in-situ annealing of 500°C for 1 hour in vacuum. Mn concentration in the phosphor films was varied by adjusting the RF power applied to each of the two solid sputtering targets ZnS (SuperVac®, Purity 99.99%) and ZnS:Mn (SuperVac®, 99–1wt.%, Purity 99.95%), both produced by Testbourne Ltd via their proprietry hot pressing technique. Comparative films were also made from sputtering from a single pressed powder ZnS:Mn target (Phosphor Technology Ltd – 0.43 wt.% Mn prepared using a hydraulic target press system). Each target had a 76.2 mm diameter and a 4.4 mm

thickness. An average of ±3% thickness variation across the resultant thin films was measured using a Dektak 6M stylus profilometer.

4.3 Photoluminescence optimisation

4.3.1 Experimental and analysis conditions

Time integrated photoluminescence spectra were obtained by exciting the surface of the ZnS:Mn thin film phosphor with the 1mm diameter beam of a N_2 laser (337 nm - photon energy = 3.68 eV, i.e. just above the band gap of ZnS). The luminescent PL emission was collected via an optical fibre and the spectra characterised with an Ocean Optics S2000 spectrometer (see Figure 3-17). The absolute maximum intensity of each spectrum, ranging from 582 to 586 nm, was retrieved for the different Mn concentrations. In Figure 4-1, these spectra are plotted for various nominal concentrations as determined by power ratio.

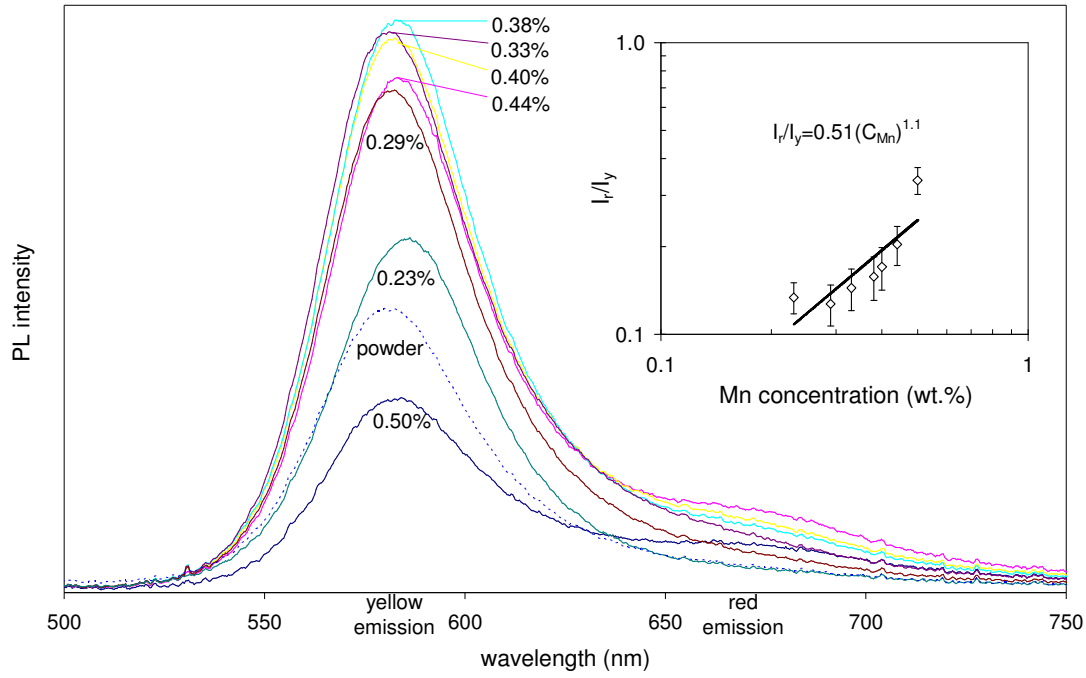

Figure 4-1: Photoluminescence spectra for different nominal manganese concentrations. In the inset, the variation of relative photoluminescent intensity at 670 nm to its peak vs. nominal Mn concentration.

The main photoluminescent peak for a ZnS:Mn thin film is the yellow 585 nm emission which occurs at about 2.1 eV. However, the inset figure demonstrates that these photoluminescent spectra exhibit also a small 'knee' for concentrations higher than 0.29 wt.% at around 670 nm. This additional red emission occurs at about 1.85 eV and becomes more pronounced at higher Mn concentration. The intensity ratio $\frac{I_r}{I_y}$ (I_r and I_y are respectively the intensities of yellow and red emissions) increases with increasing Mn concentration. For concentrations ranging from 0.28 to 0.44% wt.% Mn, these results follow the relationship: $\frac{I_r}{I_y} \propto (C_{Mn})^{1.1}$ within experimental errors, compared to a 1.4 power reported by Goede and Dang Dinh obtained from (Zn,Mn)S mixed crystals [85] and is almost equivalent to a linear $\frac{I_r}{I_y} \propto C_{Mn}$. However, for the two extreme concentrations – 0.23 and 0.5 wt.% Mn – the results are slightly out of this trend.

4.3.2 Results

It is important to mention that all the films examined were similar in terms of thickness (±5%), adhesion and visual appearance. In addition, for these films the variation was in doping, and no change in XRD spectra was observed between samples.

The peak photoluminescent intensity (at 585 nm) as a function of the Mn concentration is shown in Figure 4-2. The target power was kept fixed at 50 W for the ZnS electrode and varied from 15 to 50 W for the ZnS:Mn electrode, while the single pressed target was sputtered at a power of 80 W.

The photoluminescent optimum was obtained at a 0.38 ratio of the rf power supplied to the two targets (power ratio defined as: $P = \frac{P_{doped}}{P_{doped} + P_{undoped}}$, $P_{undoped}$ was kept constant while P_{doped} was varied), which is closely related to the nominal final Mn concentration in the film (i.e. 0.38 wt.% Mn). However, for this study, it was the nominal Mn concentration that was important, since the use of luminescence decay or red/yellow emissions ratio can then be implemented for `optimum' dopant monitoring in the actual films, rather than relying on subsequent indirect and destructive materials characterisations.

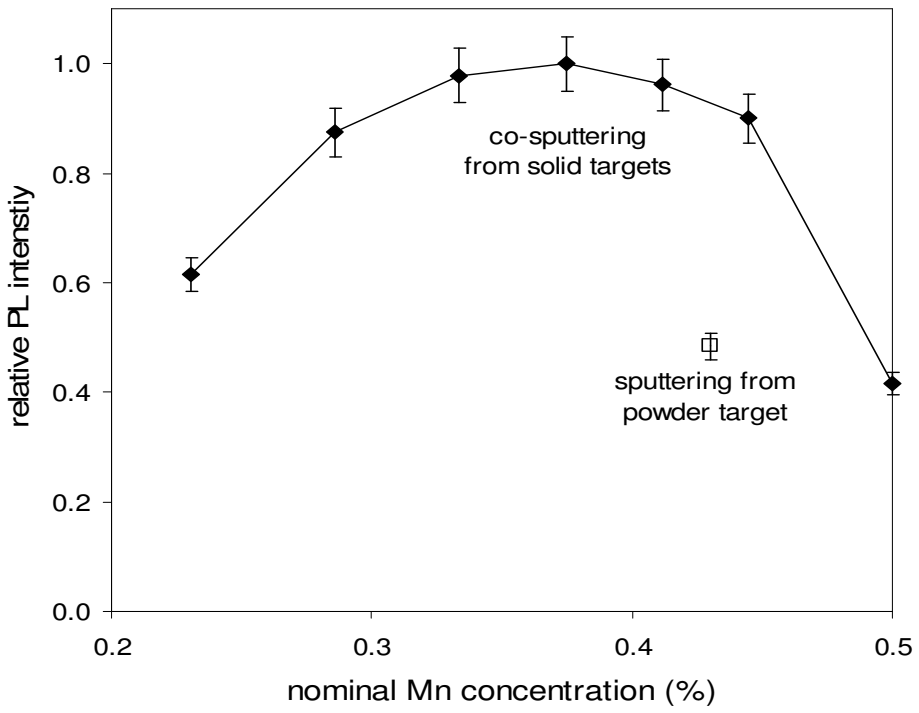

Figure 4-2: Integrated time photoluminescence intensity as a function of nominal Mn concentration (represented by co-sputtering power ratio applied) for 800 nm thick films of ZnS:Mn on Si at room temperature, with excitation from an N2 laser at 337nm

4.4 Optimum deposition conditions using decay

4.4.1 Experimental and analysis conditions

Using the pulsed laser irradiation from the N_2 laser to excite the phosphor, the transient photoluminescence emission from the sample was collected through a UV filter and a monochromator, and measured via an Electrons Tube 9558QB photomultiplier connected to a Gould DSO 4072 digital storage oscilloscope. A value of decay time constant τ was determined by fitting the transient luminescent data to a single exponential decay $I = I_0 e^{\frac{-t}{\tau}}$ where I_0 is the photoluminescence intensity at the laser irradiation pulse cut off time.

4.4.2 Results

By applying N_2 laser excitation pulses of 4 ns width and a repetition rate of 20 Hz, the photoluminescent emission was recorded and noise reduction was performed by digitally averaging the response over 256 cycles. The photoluminescent decay curves from 6 different concentrations are illustrated in Figure 4-3(a). The photoluminescence rises sharply with the application of the excitation pulse and then decays exponentially.

For this work, as illustrated in Figure 4-3(b), the double exponential decay of ZnS:Mn can be approximated to be composed of a first quick single exponential decay (directly after the laser pulse) within the first 0.05 to 0.15 ms, followed by a slower single exponential decay within the period 0.15 ms to 1 ms. For the purpose of this Mn concentration comparison, the decay constant was calculated using a single exponential fit to the luminescent decay during a fixed time domain of 0.2 to 0.5 ms after the end of the laser pulse. This period was chosen because of its good

curve fitting (with a $0.93 < R^2 < 0.99$), its measurement consistency and the elimination of interference from the laser pulse.

The results showing the average decay constant as a function of Mn concentration are represented in Figure 4-4. These results clearly show the influence of the manganese concentration on the decay constant. With increasing the concentration of Mn^{2+} ions in the host ZnS lattice, the after-glow period (when the excitation has ceased) decreases. This confirms previous comments on the effect of higher Mn concentrations [67, 80, 86], and is indicative of the effect that is associated with Mn-Mn ion interactions leading to non-radiative decay probability increase. What is interesting in the results presented here, and potentially of value in process control systems, is the clear demonstration that there is a direct correlation between the PL luminescent decay constant measured in this way, and the nominal Mn concentration as shown in Figure 4-4. This demonstrates the potential for active monitoring of the luminescent quality of the film, potentially during deposition.

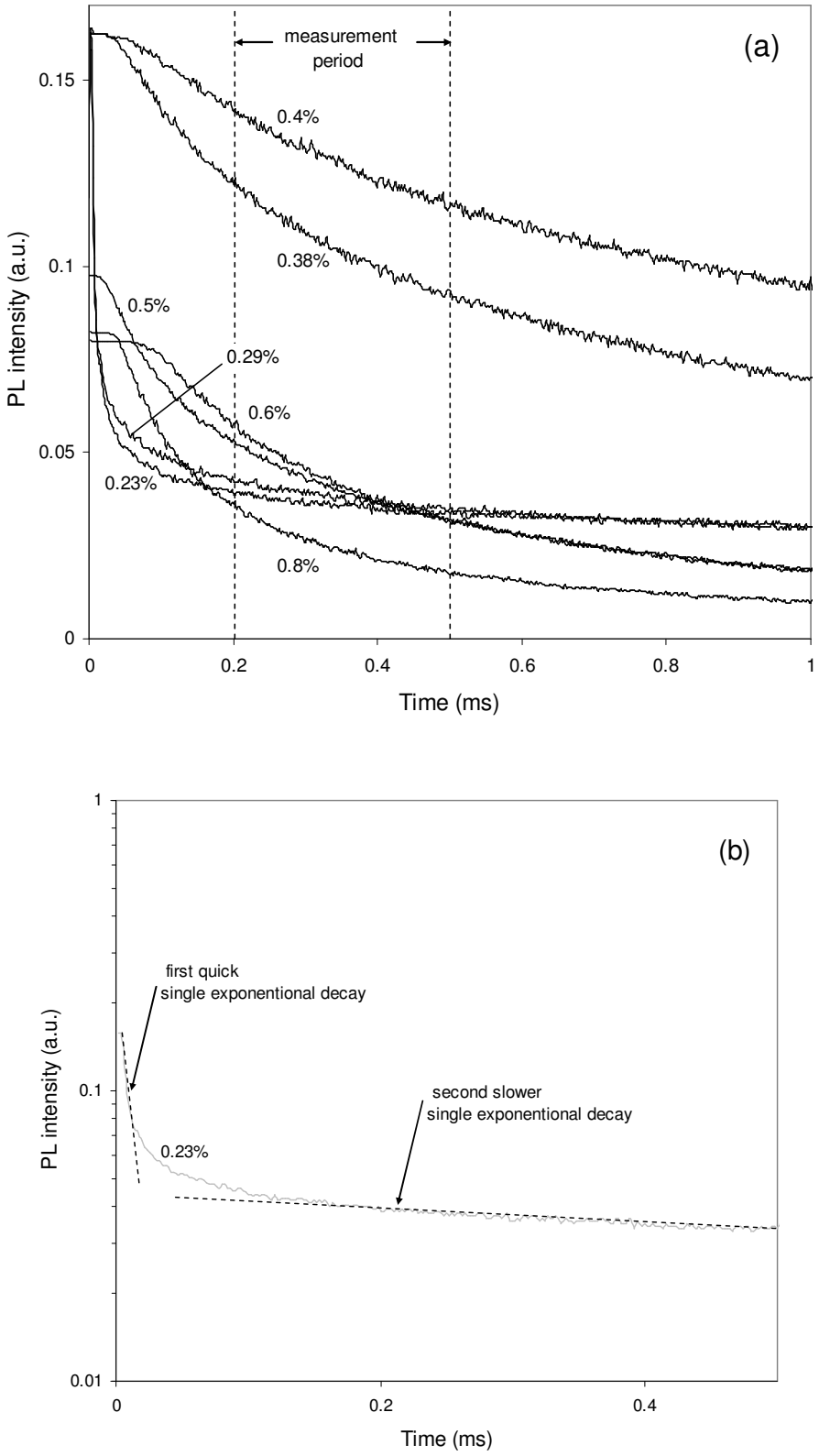

Figure 4-3: (a) Photoluminescence decay curves of 800 nm thick films of ZnS:Mn on Si at room temperature at different nominal Mn concentrations (represented by co-sputtering power ratio applied). Dashed lines indicate the time domain used for decay constant determination. (b) Example showing the double exponential decay

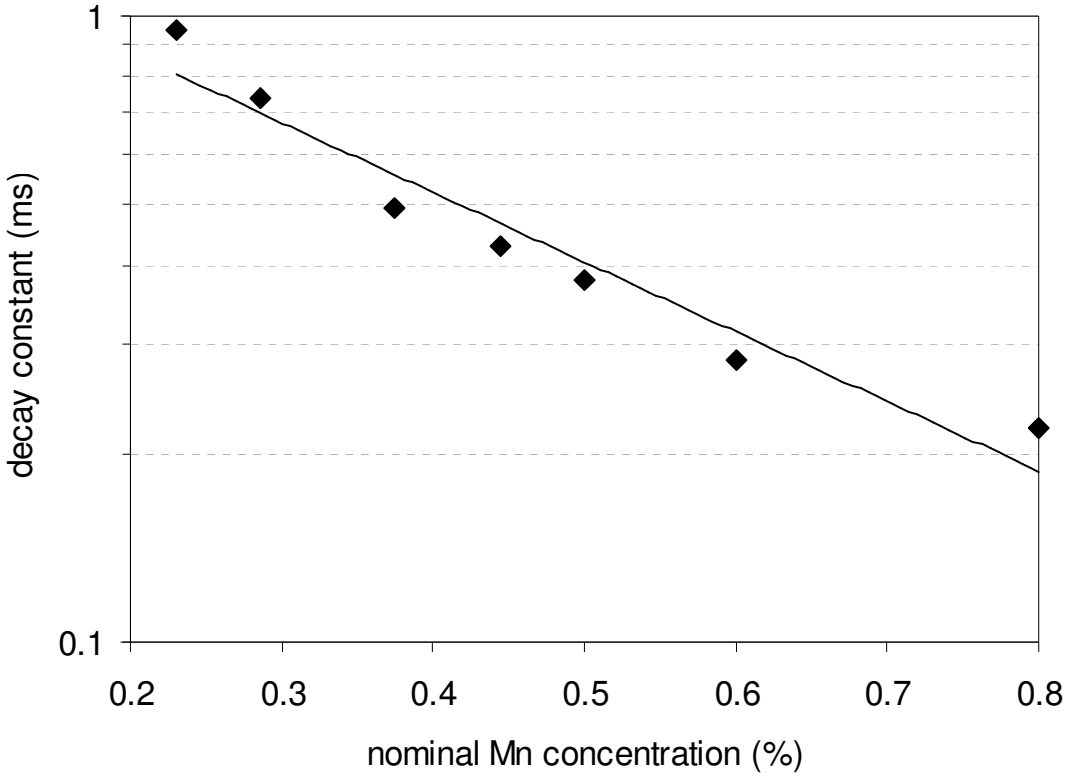

Figure 4-4: Photoluminescence decay constant as a function of nominal Mn concentration (represented by co-sputtering power ratio applied) for 800 nm thick films of ZnS:Mn on Si at room temperature.

4.5 Electroluminescence optimisation

4.5.1 Experimental and analysis conditions

For comparison of photo and electro-luminescent properties, a series of equivalent EL test devices were fabricated across the range of Mn concentrations studies. The two sputtered dielectric (Y_2O_3) thin films (300 nm) sandwiching the phosphor layer were deposited using the cluster magnetron system of Figure 3-1 at a temperature of 190°C in 2 mbar of Ar. Following device annealing at 500°C for 1 hour in vacuum, a sputtered indium tin oxide transparent conducting layer was deposited at 200 nm thick as the top transparent electrode layer (in a separate deposition system).

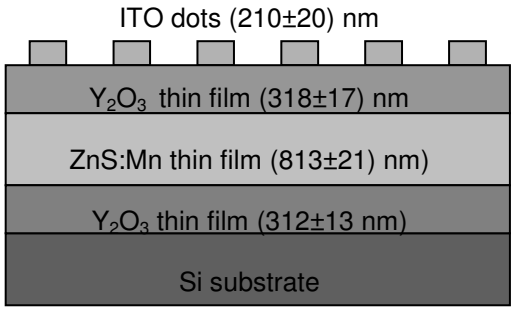

Figure 4-5: Diagram of the TFEL device structure used for characterisation studies.

Luminous intensities were measured using a LS110 luminance meter coupled to a computer controlled system by applying a high voltage sinusoidal waveform to excite the thin film electroluminescent devices.

4.5.2 Results

For electroluminescent evaluation of the co-sputtered films, a 1 kHz sinusoidal waveform voltage was applied to the test TFEL devices and luminance was recorded as a function of drive voltage applied, as shown in Figure 4-6 with six different nominal Mn concentrations (note: voltages shown here are ground to peak values rather than RMS, since this is the convention in ACTFEL studies). Figure 4-7 shows the operating luminance (defined in this work as the threshold voltage, V_{th}, plus 50 V) vs Mn concentration. The results show that with these films, the `optimum' electroluminescence is obtained for a similar nominal Mn concentration (~0.36 Mn wt.%) compared to the photoluminescence results achieved from a different set of wafers, which also compares favourably to results obtained previously from powder targets which showed an optimum at 0.43 wt.% [67]. Moreover, Figure 4-8(a) shows the increase of threshold voltage (determined as shown in Figure 4-8(b)) when increasing the Mn concentration, which was also observed previously [87-89] Above

0.5 Mn wt.% the threshold voltage tends to increase less rapidly. It is believed that this increase in electric field with Mn concentration occurs through the lowering the Fermi level [87].

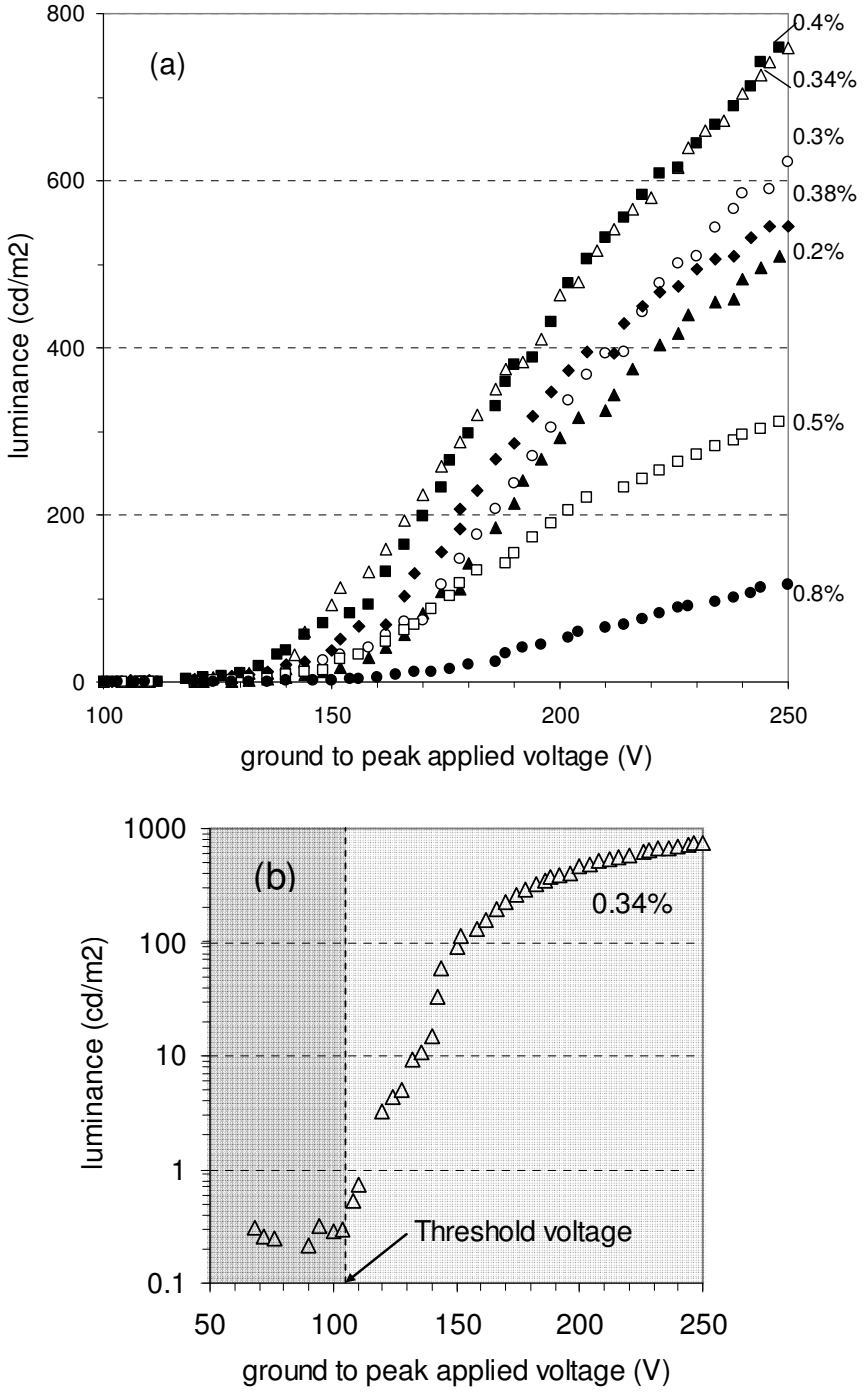

Figure 4-6: (a): Luminance vs drive voltage characteristics of ZnS:Mn based TFEL test devices as a function of the co-sputtering power ratio used to vary the Mn concentration (1 kHz sine wave drive voltage). (b): determination of the threshold voltage

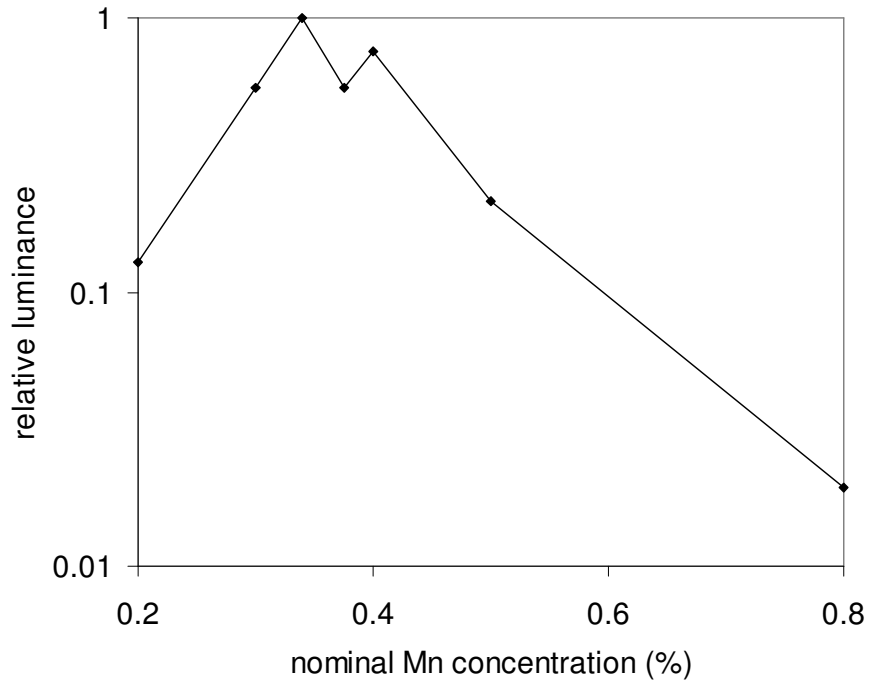

Figure 4-7: Electroluminescence luminance value vs nominal Mn concentration (represented by co-sputtering power ratio applied) at operating voltage (V_{th} + 50V, ground to peak) for TFEL devices

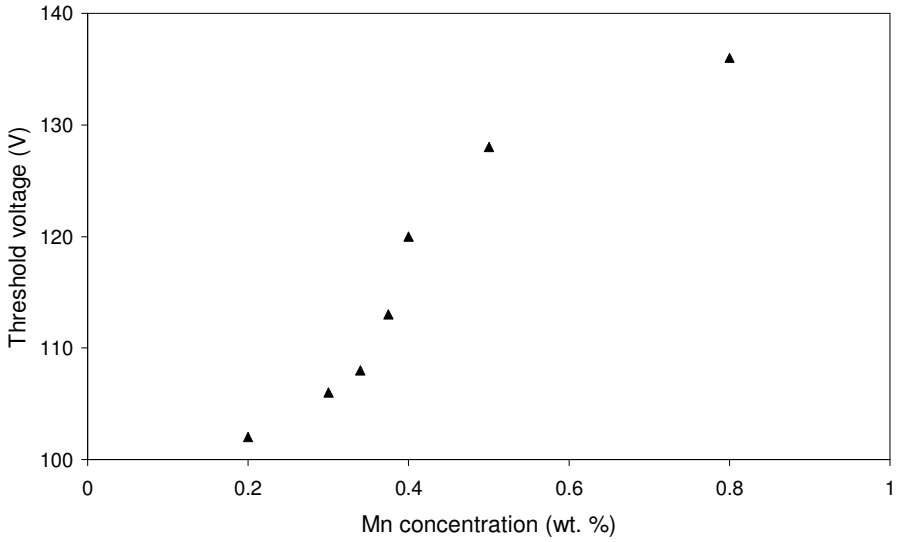

Figure 4-8 Threshold voltage vs nominal Mn concentration (represented by co-sputtering power ratio applied) for TFEL devices

4.6 Discussions and conclusions

AC excited electroluminescence within ZnS:Mn thin films is known to occur as a result of the substitutional incorporation of Mn^{2+} into the host lattice, where a Zn vacancy is occupied by the dopant ion. The 2.1 eV 3d shell transition that is responsible for the characteristic 585 nm Mn emission is spin and parity forbidden for the isolated Mn atom, and can only occur when the field is modified within the lattice. A correctly sited Mn ion is therefore termed an *emitting centre* and may be excited by impact excitation, which is thought to dominate in EL, or by energy exchange from electron-hole recombination as produced by PL excitation. However, during the early work on TFEL in the 1980s, it was reported that less than 1% of the dopant atoms are participating in the emission process, but that the cross-section for excitation is high, being of the order of the geometric cross-section – $1x10^{16}$ cm^2 [29]. This implies that the majority of dopant atoms are not correctly sited within the lattice. The nature of the dopant environment is thus highly influential on the luminescent properties, and is strongly affected by deposition conditions – particularly annealing – as well as by the actual doping density.

The rapid rise in luminescent emission by both PL and EL, as Mn concentrations is increased towards the optimum (here shown as 0.3 – 0.4 wt.%), is related to the concomitant increase in available emitting centres – i.e. substitutional Mn ions. Beyond the optimum, the rapid fall off in luminescent emission is correlated to the exponential decrease in luminescent decay time, which can be considered to be due to an increase in non-radiative decay probability associated with Mn-Mn interactions [43, 86, 90, 91]. Evidently the phenomenon of an optimum Mn concentration is achieved by a combination of these two conflicting effects. Another complete series of data were performed in a later stage of this research programme; decay results and

red/yellow emissions ratios from the first and the second batches are regrouped and compared on Figure 4-9.

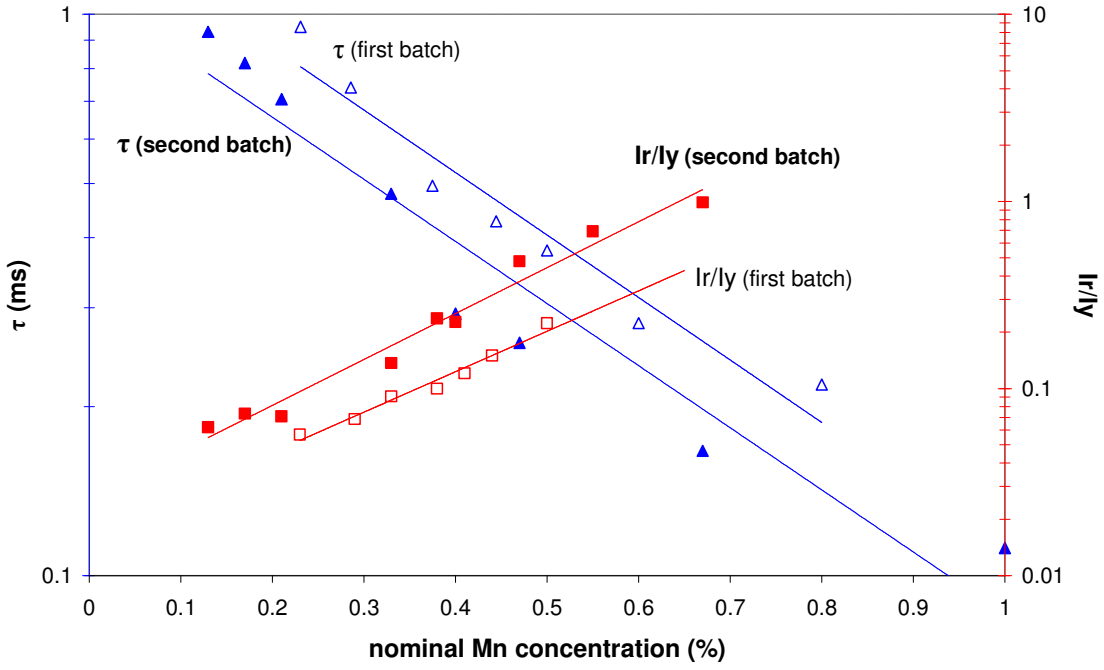

Figure 4-9: Variations of both decay constant and red/yellow emissions ratios vs nominal Mn concentration (Comparison of two batches of 800 nm thick films of co-sputtered ZnS:Mn)

On Figure 4-9, it is important to note the change of nominal Mn concentration between the two batches (0.28 % instead of 0.38 %); this nominal Mn concentration is given by the co-sputtering ratio of the electrodes used for the two targets and therefore differs from the actual Mn concentration. This 'shifting' (of 0.1% in nominal Mn concentration) can be the consequence of deposition modifications such as target age or new RF power supply, but it is believed that higher electrode powers used would be the most probable cause. Therefore, these results give clear indication that a suitable measurement of the transient luminescence and the red/yellow emissions ratios are both good indicators of the internal effective doping concentration and thus provide potential quality monitoring techniques that could be

implemented as an in-situ growth monitor. The results show this to be true for the range of doping density up to 1 wt.%. However, as shown in Figure 4-9, it is also important to note that there is a non negligible variation in results from one sample to another.

While both links between decay time as well as red/yellow emissions ratios and Mn doping have been indicated in the past, this is the first demonstration of a clear correlation of the nominal optimised Mn concentration to a measurable parameter that would be an effective performance monitor. Changes in both dopant concentration and environment would be reflected in the position on the curves of Figure 4-9 and hence could be utilised to change deposition and/or annealing conditions in order to compensate for the known variation in sputtering that results with target age and batch changes.

Furthermore, a variation in nominal Mn concentration between depositions results in a corresponding variation in the electroluminescent intensity (as shown in Figure 4-7) demonstrating the correlation between deposition control on the nominal Mn concentration and resultant performance.

In summary, the use of a co-sputtering technique for the deposition of luminescent phosphor thin films of ZnS:Mn has been demonstrated with results showing that optical measurement techniques could be utilised to monitor the effective Mn concentration and thus provide process control tools to ensure optimised batch to batch film deposition.

Chapter 5 Laser processing of ZnS:Mn thin films for TFEL devices

5.1 Introduction

Inorganic thin films of ZnS:Mn have been the most popular phosphor used for the fabrication of thin film electroluminescent (TFEL) displays due to their efficient yellow emission under high field electroluminescence. As explained in Chapter 2, post deposition thermal annealing is typically used to improve the crystallinity and dopant distribution of the deposited films and hence the overall film quality [41, 44]. Photoluminescence (PL) intensity increases with annealing temperature which results from the diffusion of Mn^{2+} into Zn vacancies. Moreover 500°C was found to be the optimum annealing temperature for the EL intensity [28].

As an alternative to thermal annealing, it is believed that laser annealing induces an in depth phase transition and promotes dopant diffusion. In ZnS, the original cubic phase appears to change to a mixed phase - hexagonal and cubic- following laser processing at 248 nm, which suggests a re-ordering and probable removal of defects [92]. The advantages of laser annealing over standard or conventional thermal annealing are related to the short processing cycles that can be achieved with UV lasers associated with localisation of the annealing effect, hence retaining the electrical properties of the lower dielectric surface.

Laser annealing of ZnS:Mn films were first reported in 1983 [49]. More recently an extensive programme of work of laser annealing at 248 nm commenced in 1997. Laser annealing was demonstrated to be beneficial to the phosphor material for TFEL devices over thermal conventional annealing method in terms of PL and EL, as shown by the NTU Display group [2, 4, 5, 42], [3, 51, 70], with results demonstrating the following:

- a major increase in electroluminescent emission [51, 93] from a combination of laser plus thermal annealing compared with thermal annealing only
- indications from both X-ray diffraction [42] and ellipsometry [53] that a phase change occurs in the upper 200 nm of film
- exploratory comparison with a laser annealing model suggests substantial temperatures rises in the films during a laser annealing pulse [2]

For the work presented here, this laser processing technique has been applied to investigate the combined effect of laser processing and varying dopant concentration.

Phosphor thin films with various Mn concentrations were laser annealed and analysed using an experimental system modified by the author to provide a scanning sample stage. Full EL devices were also fabricated and tested.

In addition, to investigate the potential for improved EL efficiency in the resultant display devices, thin films were laser processed with 248 nm radiation, after only growing a 200 nm layer. This was followed by further growth of 200 nm of film which was then exposed to 248 nm radiation. The process continued until the suitable film thickness was reached for an EL device (typically 800 nm). It was anticipated that this process of successive layer processing would produce a highly efficient luminescent layer in comparison to the previous work where only the upper 200 nm was modified due to the optical absorption of the laser energy. As such, this would demonstrate the potential for the development of a novel processing technique to potentially maximise the benefit of laser annealing through the full active volume of the emitting phosphor layer.

5.2 Experimental

5.2.1 Thin film deposition

Thin films of ZnS:Mn were co-sputtered via the simultaneous sputtering of ZnS and ZnS:Mn (1wt%) solid targets onto a rotating 100 mm diameter (100) n-type Si wafer substrate (with a target distance of 15 cm) using a custom built Kurt Lesker Torus four-electrode magnetron system (see Figure 3.1 for details). The layers thicknesses were determined by using an interferometer during growth. An average of ± 3 % thickness variation across the thin films was measured using Dektak 6M stylus profilometer.

The substrate temperature was maintained at 190°C (± 10 °C) during deposition in 0.40 Pa of Ar. The vacuum deposition chamber had a base pressure of 1 x 10^{-4} Pa and the deposition could be followed by an in-situ annealing of 500°C for 1 hour in vacuum. Films were first grown with different Mn concentrations for the measurements presented in the first part of this chapter and with a fixed Mn concentration for the measurements presented in the second part of this chapter. The Mn concentrations were selected according to the optimised parameters identified by the work reported in Chapter 4 [94] and the films were deposited by setting the suitable RF power applied to each of the two solid sputtering targets ZnS and ZnS:Mn (1 wt.%) .

5.2.2 Laser annealing

The laser utilised for this investigation was a Lambda Physik LPX 305i excimer laser charged with Krypton Fluoride (KrF), emitting pulses of 20 ns at 248 nm (5.13 eV photon energy). An Excitech homogeniser EX-HS-700D was used to convert the non-uniform rectangular beam into the top hat profile required for a uniform density

profile. On-line energy settings of the 20 ns pulsed KrF (248 nm) laser beam were achieved using HOYA fused silica plates or an iris to attenuate the beam. The irradiated square surface was fixed to 5 mm by 5 mm (for the varying Mn concentration experiments) and 3 mm by 3 mm (for the successive laser annealing experiments) allowing fluences up to 1.4 J/cm^2. The sample was situated in a pressure cell (with UV grade window) mounted on two automated translation stages to allow accurate automation of laser processing – step and repeat sample positioning. The use of the pressure cell is to minimise ablation [54, 56], which results in material loss. Argon gas was injected into the pressure cell to achieve a 150 psi pressure (~10 bars). If more than 1 pulse was applied to the surface of the sample, a frequency of 1 Hz was used for the remaining pulses. A systematic calibration for the laser annealing process is required; the calibration curve is shown in Figure 3-14.

5.2.3 Photoluminescence characterisation

Time integrated photoluminescence spectra were obtained by exciting the surface of the ZnS:Mn thin film phosphor with the 1mm diameter beam of a N_2 laser (337 nm - photon energy = 3.68 eV, i.e. just above the band gap of ZnS). The luminescent PL emission was collected via an optical fibre and the spectra characterised with an Ocean Optics S2000 spectrometer. The maximum intensity of each spectrum was recorded for the different Mn concentrations at the characteristic Mn peak emission wavelength of 585 nm.

5.2.4 Electroluminescence characterisation

For comparison of photo and electro-luminescent properties and based on successful results obtained from PL examinations, a series of equivalent EL test devices (as illustrated in Figure 5-1) were fabricated with the same Mn concentrations. The two sputtered dielectric (Y_2O_3) thin films (300 nm) sandwiching the phosphor layer were deposited at a temperature of 190°C in 2 mbar of Ar. Following device annealing at 500°C for 1 hour in vacuum, a sputtered indium tin oxide transparent conducting layer was deposited through a 1 mm diameter contact mask (aligned with laser annealed processed areas) at 200 nm thick as the top transparent electrode layer (in a separate deposition system).

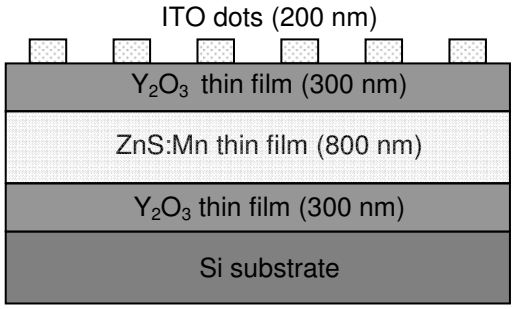

Figure 5-1: Schematic diagram of the cross section for the fabricated thin film electroluminescent test devices

Luminous intensities were measured using a LS110 luminance meter coupled to a computer controlled system by applying a sinusoidal waveform to excite the thin film electroluminescent devices.

5.3 Variation of Mn concentration results

5.3.1 Phosphor thin films

To examine the effect of laser annealing combined with or without thermal annealing on co-sputtered ZnS:Mn thin films with different Mn concentration, various

configurations of irradiated square (5 mm by 5 mm) were used to evaluate photoluminescence performance. These combinations of number of pulses and fluences are represented in Figure 5-2. For consistency, experimentation was performed on each wafer (deposited at different nominal Mn concentration) as shown in Figure 5-2 – i.e. with the wafer cleaved and one half unannealed prior to laser processing, and the other half thermally annealed to 500 °C for 1 hour.

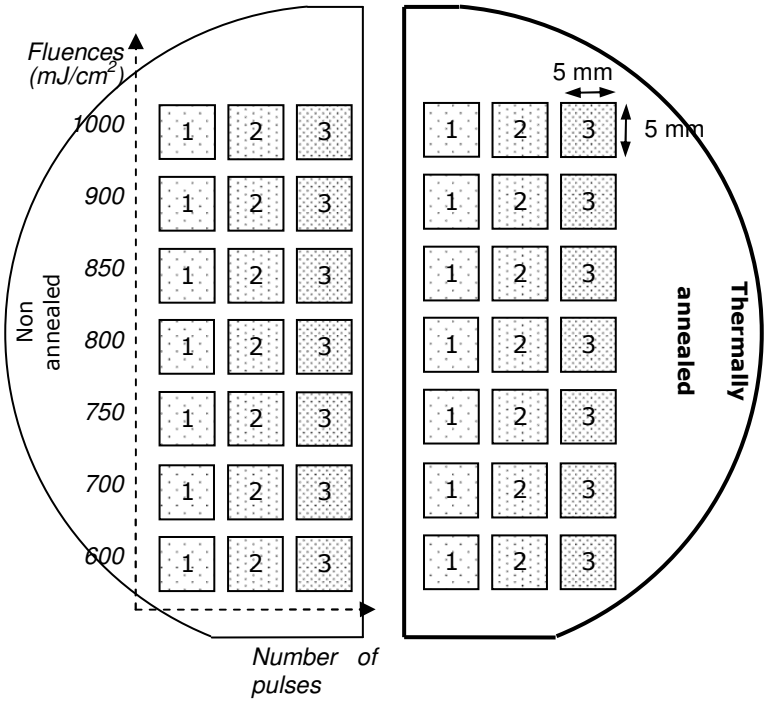

Figure 5-2: Sample pattern of laser processed ZnS:Mn thin film deposited on a Si wafer

5.3.1.1 Photoluminescence

An example of photoluminescence spectra obtained for a non-thermally annealed sample is shown in Figure 5-3.

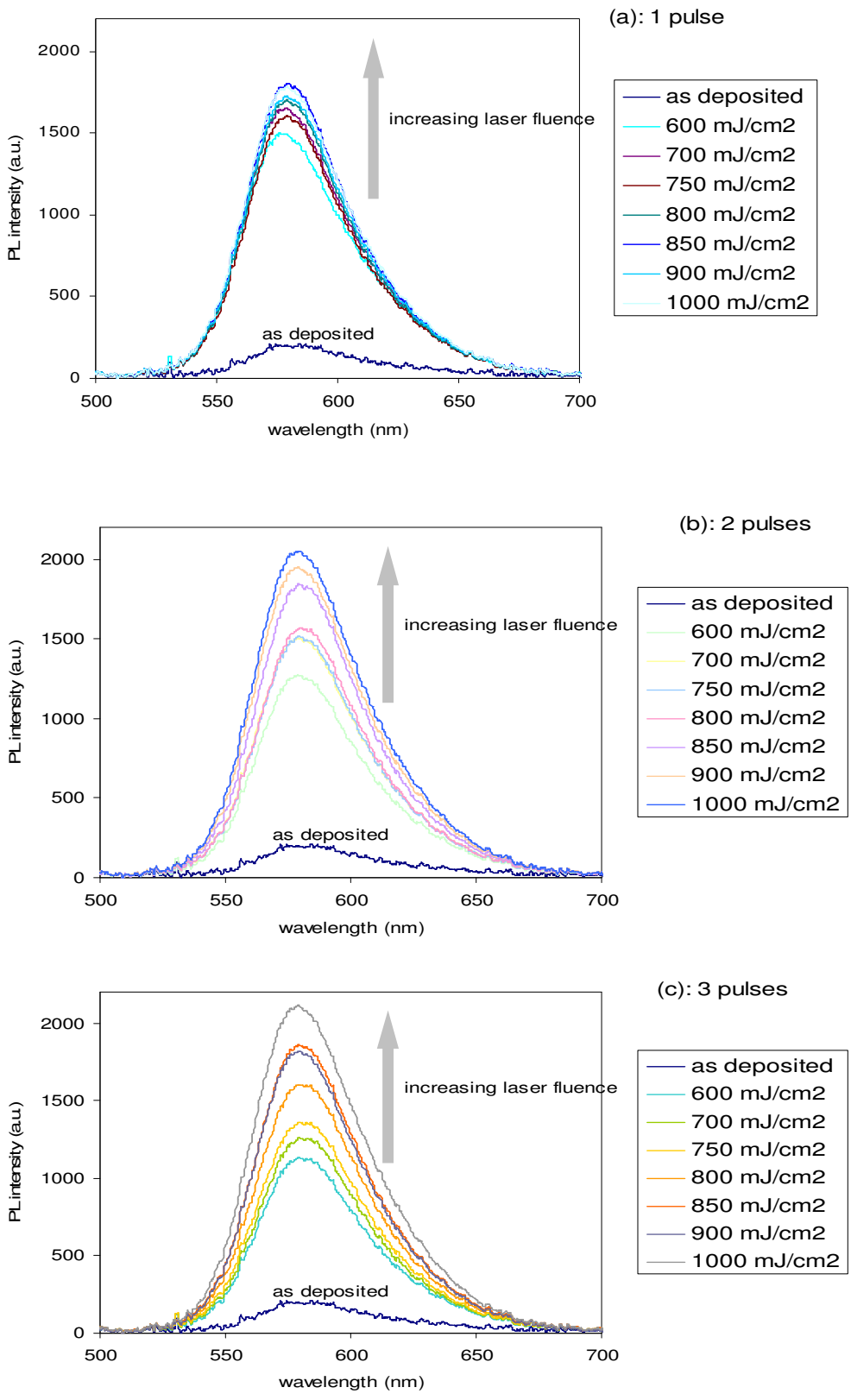

Figure 5-3: Photoluminescence spectra for a non-thermally annealed co-sputtered ZnS:Mn thin film deposited on Si with fluences ranging from 0.6 to 1.0 J/cm^2 with 1 (a), 2 (b) and 3 (c) pulses

The peak photoluminescent intensity as a function of fluence and number of pulses is shown in Figure 5-4 for three co-sputtered ZnS:Mn thin films with different Mn concentrations and one sputtered thin film from a ZnS:Mn powder target.

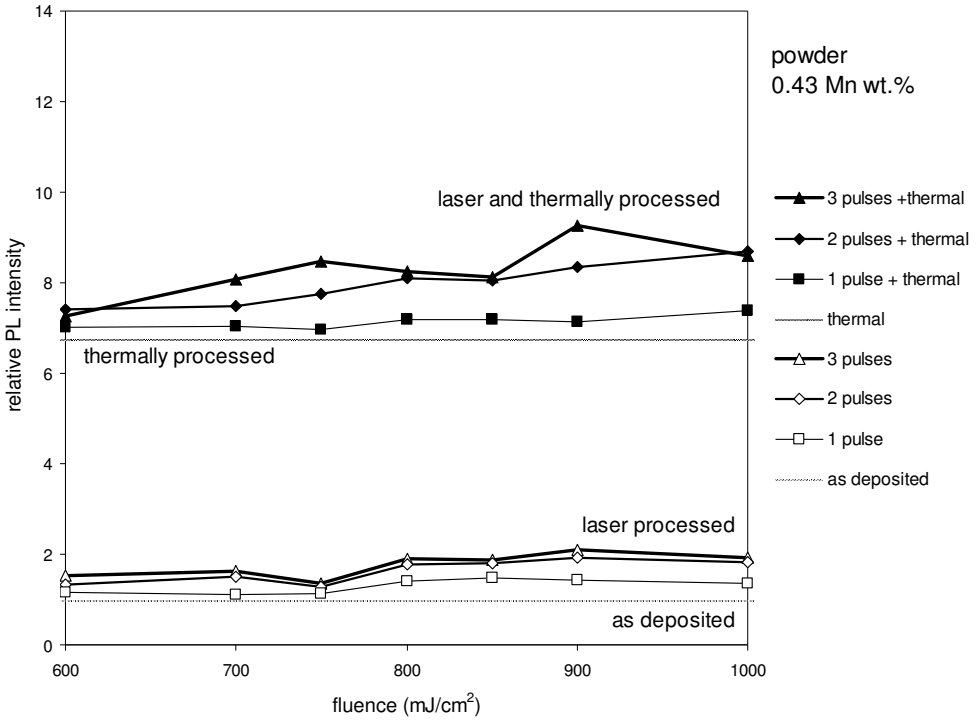
powder
0.43 Mn wt.%
laser and thermally processed
thermally processed
laser processed
as deposited
relative PL intensity
fluence (mJ/cm2)
3 pulses +thermal
2 pulses + thermal
1 pulse + thermal
thermal
3 pulses
2 pulses
1 pulse
as deposited

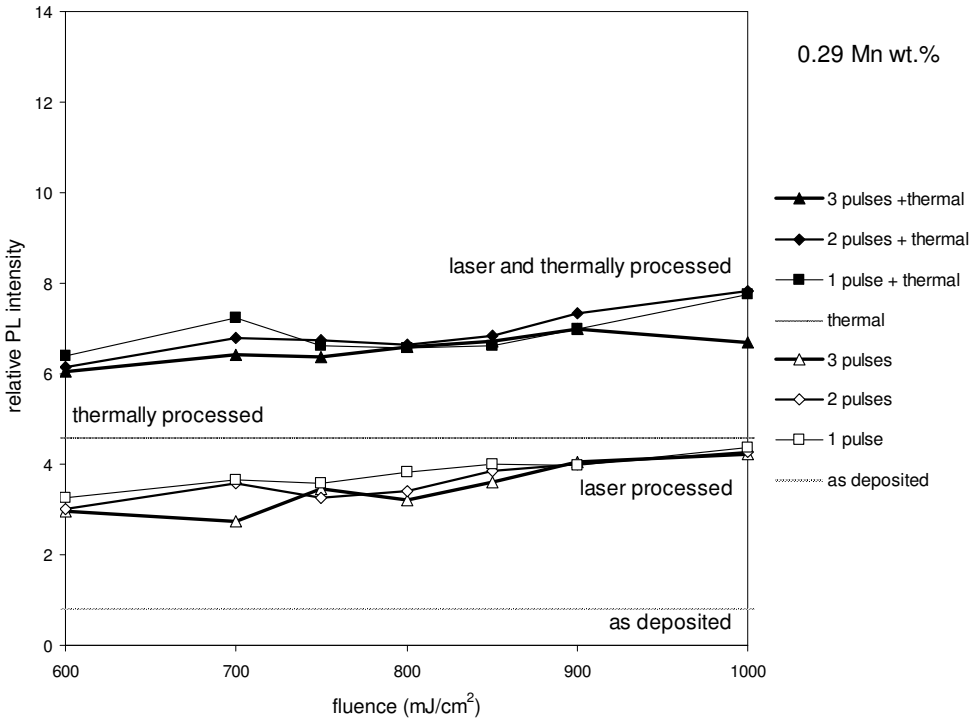
0.29 Mn wt.%
laser and thermally processed
thermally processed
laser processed
as deposited
relative PL intensity
fluence (mJ/cm2)
3 pulses +thermal
2 pulses + thermal
1 pulse + thermal
thermal
3 pulses
2 pulses
1 pulse
as deposited

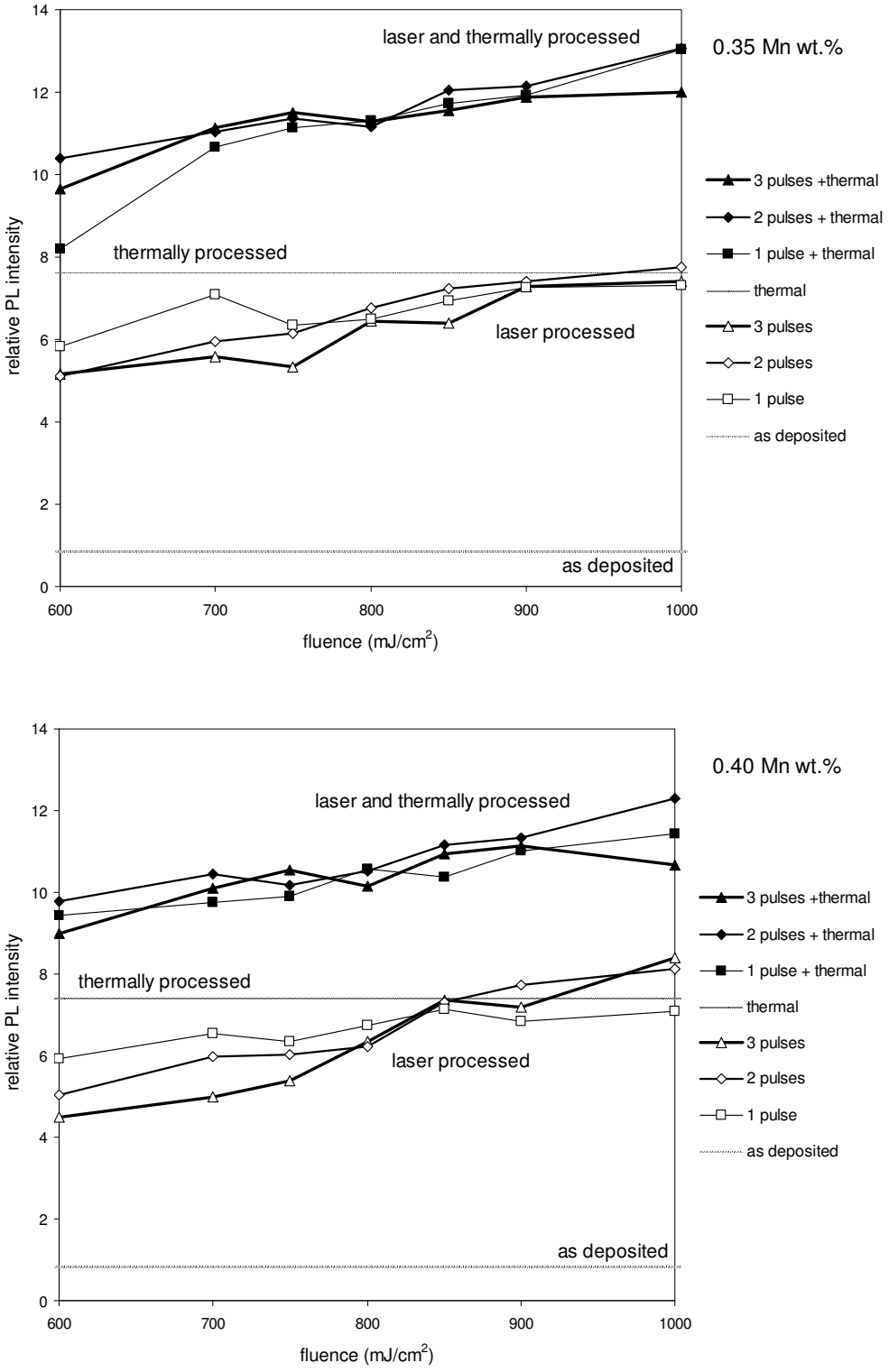

Figure 5-4: Photoluminescence (PL) improvements resulting from laser processing of different Mn concentration co-sputtered thin films and film sputtered from powder target (0.43 Mn wt %) at different fluences and numbers of pulses of 800 nm thick films of ZnS:Mn on Si at room temperature at different relative Mn concentrations. The relative PL intensities are compared to the as deposited thin film from powder target.

These results demonstrate clearly the benefit of laser annealing on luminescence of thin films of ZnS:Mn. Using laser annealing in combination with thermal annealing can enhance the photoluminescence up to 13 times and 12 times respectively for 0.35 and 0.40 Mn wt % concentrations, which are around the optimum value of (0.38 Mn wt %), compared to the as deposited thin film from powder target. As deposited films from powder target were used as the sample reference as the objective was first to compare the performance obtained from solid targets to most extensively used powder target. This improvement is more significant for the co-sputtered thin films from solid targets than for the sputtered thin film from powder target, especially for the cases without thermal annealing (up to 4 times more improvement).

There is an almost linear rise in photoluminescence intensity with fluence for all the Mn concentrations and number of pulses except for laser and thermally processed with 3 pulses above 850 mJ/cm^2. This saturation could be attributed to an excessive ablation resulting in substantial reduction of the phosphor thickness. Although laser annealing with 3 pulses produces the best photoluminescent intensities for the powder based thin films, it not clear whether or not there is an optimum number of pulses for the laser annealed co-sputtered thin film. However, laser annealing using 2 pulses seem to generally give the best results.

These analysis results also show that using laser annealing, the photoluminescent peak intensities still remain to be the greatest for thin films with Mn concentration around the ‘optimum’ achieved in Chapter 4 based on thermal annealed films. However, this statement could be invalid for non-thermally annealed samples because of the continuous but low increase in photoluminescent peak intensity, suggesting a higher Mn concentration optimum.

5.3.1.2 Surface roughness

The Wyko Optical Profilometer was used to measure the surface roughness for "as deposited", laser annealed only, thermally annealed only and laser annealed and thermally annealed ZnS:Mn thin film samples. Figure 5-5 shows a selection of these results obtained for an optimised film with a sampling area of 0.46 mm by 0.60 mm and PSI mode used.

As deposited

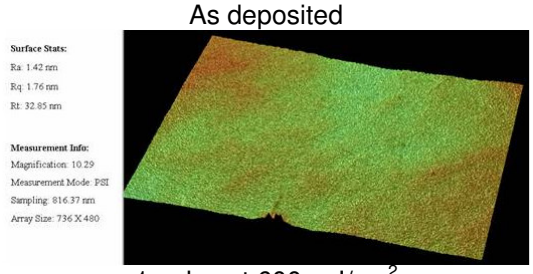

1 pulse at 600 mJ/cm^2

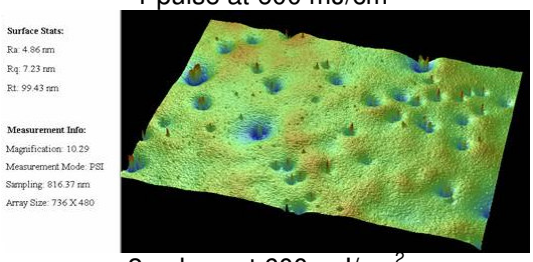

2 pulses at 600 mJ/cm^2

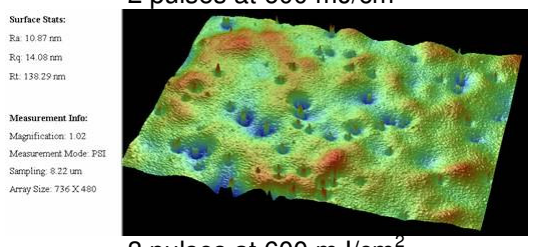

3 pulses at 600 mJ/cm^2

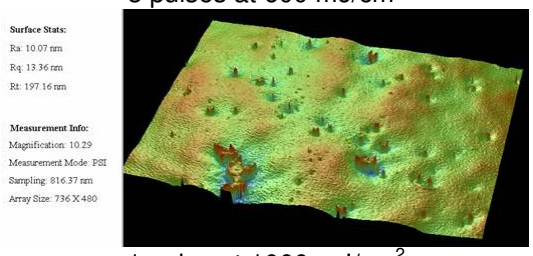

1 pulse at 1000 mJ/cm^2

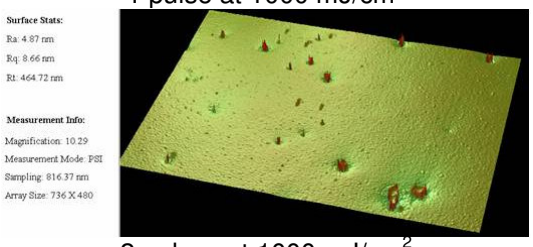

2 pulses at 1000 mJ/cm^2

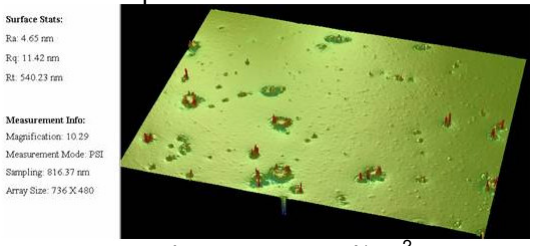

3 pulses at 1000 mJ/cm^2

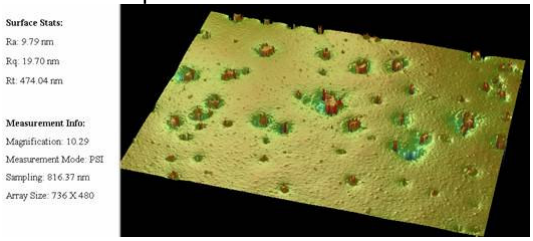

TA

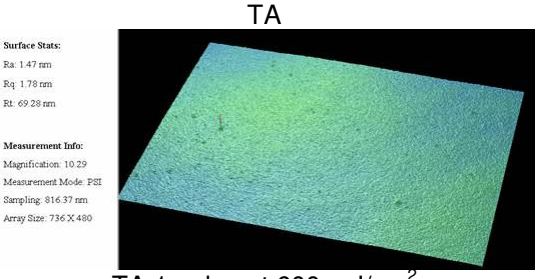

TA 1 pulse at 600 mJ/cm^2

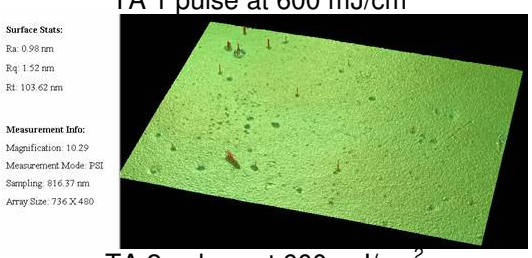

TA 2 pulses at 600 mJ/cm^2

TA 3 pulses at 600 mJ/cm^2

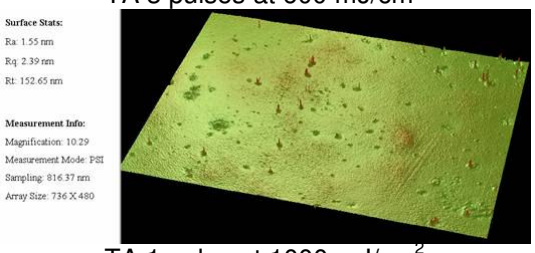

TA 1 pulse at 1000 mJ/cm^2

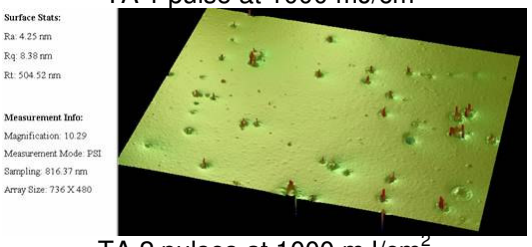

TA 2 pulses at 1000 mJ/cm^2

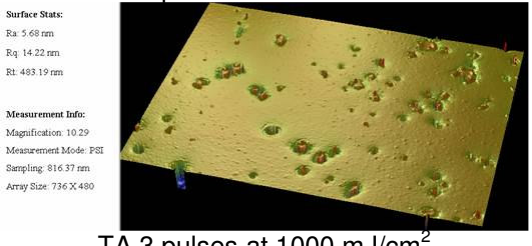

TA 3 pulses at 1000 mJ/cm^2

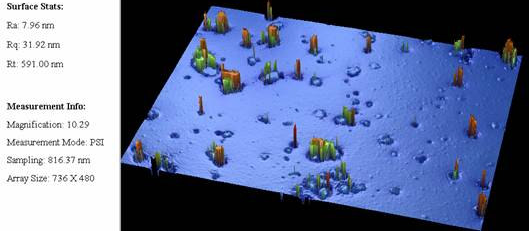

Figure 5-5: (on previous page) Optical profilometer images of ZnS:Mn thin films – left column showing non thermally annealed samples and right column showing thermally annealed (TA) samples.

These results are summarised on Figure 5-6:

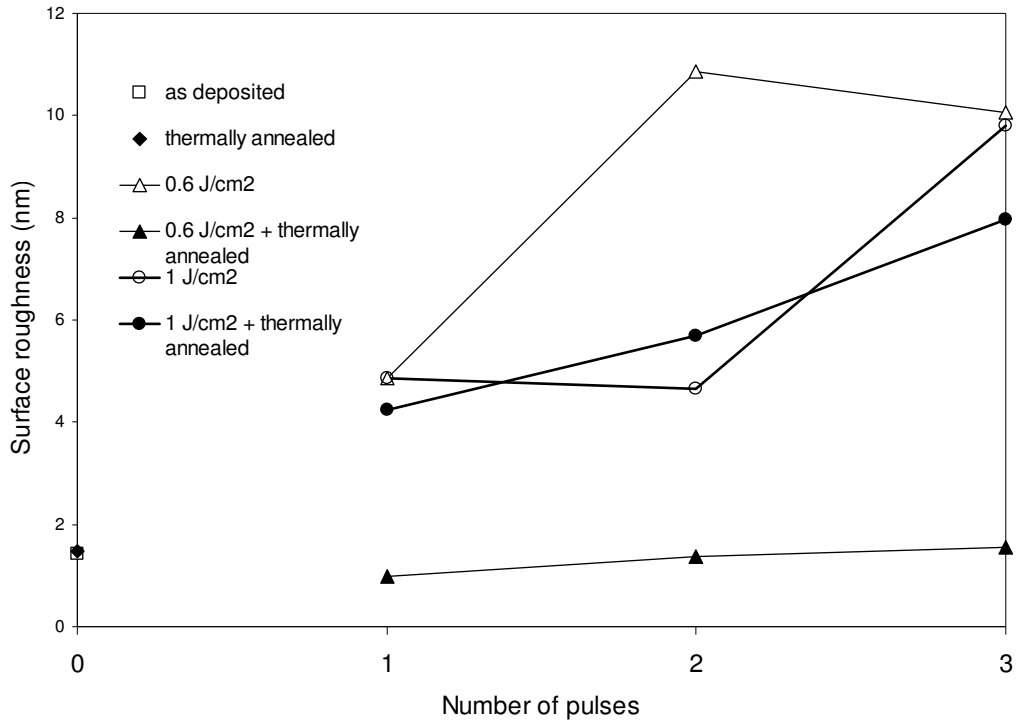

Figure 5-6: Surface roughness in function of number of pulses for low (0.6 J/cm^2) and high (1 J/cm^2) fluences of an 800 nm ZnS:Mn thin film deposited on Si with and without thermal annealing

The results from the graph in Figure 5-6 indicate that the average surface roughness of the thin films is very low (about 5 nm), which is important for the fabrication of electroluminescent devices, providing a good interface states at the boundary of the phosphor layer and the insulting layer.

Surface morphology comparison of these samples shows that the surface is nearly unchanged using thermal annealing only compared to as deposited samples. However, there is a surface improvement when adding thermal annealing to pulsed

laser annealing. At low fluence (600 mJ/cm^2), this combination improves even more the low surface roughness of the as deposited (1.42 nm) or thermally annealed (1.47 nm) to as low as 0.98 nm.

Finally, it is also important to note that a higher number of pulses from the laser degrades the surface roughness especially at high fluences which may be linked with the decrease in photoluminescence intensity results with 3 pulses.

5.3.1.3 X-ray diffraction

X-Ray Diffraction (XRD) measurements were undertaken for the ZnS:Mn thin films. XRD data for the thermally annealed and laser annealed samples are shown on Figure 5-7. Table 5-1 regroups the Miller indices in terms of the crystalline nature and diffraction angle.

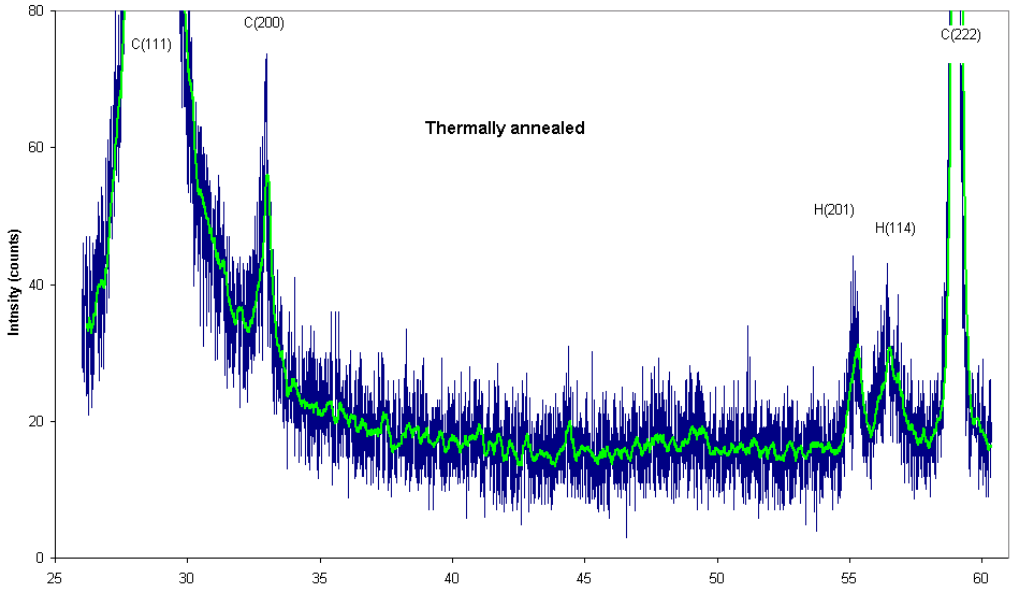

(a)

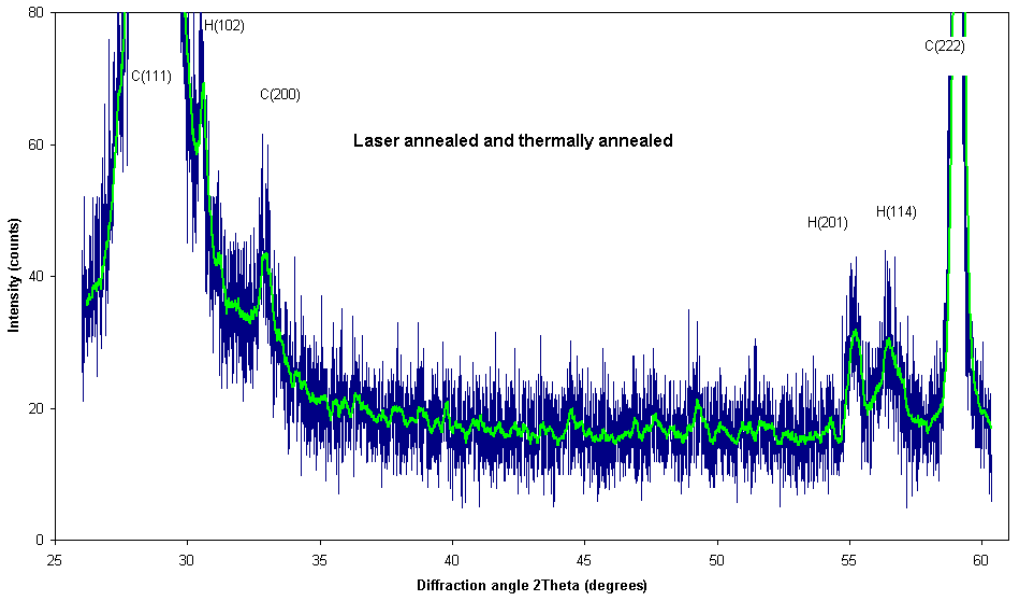

(b)

Figure 5-7: XRD patterns of thermally annealed samples at 500 °C (a) and pulsed laser annealed (2 pulses) at a fluence of 1 J/cm^2 and thermally annealed samples at 500°C (b). "C" stands for cubic phase and "H" for hexagonal phase

Cubic	(hkl)	111	200	222
	2θ (°)	28.6	33.1	59.3
Hexagonal	(hkl)	102	201	114
	2θ (°)	30.5	55.6	56.3

Table 5-1 Expected diffraction peaks for XRD pattern of ZnS:Mn [2]**. (hkl) are the Miller Indices and 2θ is the diffraction angle**

XRD analysis of these films gives some evidence of improved crystallinity associated with the improvement in photoluminescence. In particular, XRD analysis of these two types of ZnS:Mn thin films shows that they both possess a mixed phase (cubic and hexagonal) which confirms previous results discussed in Chapter 2. The preferred orientation of the ZnS:Mn thin films is indicated by the cubic (111) plane showing the highest intensity. The noticeable difference between these two types of samples is the presence of a small peak with an hexagonal (102) plane in the XRD pattern of the laser and thermally annealed ZnS:Mn film on Figure 5-7(b). This supplementary diffraction line corresponds to a crystalline quality improvement with the formation of a hexagonal wurzite structure as observed in previous work [21].

5.3.2 TFEL devices

The effect of the laser fluence and the number of pulses was studied for thermally annealed and non-thermally annealed ('as deposited') following the sample pattern represented in Figure 5-8.

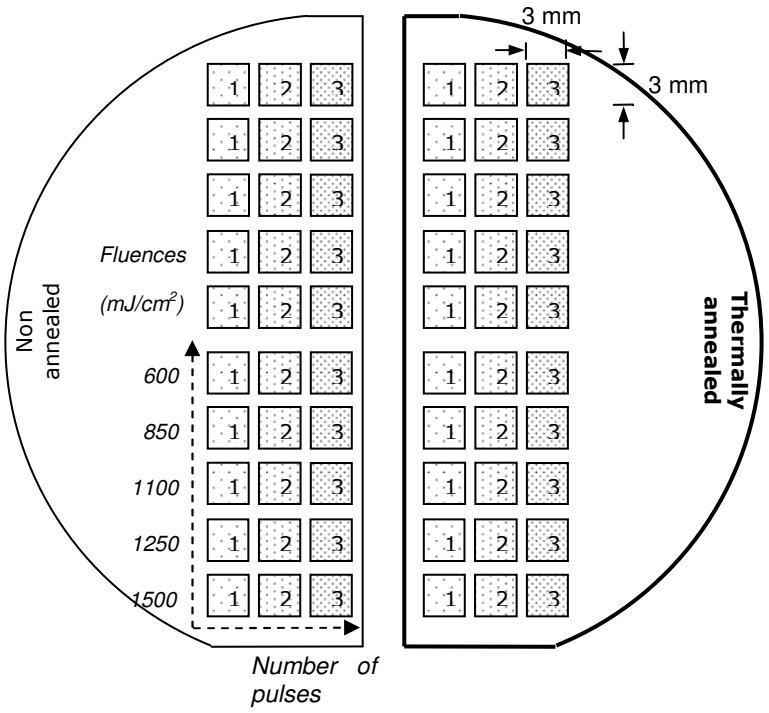

Figure 5-8: Sample pattern of laser processed ZnS:Mn thin film on 300nm Y_2O_3 layer

5.3.2.1 Electroluminescence

These samples were laser processed with different fluences using the calibration curve from Figure 3-14. Figure 5-9 shows some of the important results from this investigation (normalised to the peak luminance obtained at 500 V for the as-deposited sample). Based on the previous results and due to instability of non thermally annealed samples, only the combined effect of laser and thermal annealing is presented here.

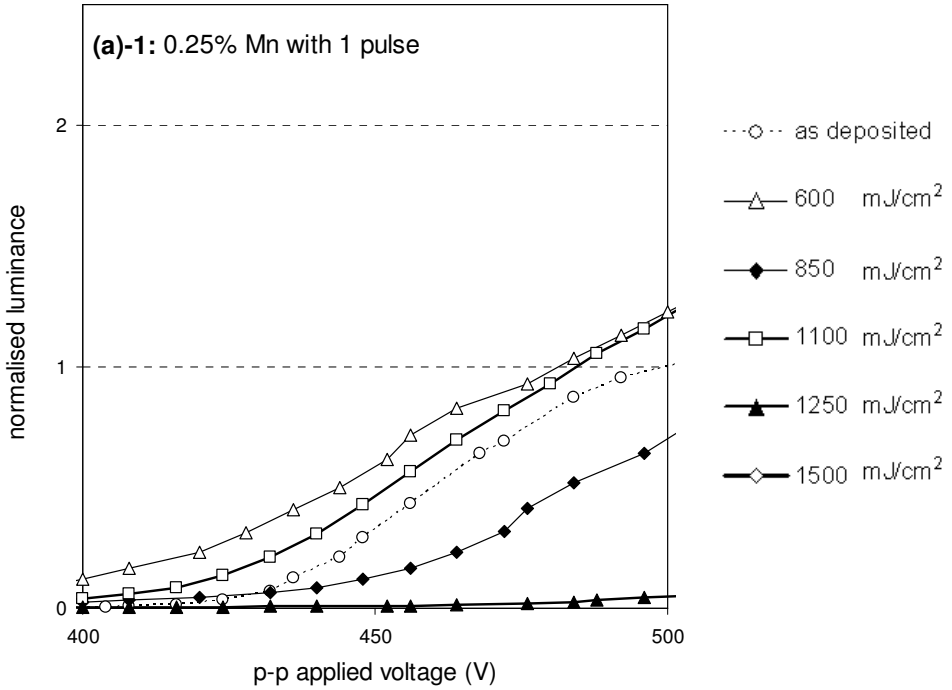
(a)-1: 0.25% Mn with 1 pulse
normalised luminance
p-p applied voltage (V)
as deposited
600 mJ/cm2
850 mJ/cm2
1100 mJ/cm2
1250 mJ/cm2
1500 mJ/cm2

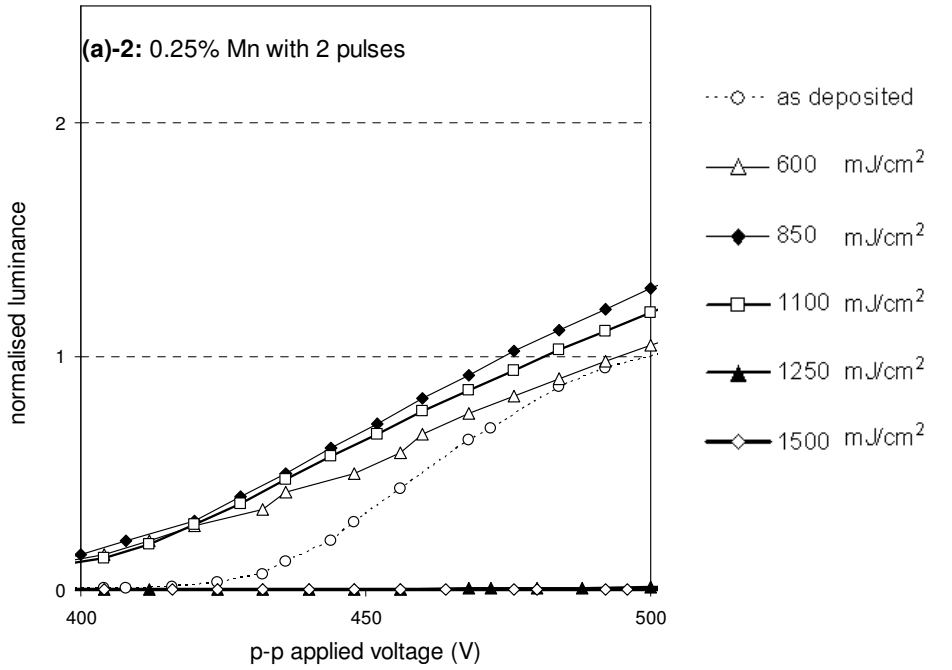
(a)-2: 0.25% Mn with 2 pulses
normalised luminance
p-p applied voltage (V)
as deposited
600 mJ/cm2
850 mJ/cm2
1100 mJ/cm2
1250 mJ/cm2
1500 mJ/cm2

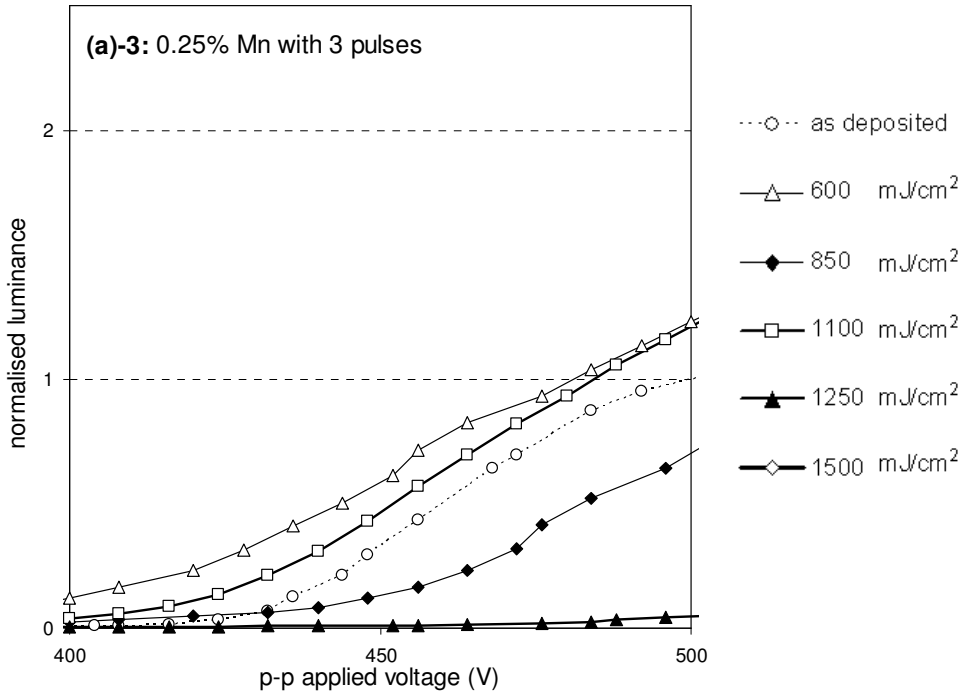
(a)-3: 0.25% Mn with 3 pulses
normalised luminance
p-p applied voltage (V)
as deposited
600 mJ/cm2
850 mJ/cm2
1100 mJ/cm2
1250 mJ/cm2
1500 mJ/cm2

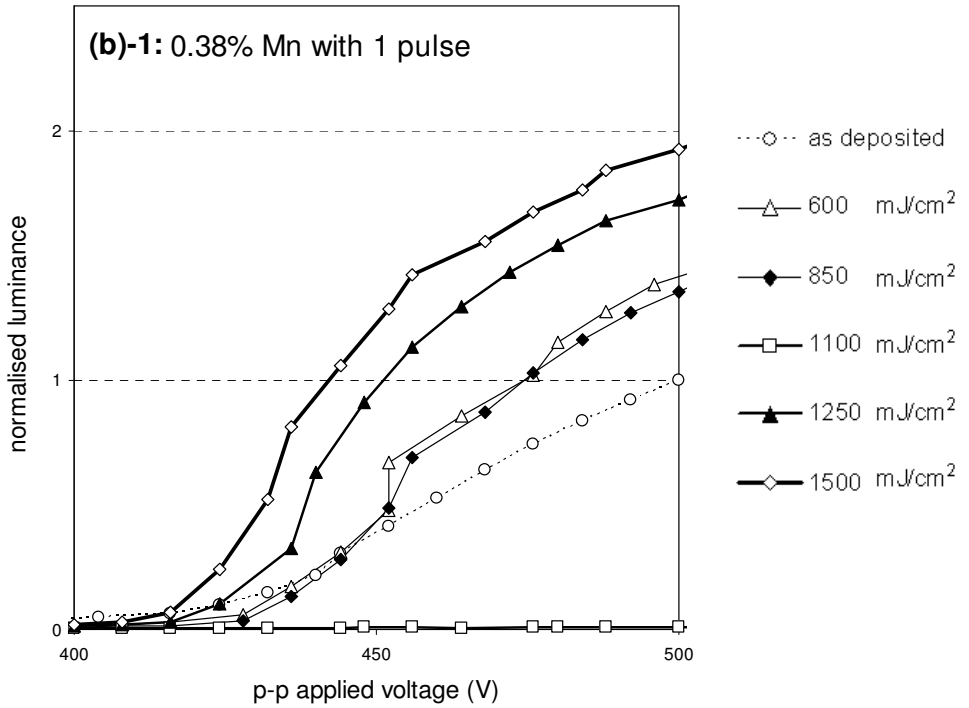
(b)-1: 0.38% Mn with 1 pulse
normalised luminance
p-p applied voltage (V)
as deposited
600 mJ/cm2
850 mJ/cm2
1100 mJ/cm2
1250 mJ/cm2
1500 mJ/cm2

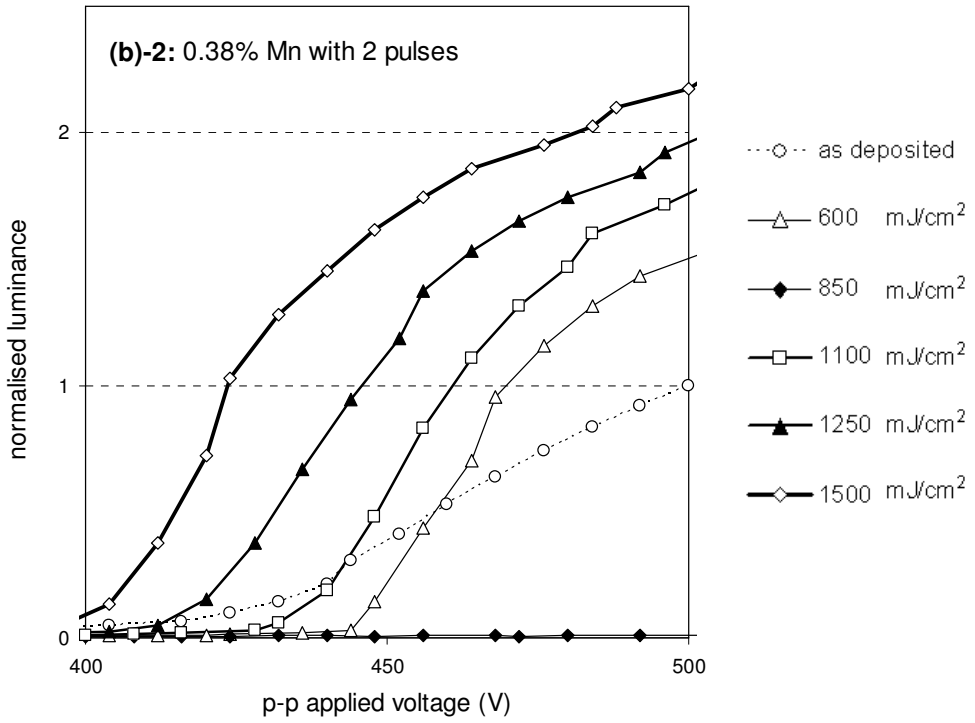
(b)-2: 0.38% Mn with 2 pulses
normalised luminance
p-p applied voltage (V)
0
1
2
400
450
500
as deposited
600 mJ/cm2
850 mJ/cm2
1100 mJ/cm2
1250 mJ/cm2
1500 mJ/cm2

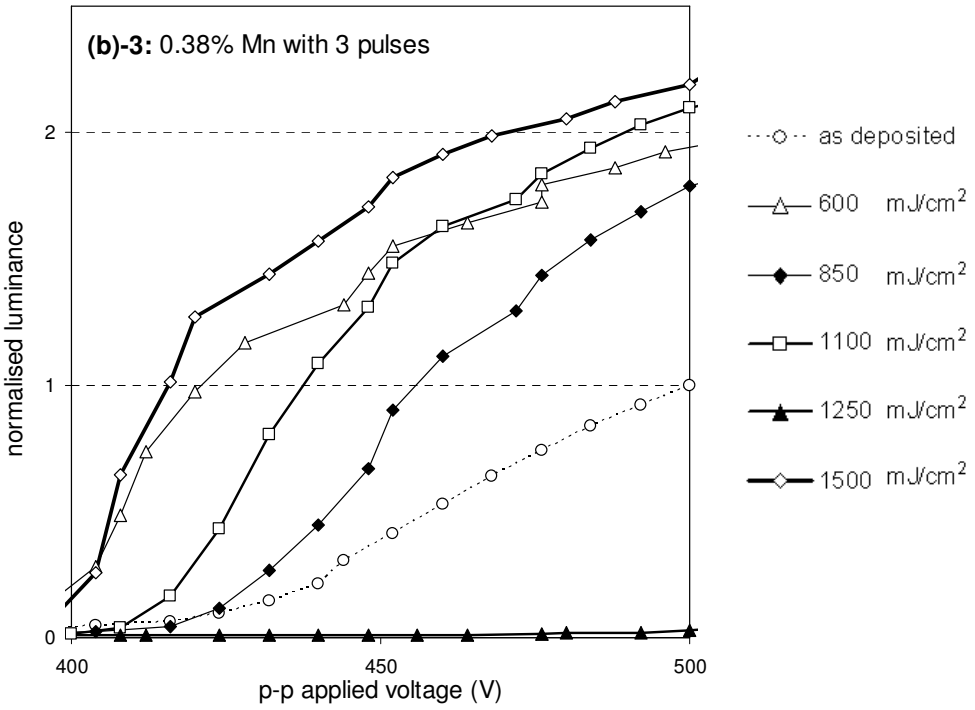
(b)-3: 0.38% Mn with 3 pulses
normalised luminance
p-p applied voltage (V)
0
1
2
400
450
500
as deposited
600 mJ/cm2
850 mJ/cm2
1100 mJ/cm2
1250 mJ/cm2
1500 mJ/cm2

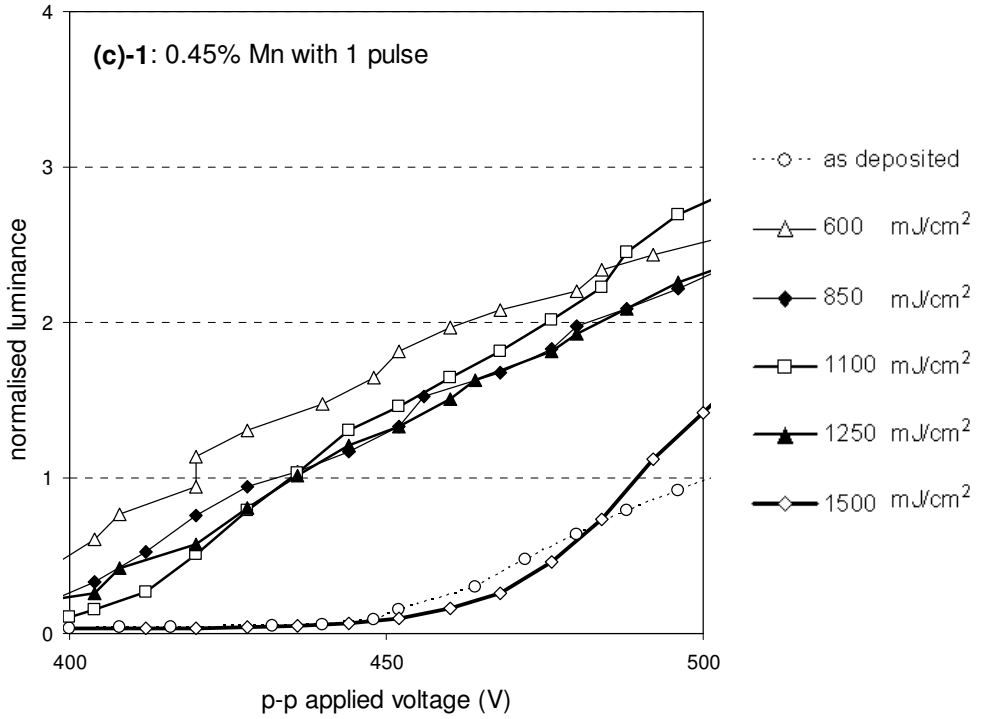
(c)-1: 0.45% Mn with 1 pulse
normalised luminance
p-p applied voltage (V)
as deposited
600 mJ/cm2
850 mJ/cm2
1100 mJ/cm2
1250 mJ/cm2
1500 mJ/cm2

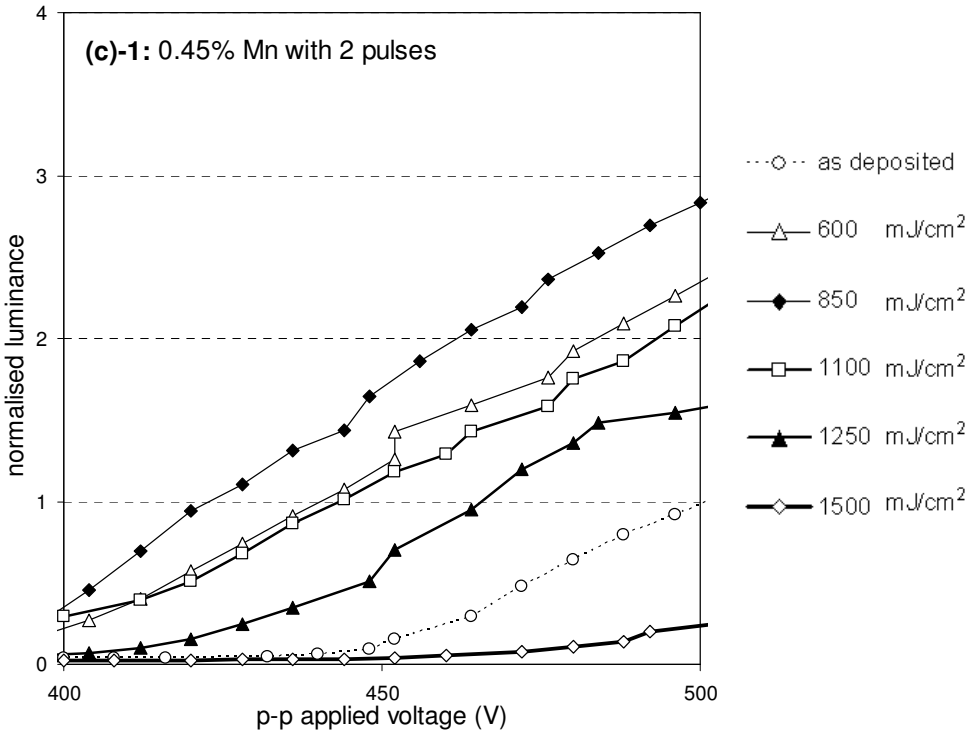
(c)-1: 0.45% Mn with 2 pulses
normalised luminance
p-p applied voltage (V)
as deposited
600 mJ/cm2
850 mJ/cm2
1100 mJ/cm2
1250 mJ/cm2
1500 mJ/cm2

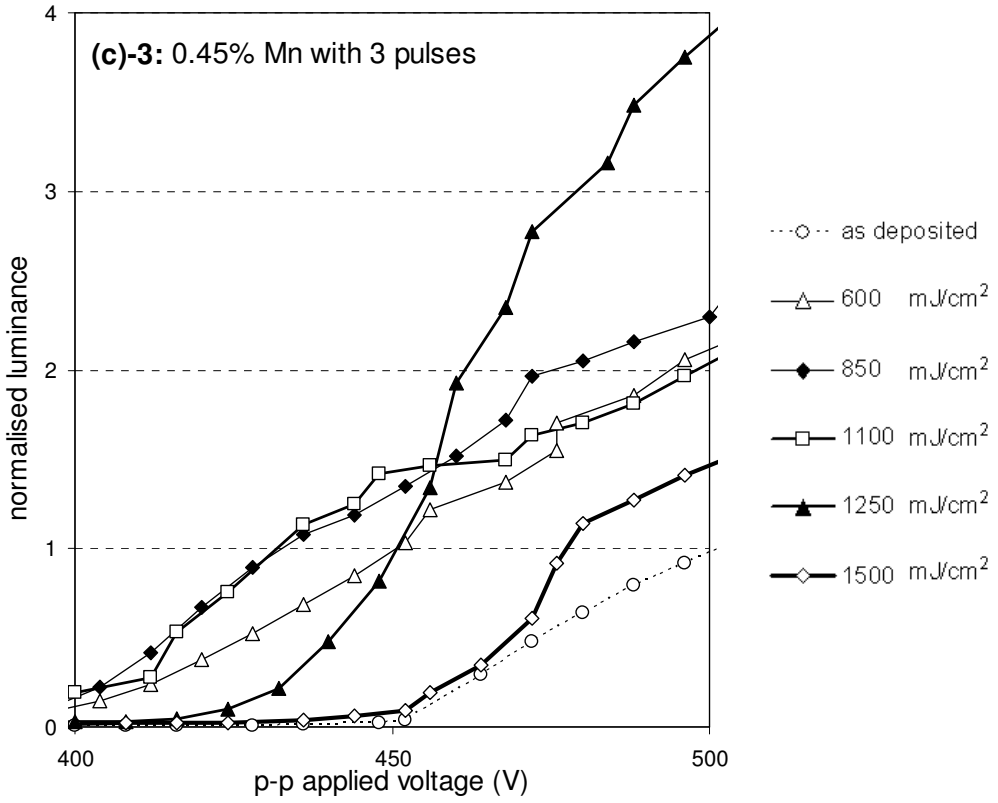

Figure 5-9: Normalised luminance vs drive voltage characteristics of laser and thermally annealed ZnS:Mn based TFEL test devices as a function of fluences and number of pulses applied to the surface of the phosphor for 3 different Mn concentrations: (a), (b) and (c) with 1, 2 and 3 pulses (normalised to the peak luminance of the unprocessed, as-deposited, sample at 500 V).

Figure 5-10 summarises these results obtained for three different dopant concentrations with the normalised luminance obtained at operating voltage (here chosen as 500 V peak to peak) vs fluence for 1, 2 and 3 irradiation pulses.

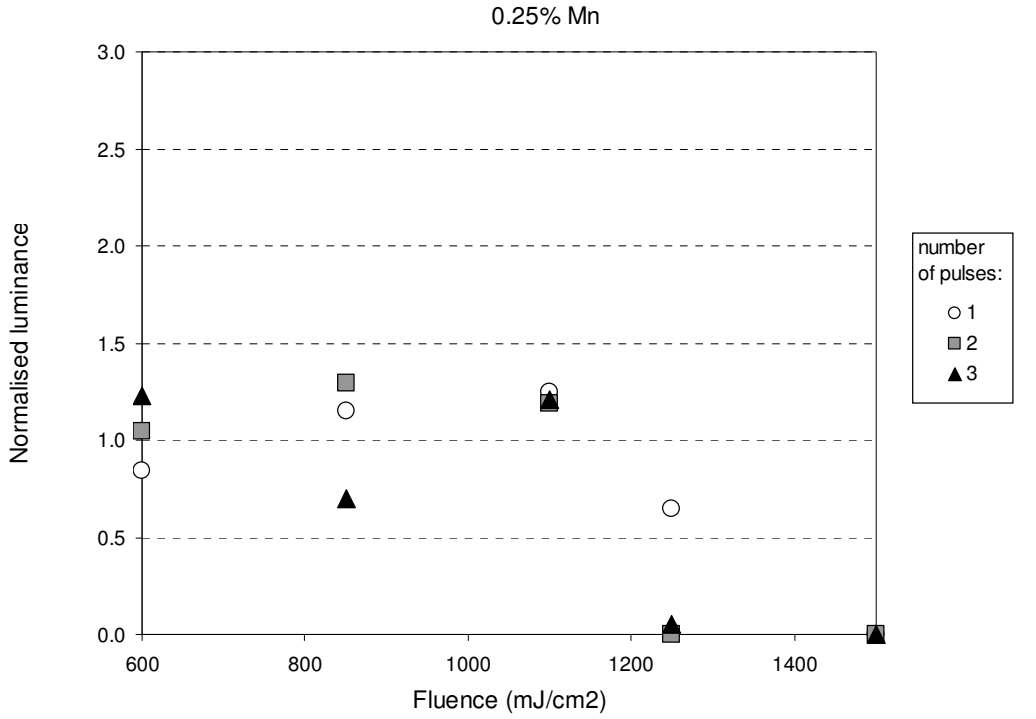
0.25% Mn
Normalised luminance
3.0
2.5
2.0
1.5
1.0
0.5
0.0
600
800
1000
1200
1400
Fluence (mJ/cm2)
number of pulses:
1
2
3

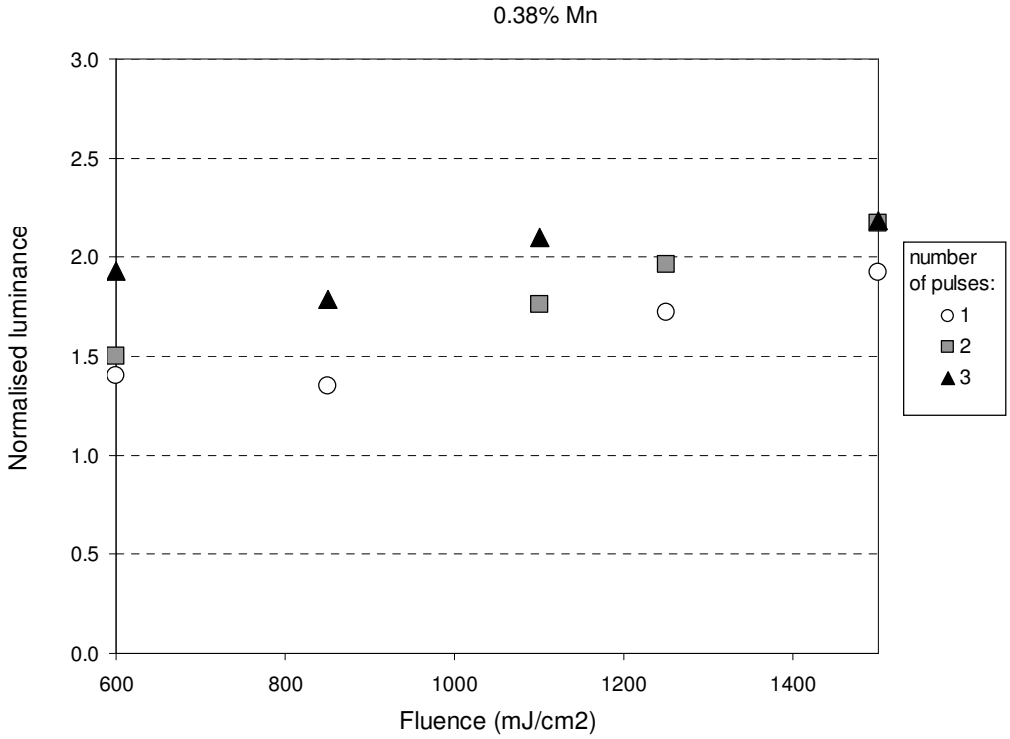
0.38% Mn
Normalised luminance
3.0
2.5
2.0
1.5
1.0
0.5
0.0
600
800
1000
1200
1400
Fluence (mJ/cm2)
number of pulses:
1
2
3

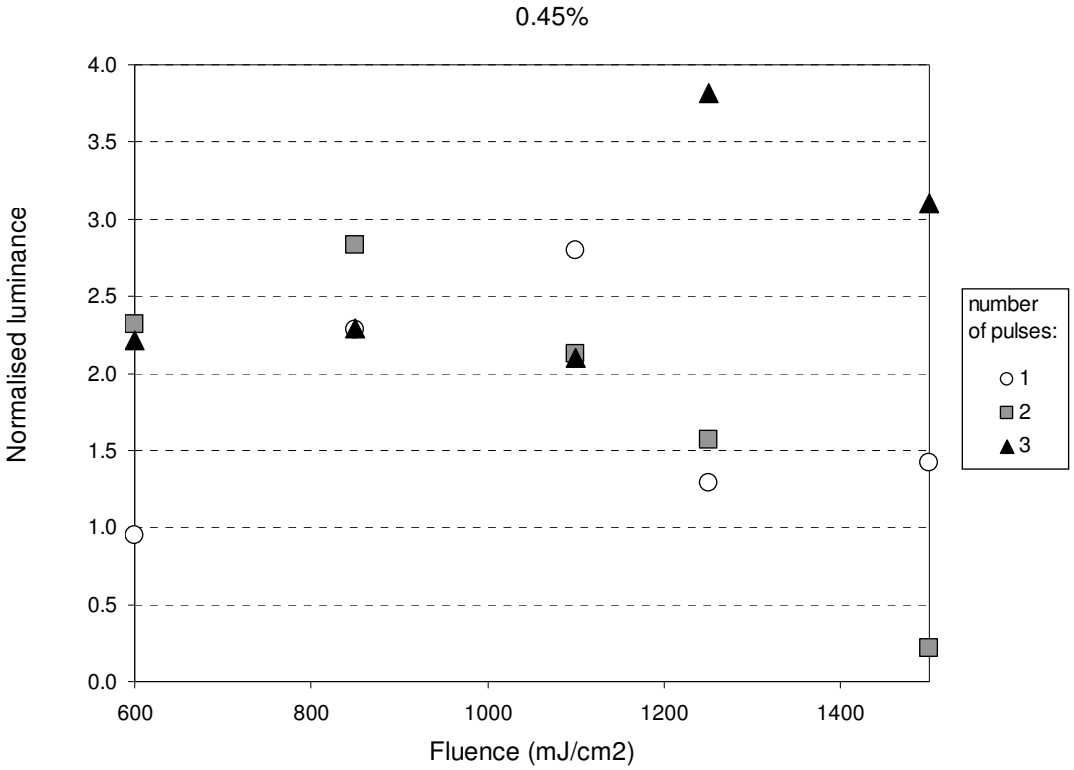

Figure 5-10: Normalised luminance at operating voltage vs fluence of ZnS:Mn laser and thermally annealed based TFEL test devices as a function of number of laser pulses applied to the surface of the phosphor for 3 different Mn concentrations (normalised to the peak luminance of the unprocessed, as-deposited).

This present study aims at determining the effect of laser annealing (with laser annealing) combined with Mn concentration on electroluminescence properties of TFEL devices. These results demonstrate again the benefit of laser processing. Depending on the number of pulses and fluence chosen, each of the three sets of devices with different Mn concentration could result with an enhanced luminance compared to those obtained with thermally annealed only samples. In some cases, this improvement would be equivalent to an increase of more than 200% of luminance. However, for the low Mn concentration results, less than half of the results showed an improvement as depicted on first graph of Figure 5-10 (mainly at low fluences, 1.1 J/cm^2 and below), and the luminance was only increased by 30% at

best (Figure 5-11) for devices with lower luminance. In comparison, devices with the highest Mn concentration showed much larger improvements, up to a 380% increase (1.25 J/cm^2 with 3 pulses). Devices with optimum Mn concentration exhibited luminances just below 1000 cd/m^2, as illustrated on Figure 5-11; however, they showed in general less percentage of improvement compared to the latter, at best 215% increase. In other words, laser annealing was less beneficial to lower Mn concentration TFEL devices.

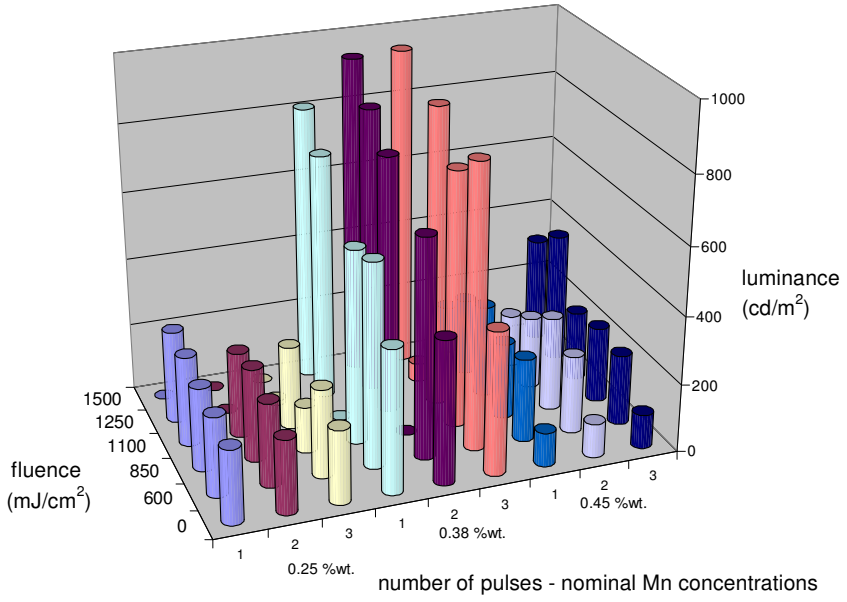

Figure 5-11: Luminance at operating voltage vs fluence of ZnS:Mn laser and thermally annealed based TFEL test devices as a function of number of laser pulses applied to the surface of the phosphor for 3 different Mn concentrations

These results indicate that the luminance improvement, caused by the highly localised annealing process, can lead to a redistribution of the Mn ions in the ZnS film and reduce the concentration of shallow states (i.e. the donor impurities are near the conduction band with an energy difference up to 0.2 eV [95]) which influence the structural and optical characteristics of these devices.

The next step would be to further investigate this study with the implantation of TFEL devices with Mn concentration closer to the optimum. It is anticipated that, from these results, TFEL devices with slightly higher Mn concentration than the optimum and with suitable laser processing parameters would produce enhanced electroluminescence.

5.4 Laser treatment of successive deposited ZnS:Mn layers for electroluminescent devices

In the previous part of this chapter only the top surface was laser annealed and consequently only the upper region of the film (about 200 nm) was modified due to the optical absorption of the laser energy. As an attempt to modify the whole phosphor film and therefore improve EL efficiency, a series of experiments were undertaken to examine the feasibility, and effect, of using successive laser processing of 200nm layers deposited sequentially. Films of ZnS:Mn were deposited 200nm at a time – with growth interrupted to undertake laser processing. A matrix of layer deposition and processing variations was designed to investigate the effect of annealing individual 200nm layers, and in different sequences – as illustrated in Figure 5.11.

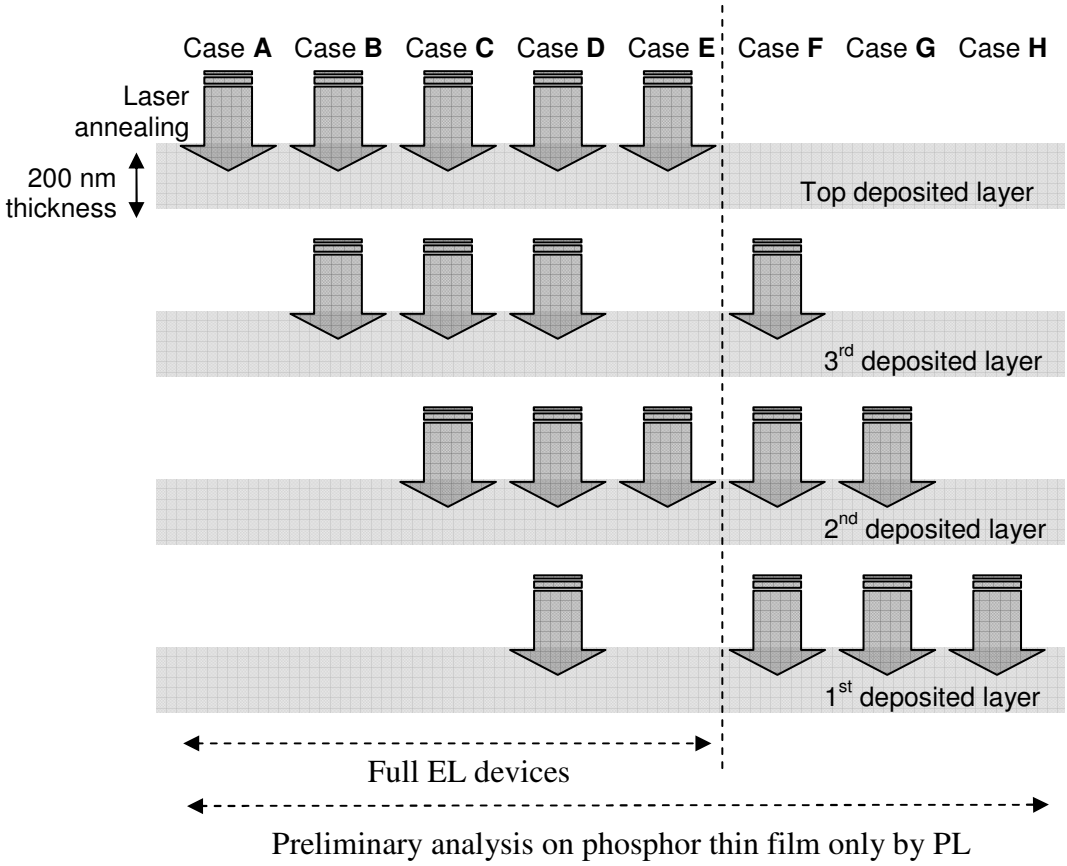

Figure 5-11: Schematic diagram of the sequential laser annealing used for successive deposited 200 nm layers of ZnS:Mn on Si and on Y_2O_3/Si – e.g. in case A only the top phosphor layer (layer 4) is irradiated, in case C the top 3 layers, and in case E layer 4 and layer 2.

5.4.1.1 Photoluminescence analysis

For the phosphor thin film only, eight cases of laser annealing (cases A-H) were performed with six fluences for each case and with single, double or triple pulse irradiation resulting in an array of 144 sequentially irradiated squares on the top surface as represented in Figure 5-12.

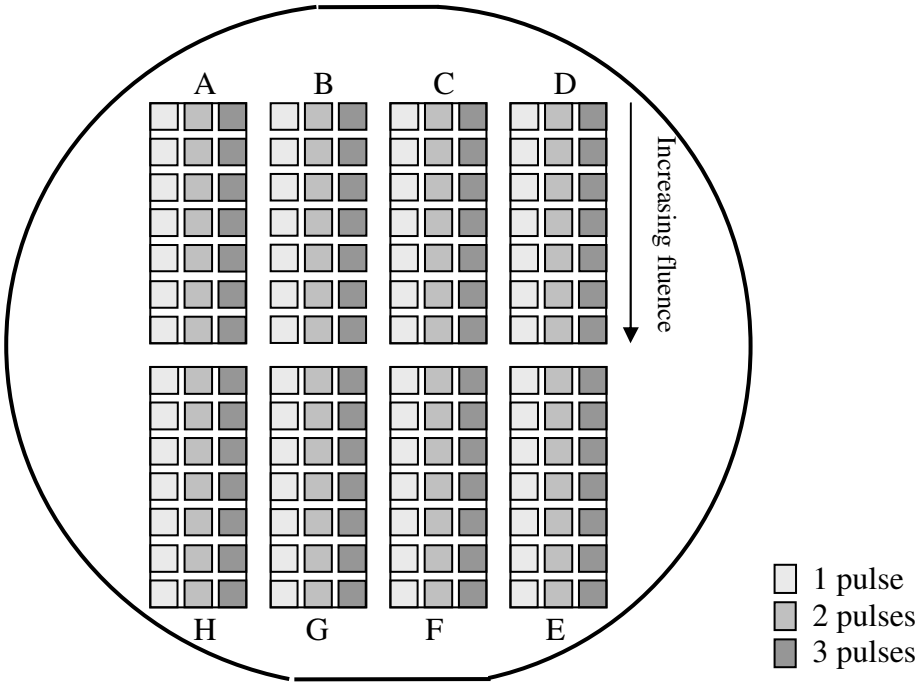

Figure 5-12: Simplified schematic diagram of a wafer used for the laser annealing with photoluminescence analysis

Non-laser annealed areas were also measured for photoluminescence intensity and the results given on Figure 5-13 are relative to the PL intensity data obtained for these non-laser annealed areas. It is important to note that the phosphor thin film did not undergo any post deposition thermal annealing.

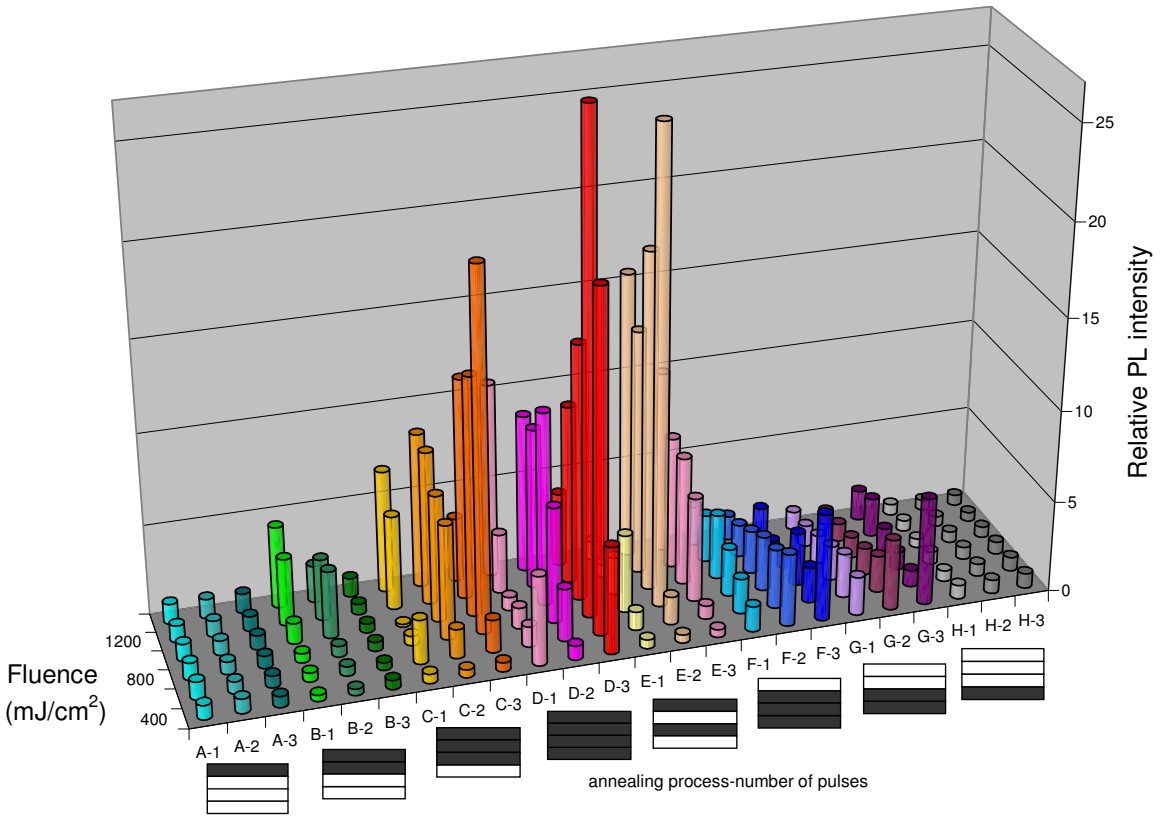

Figure 5-13: Relative photoluminescence (PL) intensity obtained after sequential laser annealings of successive deposited 200 nm layers of ZnS:Mn on Si for cases A-H

These results show clearly the benefit on photoluminescence (PL) efficiency by laser annealing successively deposited layers of a whole phosphor thin film. Indeed, by increasing the number of layers successively laser annealed, the PL intensity is raised dramatically. This effect is further enhanced by selecting the appropriate fluence and number of irradiation pulses. In this work 800 J/cm^2 and 3 pulses were found to be the optimum laser annealing parameters where the PL intensity was increased by a factor of 39 from case A to case D and by a factor of 9 in average over all the results obtained for A and case D. Moreover, this effect is greater for 'top to bottom' laser annealing (cases A to C) than 'bottom to top' laser annealing (cases H to F), the PL obtained for case C is twice better than case F.

5.4.1.2 Electroluminescence analysis

Following the results obtained on photoluminescence, five successive annealing cases were performed on full EL devices at four fluences. Three repeat samples were produced for each combination for the interest of reproducibility of testing by electroluminescence. Post thermal annealing was also applied to some devices to investigate the combined effect. The phosphor layer was laser annealed as represented in Figure 5-14 with different successive layer annealing as per Figure 5-11.

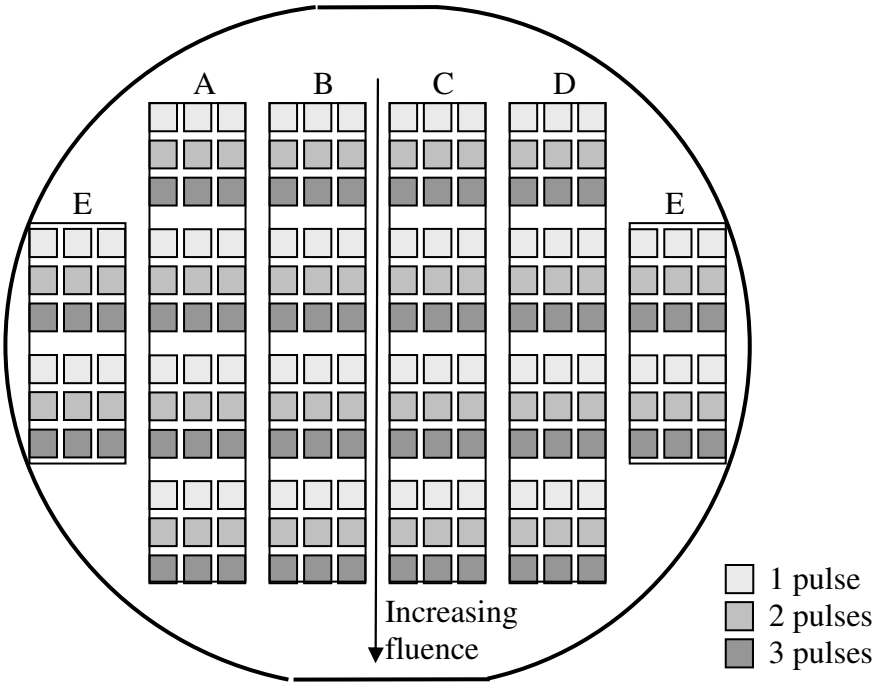

Figure 5-14: Simplified schematic diagram of a wafer used for the laser annealing with electroluminescence analysis

Results obtained with three irradiation pulses are presented here in Figure 5-15. Non-laser annealed test devices were also measured for electroluminescence output which corresponds to a fluence of 0 on the graph.

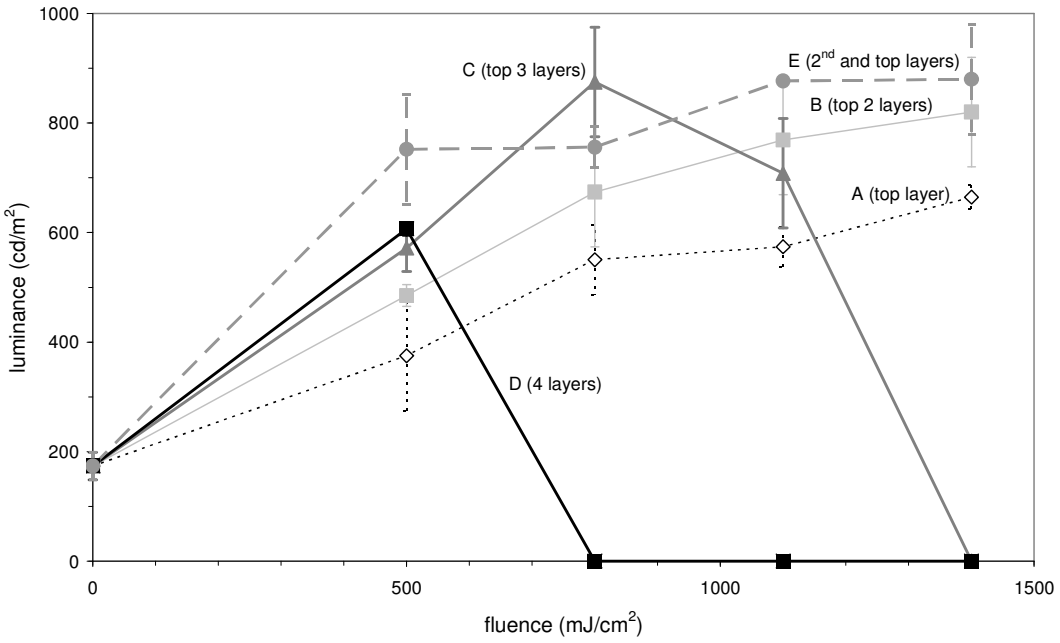

Figure 5-15: Luminance from thin film electroluminescent devices obtained after sequential laser annealings of successive deposited 200 nm layers of ZnS:Mn on Y_2O_3/Si at operating voltage of V_{ppk} = 600 V (V_{RMS} = 212 V)

As with the photoluminescence analysis, these AC excited electroluminescence results demonstrate the improvement of TFEL devices performance by successive laser annealing of deposited layers compared to single top surface laser annealing. The major difference compared to the with PL results is observed for a high number of laser annealed layers and high fluences - where TFEL devices suffer breakdown effects and exhibit zero luminescence. Indeed the maximum luminances of 500 mJ/cm^2 and 1100 J/cm^2 could only be reached for 4 and 3 successively laser annealed layers (cases D and C respectively) to have working devices.

5.5 Discussions and conclusions

TFEL devices suffered electrical breakdown with the combination of all layers being laser annealed and at high fluences. This failure phenomenon is obviously associated with the damage of the bottom dielectric (Y_2O_3) properties; this is most certainly due to a high penetration depth of the laser beam, as associated heating being greater than the phosphor thickness. In other words, to effectively laser anneal a phosphor thin film of a TFEL device, the penetration depth from the laser used should be high enough to obtain the desired rearranged mixed cubic/hexagonal phase in the whole thickness but not too high to modify the electrical properties of the underlying dielectric. If the fluence is high enough, transformation from cubic/hexagonal to cubic phase can occur. This transition has been called 'effective transition depth' and was found to be equal to 150 nm for a fluence of 0.5 J/cm^2 from a thermal simulation performed previously by NTU Display Group [2] also using a KrF laser for ZnS:Mn thin films. Extrapolating the data, as shown on Figure 5-16, obtained from this simulation would give the following approximate effective penetration depths: 340 nm for 0.8 J/cm^2, 470 nm for 1.1 J/cm^2 and 560 nm for 1.4 J/cm^2. These data indicate that the fluence values chosen for the work reported here were probably too high, and would ideally be repeated at lower fluences as future work. Moreover from this extrapolation, for a desired effective penetration depth of 200 nm, the fluence would be approximately 560 mJ/cm^2 which could be enough to achieve total phase transformation.

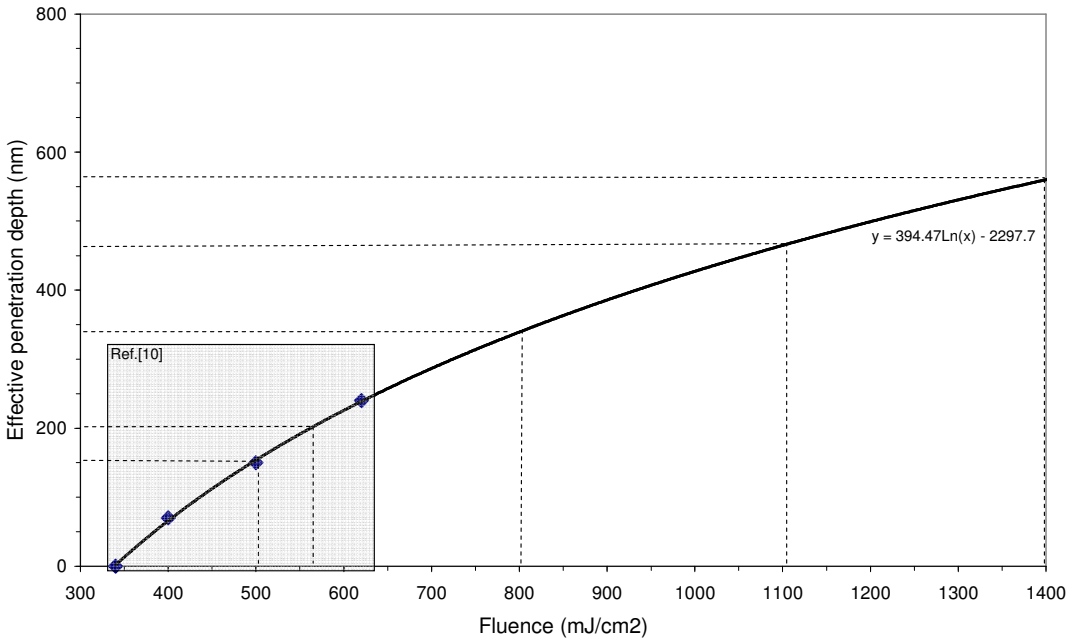

Figure 5-16: Luminance from thin film electroluminescent devices obtained after sequential laser annealings of successive deposited 200 nm layers of ZnS:Mn on Y_2O_3/Si

Large-area TFEL devices with successive laser annealed phosphor thin films on low cost glass or plastic substrates could become a key technology for many applications where high thermal annealing (using a heater) is required for functionalisation of the layers, but is not feasible due to the low temperature requirements of the substrates.

As a summary of this chapter, a detailed investigation into the effect of laser processing of ZnS:Mn phosphors for TFEL devices as a function of Mn concentration has been presented. The results demonstrate that the combination of dopant concentration variation and laser annealing conditions can be engineered to produce optimised performance – with the results highlighting how future optimisation work could be undertaken. In particular, the investigation into the use of successive laser annealing has demonstrated a novel processing technique that is

potentially capable of modifying the crystal structure of the full phosphor thickness resulting in highly enhanced TFEL devices.

Chapter 6 Performance enhancement of TFEL devices using novel fabrication processes

6.1 Introduction

The main objective of this chapter is to present an evaluation of TFEL devices fabricated using RF magnetron sputtering compared to devices produced using alternative industrial techniques. This has been possible via the involvement by the author in a series of device fabrication and characterisation studies as part of two Technology Strategy Board collaborative research and development projects concerned with EL device innovations – the HESSLIS project and the SRELD project. A range of ZnS:Mn depositions techniques were employed to compare the performance of the resultant films in these devices, including RF magnetron sputtering, Atomic layer deposition, and Hi rate Target Utilisation Sputtering (HiTUS). The author's characterisation work was used to investigate these techniques for potential application to device fabrication for sunlight readable indicator display systems (SRELD) and light emitting devices on plastic substrates (HESSLIS)

Using RF magnetron sputtering throughout this research for the deposition of the different layers which constitute the TFEL devices has shown some inconstancies. Series of batches have been produced throughout the lifetime of the sputtering targets and have been compared in terms of the luminescent properties such as PL intensity peak, intensity ratio of red and yellow emissions, decay constant, and

electroluminescence. However, the results (shown in Chapter 4) have exhibited a 'shifting' of nominal manganese concentration with similar co-sputtering target ratios. This may be due to RF magnetron sputtering instabilities which are mainly associated with the surface profile of the target through its lifetime, i.e. the race-track grows deeper into the target and evolves during its operation with an increase in deposition rate. This race-track occurs because of the physical effect of RF magnetron sputtering which produce a helicoidal trajectory to the electrons caused by the combination of magnetic and electric fields. Therefore, the target is not consumed homogenously because of the localisation of the plasma, leading to sputtering rate instabilities and poor target utilisation.

To overcome these inconsistencies and to reduce the sulphur densities acting as donors in zinc sulphide films, an alternative and novel deposition system was investigated with reactive sputtering in an argon-hydrogen sulphide ($Ar:H_2S$) environment for the deposition of thin film phosphors at Plasma Quest Limited (PQL) – as part of the HESSLIS collaborative project, which is explained in the first part of this chapter. This system has demonstrated higher process stability, higher growth rates and higher film densification than the traditional RF magnetron sputtering used previously in this research, and is likely to be the deposition method of choice for any future exploitation of the research.

In the second part of this chapter, the results from films deposited by atomic layer deposition are presented as an alternative technique with potentially higher thin film quality than RF magnetron sputtering. This deposition technique was applied for the fabrication of LETFEL devices (see Chapter 2) through a collaborative project examining the use of LETFEL technology in avionic display applications - SRELD (Sunlight Readable ELectroluminescent Display).

6.2 High target utilisation sputtering (HiTUS) vs RF magnetron sputtering

6.2.1 Experimental

Unlike traditional RF magnetron sputtering, where the plasma is generated in the region of the electrode, high target utilisation sputtering (HiTUS) from PQL relies on the generation of plasma remotely from the targets. The system is represented in Figure 6-1.

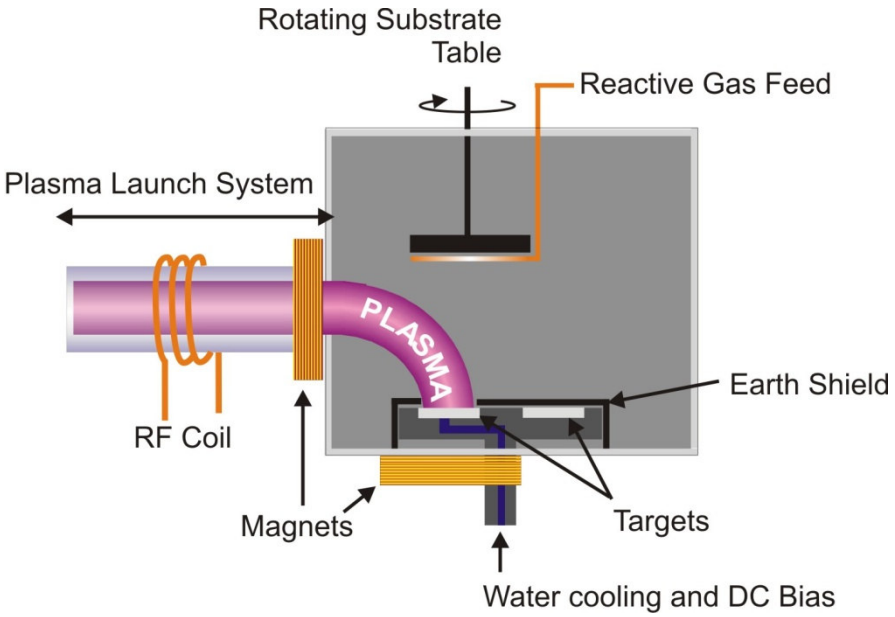

Figure 6-1: Schematic diagram of HiTUS system [10]

An RF coil antennae surrounding a quartz glass tube is located in a side arm (referred to as the plasma launch system, or PLS) adjacent to the vacuum chamber. The plasma is initiated here and amplified by a launch electromagnet at the exit of the PLS. A steering electromagnet is then used to focus and control the direction of the plasma. With careful control of the current flowing through each of these electromagnets, the plasma beam can be directed such as to cover the full surface area of the target. With the application of a sufficient negative bias, argon ions are

then accelerated into the target resulting in a high current density over the full surface area of the target. Hence the target is uniformly eroded resulting in a significant reduction in target poisoning over conventional magnetron sputtering and hence also a much improved deposition rate when depositing non-metallic thin films such as phosphors.

The PQL HiTUS system used for this work accommodates four 4 inches (~10 cm) diameter, 6 mm thick water cooled targets. This allows for the deposition of complete devices without needing to break the vacuum and potentially introduce contaminants.

6.2.1.1 HiTUS deposition

All HiTUS depositions in this collaborative project were undertaken by Dr. Steve Wakeham (from PQL) and all materials were deposited from a metallic target in a reactive gas mixture of argon and either oxygen or hydrogen sulphide. Prior to depositing each layer, the substrates were immersed in a diffuse, high density plasma. This is easily achieved using HiTUS by switching off the steering electromagnet. The impinging low energy (less than 50 eV) argon ions remove volatile species from the substrate surface helping to promote adhesion of subsequent layers. After this substrate pre-conditioning, the target is sputter cleaned for up to 5 minutes prior to admission of the reactive gas. Deposition conditions are then allowed to stabilise for a further 5 minutes before the shutter, which is located immediately adjacent to the substrates, is opened and deposition commences.

Both the Y_2O_3 and the ZnS:Mn were also deposited with no substrate heating, making this procedure directly transferable to plastic substrates. Yttrium and ZnS:Mn

(0.4%, 0.5%, and 0.6% Mn) targets were used for the reactive depositions (A summary of the deposition conditions used for each of the materials within the EL structure is given in Table 6-1.

Material	Process pressure (mbar)	RF power (kW)	DC power (kW)	Sub. Temp. (°C)	Dep. Rate (nm/min)
ITO	3.6×10^{-3}	1.0	0.81	< 70 °C	87
Y_2O_3	4.0×10^{-3}	1.99	1.50	< 70 °C	28
ZnS:Mn	7.7×10^{-3}	0.79	0.20	< 70 °C	52

Table 6-1: HiTUS deposition parameters

6.2.1.2 RF magnetron sputtering

For a comparative study, two separate RF magnetron sputtering systems from NTU were also used for the deposition of Y_2O_3 and ZnS:Mn (undertaken by the author) and ITO (undertaken by Dr. Costas Tsakonas). A base pressure of 1.2×10^{-6} mbar was used for the Y_2O_3 and ZnS:Mn layers and the second system used to deposit the ITO was evacuated to a base pressure of 1.6×10^{-7} mbar. Diffusion pumps backed by rotary pumps were used to attain this vacuum in both plants. The substrates were loaded into the main chamber through a side load lock. Two RF magnetron electrodes were positioned at 30º to the vertical and 15 cm from the substrate surface for the dielectric/phosphor depositions. The same configuration was used for the ITO coatings but with a target-substrate separation of 10 cm. The two main chambers were equipped with mass flow controlled gas lines providing 100% Argon for the EL device layers (dielectric and phosphor films) and 0.2 % Oxygen/Argon for the ITO contacts.

Alkali-free borosilicate glass and n-type silicon substrates were used in this study. Prior to deposition the glass and Si wafers were baked at 350ºC and 500ºC respectively. All targets were pre-sputtered for between 2 and 5 minutes prior to deposition. The optimised ZnS:Mn layers (see Chapter 4) were deposited by co-sputtering a 99.99% pure ZnS target and a 99.95% pure ZnS target doped with 1.0 wt.% Mn. Two RF power supplies providing 80 W to the ZnS target and 40 W to the target doped with Mn. All targets were provided by Testbourne UK. Table 6-2 shows the growth parameters for all layers (the total power on both targets is shown for the ZnS:Mn layer).

Material	Process pressure (mbar)	RF power (W)	Sub. Temp. (°C)	Dep. Rate (nm/min)
ITO	2.66×10^{-3}	50	180 °C	4
Y_2O_3	6.66×10^{-3}	120	200 °C	1.5
ZnS:Mn	6.66×10^{-3}	120	200 °C	3.7

Table 6-2: RF magnetron sputtering deposition parameters

6.2.1.3 Comparison of sputtering techniques

The primary difference between the two sputtering techniques described above is that HiTUS decouples the ion density, which is controlled by the RF antennae power supply, from the ion energy, which is controlled by the DC bias applied to the target. This offers greater control over the growth process due to the independent control of multiple sputtering parameters.

From Tables 6-1 and 6-2 it is clear that the HiTUS system also enables growth rates in excess of an order of magnitude greater than those offered by RF magnetron sputtering. Whilst higher deposition rates can be achieved using magnetron

sputtering, this is to the detriment of the film properties since the RF power must be increased, with concomitant increase of the target bias, resulting in damage to film growth due to high energy ion bombardment [96, 97]. Also of note is that these high growth rates are achieved using no substrate heating hence making HiTUS ideal for applications that require plastic substrates.

6.2.1.4 PL and EL measurement facility

PL and EL measurements were performed by the author and Dr. Costas Tsakonas.

The PL measurements were carried out in a dark room and at ambient temperature using a Laser Science VSL-337 ND nitrogen laser operating at 337 nm and 4 ns pulses. A power of 400 μJ/pulse with a 20 Hz repetition rate was used. The intensity of the PL emission was measured using an S2000 Ocean Optics fibre optic spectrometer.

The EL measurements were also carried out (by the author) in a dark room. A TTi TG1010 programmable function generator, a voltage amplifier (maximum supply of 900 V peak to peak) and a Minolta LS-110 luminance meter were used to drive the devices and record their luminance. The input devices were all connected in series to a current limiting 100 kΩ resistor. All EL measurements were carried out using a sinusoidal waveform voltage at a frequency of 1 kHz with voltage increments of 8 V peak to peak and 5 s duration.

6.2.2 Photoluminescence results

Prior to making a complete electroluminescent device using ZnS:Mn as the active, light emitting layer, individual films were first optimised for photoluminescence (PL). Three different metal alloy targets were used to investigate the effect of

different Mn concentrations on the PL properties of ZnS:Mn thin films deposited by reactive sputtering using HiTUS. Single layers of ZnS:Mn with thicknesses of between 0.5 and 1.0μm were initially deposited at room temperature onto glass microscope slides from Zn targets doped with 0.4, 0.5 and 0.6 wt.% Mn. For each of the three Zn:Mn targets the H_2S flow rate was optimised to produce films that exhibited intense PL when excited by a nitrogen gas laser. As shown in Figure 6-2, the Zn target doped with 0.6 wt.% Mn consistently gave films with the highest PL intensity. It is important to note that this result differs significantly from those obtained from RF sputtered solid targets (nominal 0.38 wt.% Mn) or from powder target (0.43 wt.%). Therefore, the use of reactive sputtering with HiTUS indicates that the PL optimum is different due to altered deposition conditions, and the use of reactive sulphur, which would be expected to improve stoichiometry (this will be further investigated as future work). The peak intensity of the emitted light is centred at approximately 600 nm, which is close to the typical 580 to 590 nm characteristic emission of the Mn phosphor, but where the shift may be due to the enhanced sulphur environment – this will be investigated as future work. At the higher Mn concentrations, there is some evidence that the peak shifts to lower wavelengths.

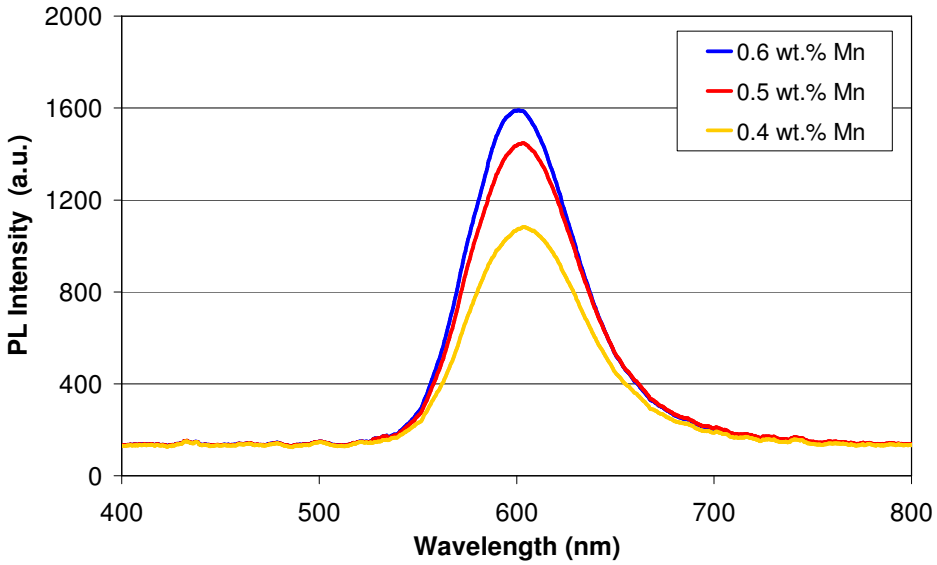

Figure 6-2: HiTUS results showing luminous intensity as a function of wavelength for ZnS:Mn films optimised with different concentrations of Mn in the target.

By increasing the H_2S flow rate during deposition the coatings are observed to become fully transparent. For optimized, fully transparent films, the deposition rate can be increased up to 90 nm/min for a target power of 0.5 kW. However, whilst this high deposition rate did produce coatings that displayed intense PL, they exhibited very poor breakdown properties when incorporated as part of an EL structure. ZnS:Mn films produced at lower powers were seen to exhibit excellent PL and EL properties. Figure 6-3 shows that for optimum PL a target power of approximately 200 W should be used, giving a deposition rate of 52 nm/min. The results of optimised ZnS:Mn films deposited using RF magnetron sputtering have also been included as a bench mark. These films were deposited at 200 °C and subsequently post annealed at 500 °C. The HiTUS films were deposited with no substrate heating or post deposition annealing. Whilst the film deposited at 200 W was slightly thicker than the others, this only accounts for a small proportion of the increase in PL intensity. The observed peak shift might be due to enhanced sulphur content.

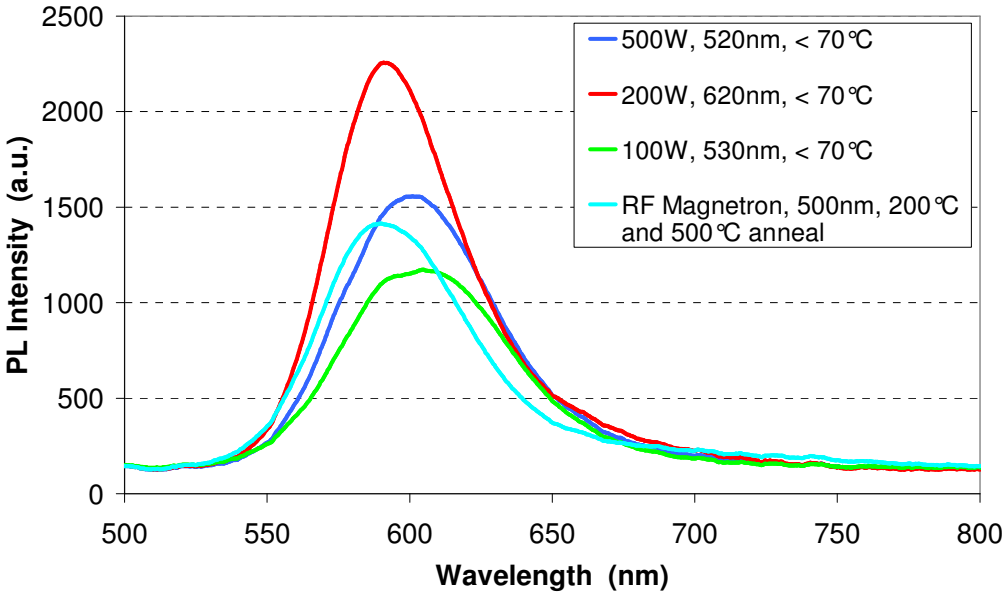

Figure 6-3: PL intensity as a function of target power for HiTUS ZnS:Mn films deposited with no substrate heating or post deposition annealing (0.6 wt.% Mn). Results of high temperature RF magnetron sputtering have been included for comparison.

Following the successful deposition of ZnS:Mn onto glass and Si substrates, single layers were also deposited onto Kapton™ (50 µm), planarised polyethylene naphathalate (PEN - 125 µm) and polyethylene terephthalate (PET - 188 µm) using HiTUS. Coatings with a thickness of up to 1.0µm resulted in no deterioration of the flexible substrates.

The positive PL results indicated that these films should be excellent candidates for EL devices. Dielectric layers of Y_2O_3 and Ta_2O_5 were also deposited onto glass and polymeric substrates with excellent transparency and breakdown properties, making possible the fabrication of completely transparent and flexible, AC thin film electroluminescent (ACTFEL) test devices.

6.2.3 Electroluminescence results

The fabrication and characterisation of ACTFEL test devices using both HiTUS and RF magnetron sputtering was undertaken by the author as part of the study of TFEL. The double insulating layer structure has been used for all devices with Y_2O_3 being used as the dielectric. Devices were initially deposited onto silicon substrates with ITO being used as the top contact. The possibility of making completely transparent devices on both glass and flexible substrate materials was then considered. The results in this section focus on a comparison of the two sputtering techniques to deposit working EL devices on both silicon and glass substrates. Working EL structures were also deposited onto planarised PET using HiTUS. Due to the higher processing temperatures employed by RF magnetron sputtering, it was not possible to deposit devices onto plastic substrates using this technique.

6.2.3.1 EL devices deposited onto Si wafers

Figure 6-4 shows the luminance as a function of applied peak to peak voltage (L-V) for an EL device deposited using RF magnetron sputtering. It is clear that heating the sample not only reduces the threshold voltage but also increases the maximum attainable luminance. This is to be expected as heating of the ZnS:Mn layer results in a greater number of Mn ions finding their energetically favoured position as substitutes for the Zn atoms within the host lattice. In this position they readily contribute to the emission of light as active, luminescent centres. When located as interstitial defects they simply act as scattering centres for electrons. The effect of annealing the complete EL structure is that the hot electrons injected from the interface states are released at lower fields and hence the threshold voltage for EL emission occurs for lower voltages. Above the threshold voltage the gradient of the

L-V curve also becomes flatter for an anneal temperature of 600 °C indicating an increased energy distribution of interface states [67]. After post annealing in a vacuum at 600 °C the luminance is seen to increase to approximately 500 Cd/m^2 at 750V.

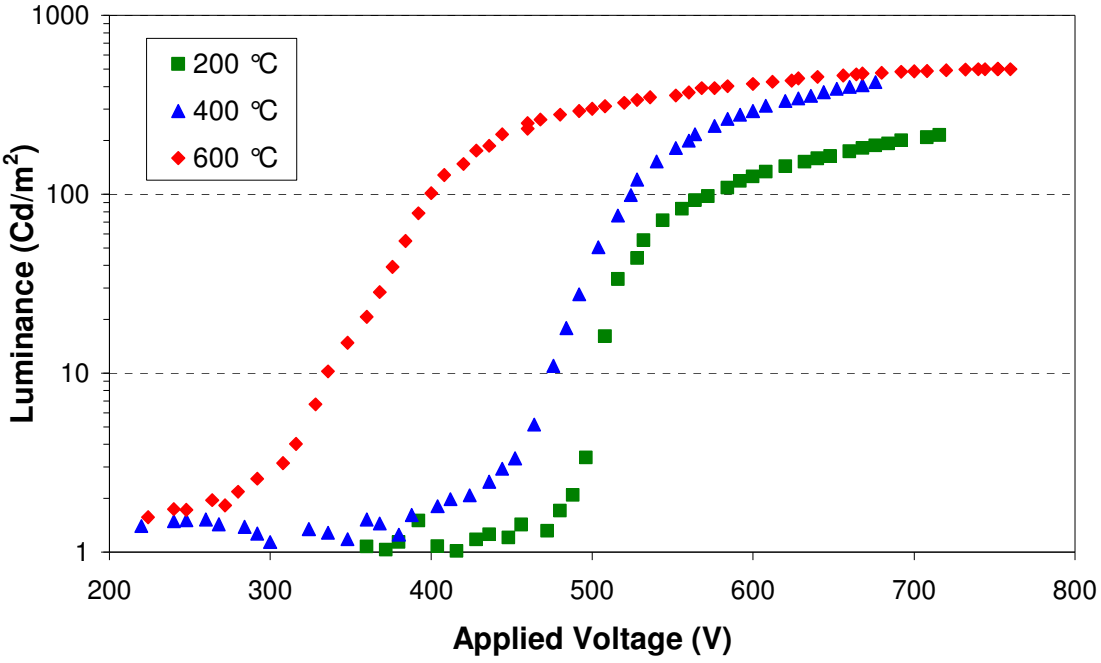

Figure 6-4: Luminance as a function of applied peak to peak voltage for an EL device on silicon fabricated using RF magnetron sputtering.

For comparison, the results of an equivalent device incorporating ITO and dielectric layers deposited using RF magnetron sputtering but with the ZnS:Mn deposited using HiTUS with no substrate heating are shown in Figure 6-5. A maximum luminance of 740 Cd/m^2 is obtained for an applied peak to peak voltage of 690 V. Of significance is the sharpness of the turn-on when the structure is heated to 600 °C. This suggests that devices made with HiTUS ZnS:Mn result in an interface region with a more concentrated distribution of trapped states. The increase in threshold voltage when increasing the anneal temperature from 400 to 600 °C is an interesting result that

may imply a modification of the density of interface states via the removal of higher energy states (traps), or possibly a modification of the high field resistivity of the ZnS:Mn leading to increased threshold for impact excitation. This is to be investigated further. An increase in luminance of approximately 315 Cd/m^2 for a rise in voltage of just 50 V is seen. The same rise in voltage for the devices fabricated using ZnS:Mn deposited by RF magnetron sputtering sees only a 17 Cd/m^2 increase from 300 to 350 V, the steepest section of the L-V curve. This makes the drive electronics potentially much easier and cheaper to implement for devices deposited using HiTUS.

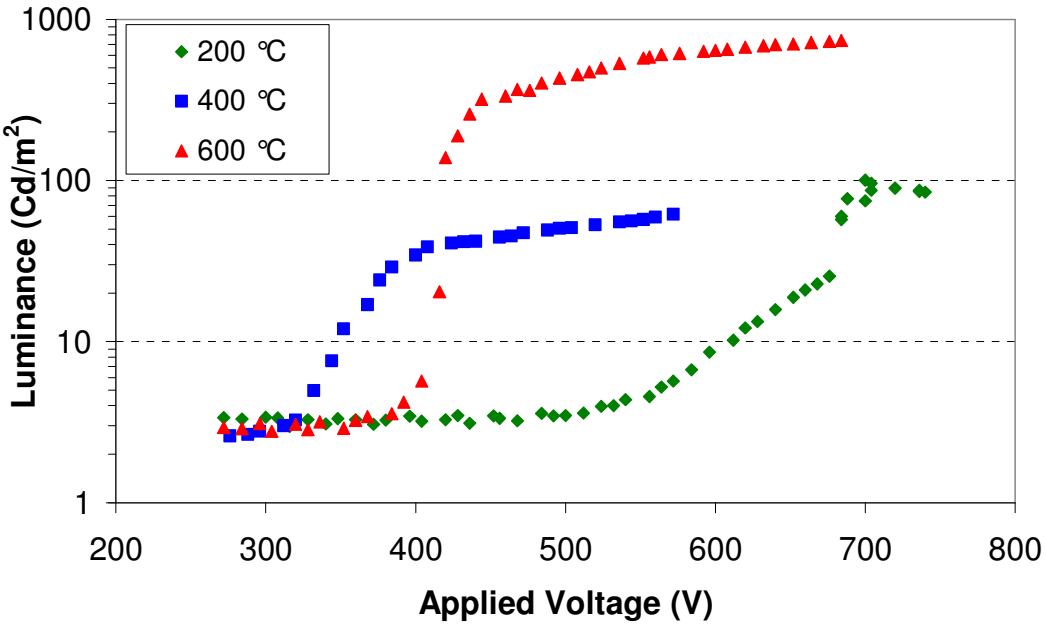

Figure 6-5: Luminance as a function of applied peak to peak voltage for an EL device on silicon fabricated using RF magnetron sputtering and HiTUS ZnS:Mn.

Other TFEL devices comprising RF sputtered ZnS:Mn phosphor and HiTUS deposited dielectrics were fabricated and L-Vs are also presented here for comparison in Figure 6-6.

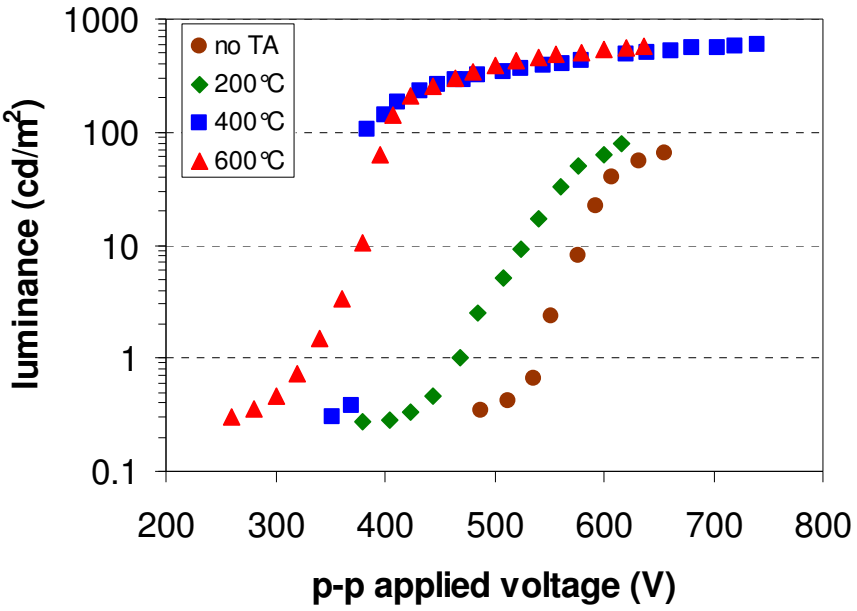

Figure 6-6: Luminance as a function of applied peak to peak voltage for an EL device on silicon fabricated using RF magnetron sputtering and HiTUS dielectric layers.

6.2.3.2 EL devices deposited onto glass substrates

Completely transparent EL devices have been fabricated on glass substrates using an ITO back contact layer. The transmission of the devices at 595 nm, taking the uncoated glass substrate as the reference, is approximately 96 % and the average visible transmission from 400 to 750 nm is 87%.

Figure 6-7 shows an L-V curve for a complete structure deposited using HiTUS, with no substrate heating or post deposition annealing. The effect of annealing at 200 °C is also shown. This results in little improvement of the device. For comparison, the results of post deposition annealing a device deposited at the substrate temperatures quoted in Table 6-2 using RF magnetron sputtering is also shown. The maximum luminance is significantly higher with substrate heating. However, this obviously precludes the use of these devices for plastic applications. Devices deposited at ambient substrate temperature using RF magnetron sputtering exhibit no PL or EL

and also breakdown very easily. It should be noted that the Y_2O_3 layer used in the HiTUS devices has not yet been optimised.

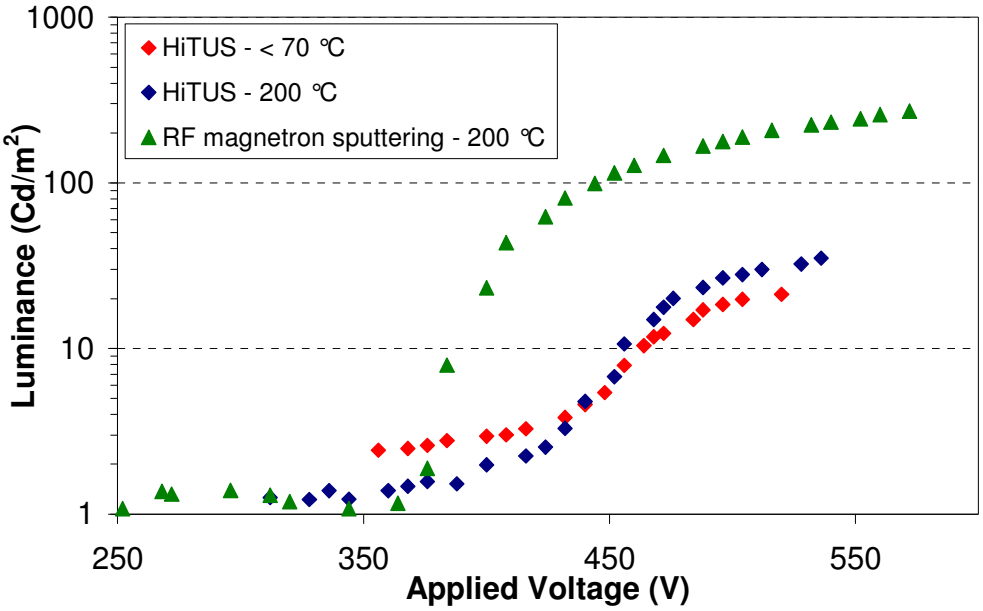

Figure 6-7: Luminance of a transparent EL structure deposited onto glass vs drive voltage with no substrate heating and with or without post deposition annealing (200°C or < 70°C) using HiTUS . Equivalent RF magnetron sputtering deposited devices at 200°C are also shown.

6.2.4 Laser annealing of HiTUS ZnS:Mn based EL devices

A series of laser annealing experiments using the Lambda Physik LPX 305i excimer laser charged with Krypton Fluoride (KrF), emitting pulses of 20 ns at 248 nm (5.13 eV photon energy) were performed on a single silicon wafer with dielectric/electrodes layers (Y_2O_3/ITO) deposited at NTU at 200° C and the optimised phosphor layer deposited at PQL using the HiTUS system. Laser annealing took place before the top dielectric layer was deposited and was undertaken by the author (and Costas Tsakonas).

Top ITO contacts of 1mm in diameter were deposited at NTU at ambient temperature. Laser fluences of 0.6, 0.8, 1, 1.2, 1.4 and 1.6 J/cm^2 were used and

various areas were irradiated by either 1 or 2 pulses at all the above fluencies as shown in Figure 6-8. The results are regrouped in the graph of Figure 6-9.

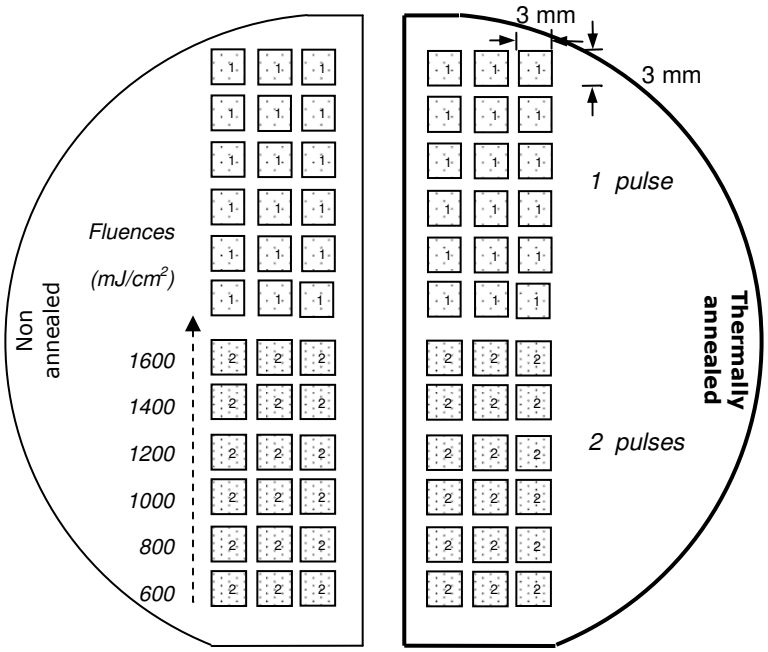

Figure 6-8: Sample pattern of laser processed HiTUS ZnS:Mn deposited on Y_2O_3/Si wafer.

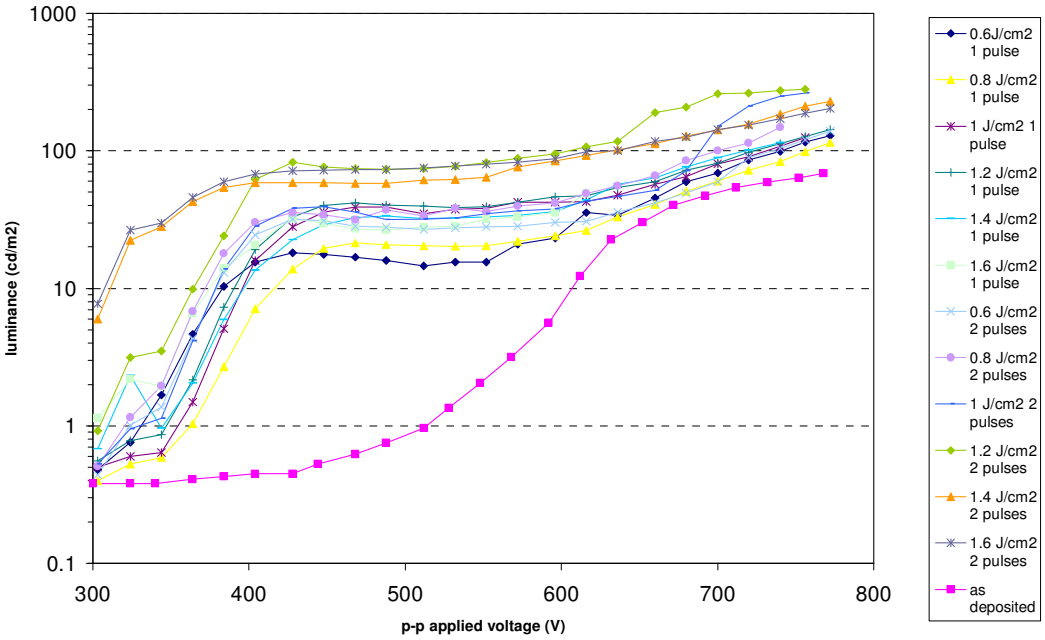

Figure 6-9: Luminance against operating voltage of HiTUS laser processed ZnS:Mn based EL devices for 1 and 2 pulses at fluences ranging from 0.6 to 1.6 J/cm^2 and non laser annealed EL devices (as deposited).

There is an unequivocal increase of luminance for all laser processed areas compared to as-deposited areas. There is also a continuous decrease of the threshold voltage for increasing laser fluence. For all laser processed areas the luminance reaches a distinct plateau before continuously increasing again. Numerical simulations indicate that the laser absorption and hence the annealing depth for ZnS thin films at 248 nm is about 200 nm and since the current ZnS layers are 800 nm thick a considerable part of the phosphor layer is not affected as significantly by laser annealing as the top 200nm layer. This may be related to the two stage luminescent emission, but is not fully understood, and is subject to ongoing work. The maximum luminance is observed for 1.2 J/cm^2 and 2 pulses at 280 cd/cm^2. The maximum luminance for the 1 pulse series is also observed for the 1.2 J/cm^2 fluence at 178 J/cm^2. The as-deposited areas achieved a luminance level on average of 68 cd/cm^2.

For comparison of EL devices performance, the luminance obtained at an operating voltage of 500 V was plotted as a function of fluence for 1 and 2 pulses as shown Figure 6-10.

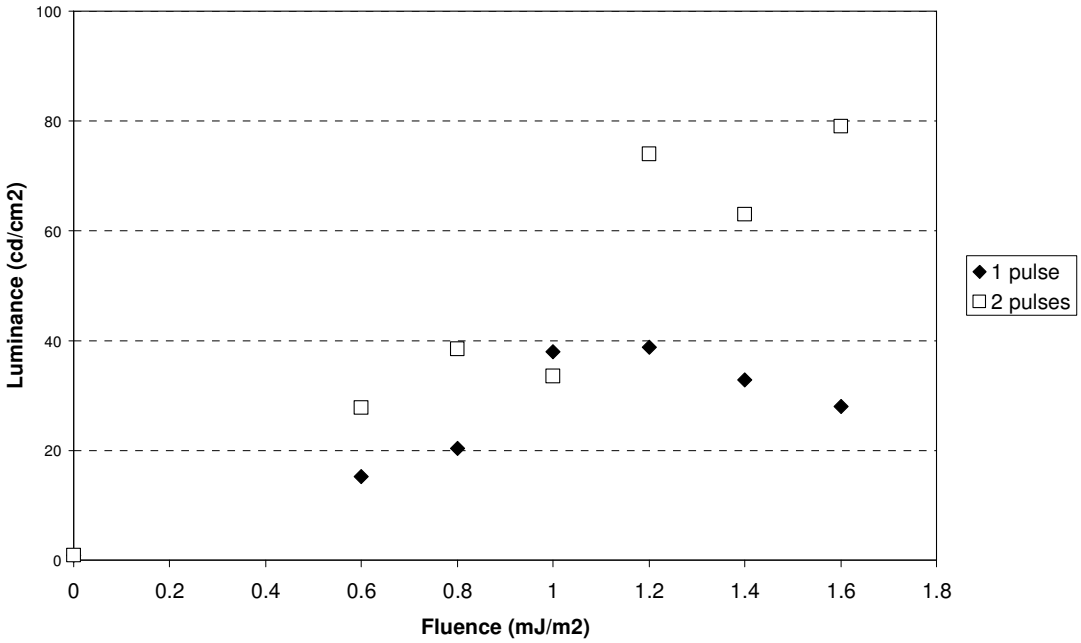

Figure 6-10: Luminance vs fluence of HiTUS laser processed ZnS:Mn based EL devices for 1 and 2 pulses.

6.3 SRELD

6.3.1 Introduction

The second collaborative project to which the work presented here contributed was the 'Sunlight Readable EL device' (SRELD) project.

This collaborative research project was based on the application of the NTU LETFEL device technology [58, 98] which is illustrated in Figure 6-11.

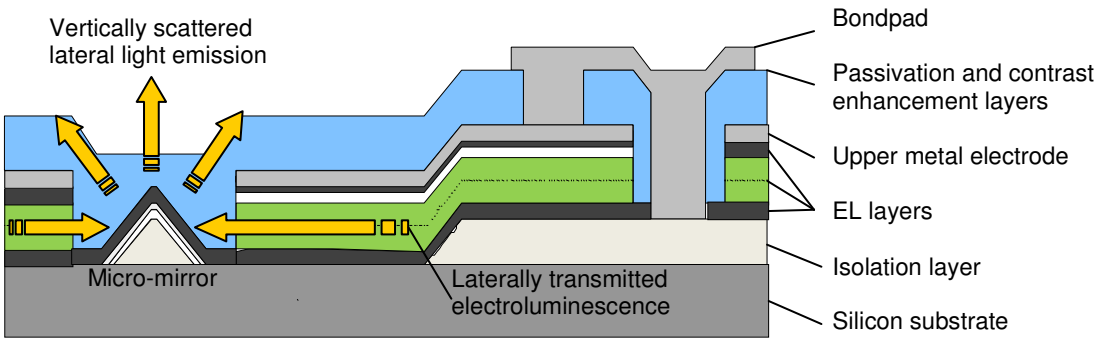

Figure 6-11: Schematic of LETFEL device principle, showing light generation by thin film electroluminescence and the light outcoupling via internal light guiding and reflection away from the substrate by micro-mirrors [32]**.**

The SRELD project aimed to transfer the lab based LETFEL technology to a commercially viable production and process route, in order to produce display devices suitable for integration into a full system to address a critical display requirement for sunlight readable vehicle displays – particularly avionic indicators.

A part of this project was to optimise the light output, undertaking evaluation trials and miniaturising the electronics. However, the initial devices exhibited poor stability that precluded further detailed evaluation and which consequently required a re-direction of the project effort to ensure the feasibility of transfer of the device fabrication to a successful process route.

Extensive testing of each layer and process identified that the quality of the deposited dielectrics was the primary area of technical development required for the success of the project, hence this became the focus of development – along with the knowledge transfer required to establish a process route for the core technology.

The project has also benefited from the collaboration with Plasma Quest Ltd. to evaluate the use of HiTUS technology as an alternative to ALD for the EL deposition.

In terms of the research work presented here, the RF magnetron optimisation of ZnS:Mn deposition was used in the early stages of device fabrication, and the author undertook the characterisation of the devices fabricated towards the end of the programme which utilised ZnS:Mn films deposited by ALD.

SRELD devices were fabricated by the Micro and Nanotechnology Centre and Qudos Ltd., at the Rutherford Appleton Laboratory using commercially available atomic layer deposition (ALD) from Planar in Finland for the ZnS:Mn films, as described in Chapter 2. Each device is comprised of 28 separately addressable light emitting legends (as illustrated on Figure 6-12), which use an array of the LETFEL micro-mirrors based on a three pointed star design as shown in Figure 6-13.

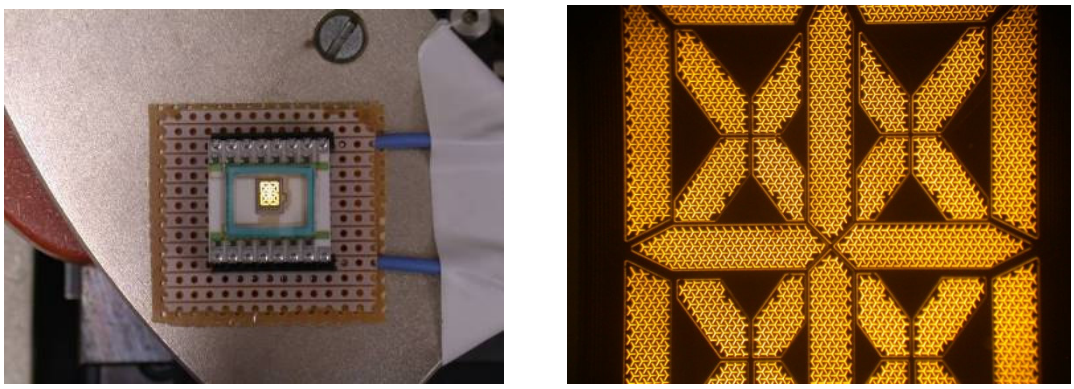

Figure 6-12: Photograph of SRELD devices chip mounted on sample holder to be tested for electroluminescence (on left) - and its close up (on right)

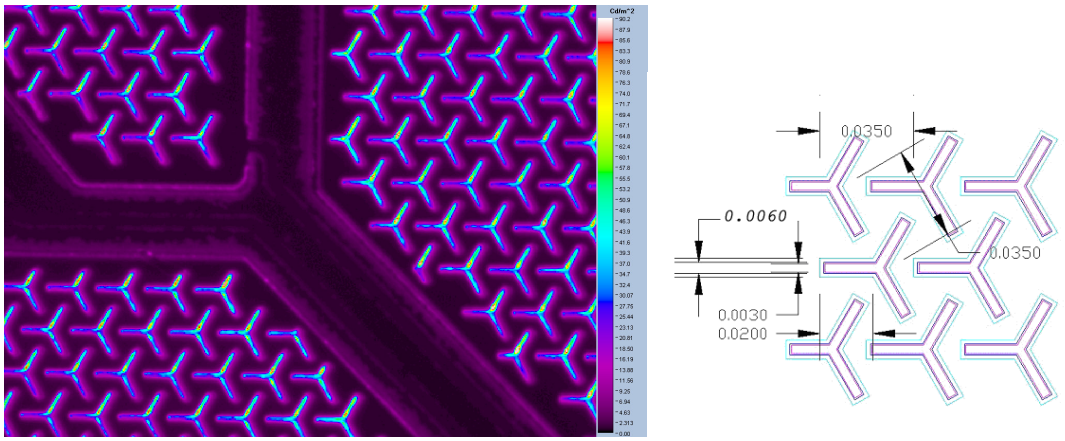

Figure 6-13: Luminance mapping from an imaging photometer of a SRELD chip mounted on a sample holder to be tested for electroluminescence showing light emission uniformity and high vision contrast (on left) - micromirror design (on right).

This design has been chosen because previous measurements have shown that this structure gives the largest outcoupling efficiency, when compared to other designs. Table 6-3 provides key design details which are associated with the micro-mirror and the various apertures and features defined on various layers for the tested devices chips.

Design No.	Micro-mirror width (µm)	Pull-back (µm)	edge stop	aperture (µm)	Micro-mirror arm length (µm)	Pitch (µm)
D1	**3**	**0.5**	**No**	**7.0**	**20**	**35**
D2	**3**	**1.0**	**No**	**7.0**	**20**	**35**
D3	**3**	**1.5**	**No**	**7.0**	**20**	**35**
D4	**3**	**2.0**	**No**	**7.0**	**20**	**35**
D5	**3**	**2.0**	**Yes**	**7.0**	**20**	**35**
D6	**3**	**1.5**	**No**	**7.0**	**40**	**60**

Table 6-3: Dimensions details for the 6 chip designs

Forming processes were applied and investigated by the author to fabricated SRELD devices in an attempt to optimise their efficiency, and the effects of AC sinusoidal

waveform voltage frequency and device ageing were tested. This work is still ongoing, but some examples of the results to date are presented on Figure 6-13. SRELD devices chips as illustrated in Figure 6-12 were tested using an experimental setup to measure electroluminescence as described before in this chapter. Devices were tested before and after each aging process at two driving frequencies: 1 kHz and 5 kHz. All devices were first aged for 2.5 hours and for 15 hours subsequently.

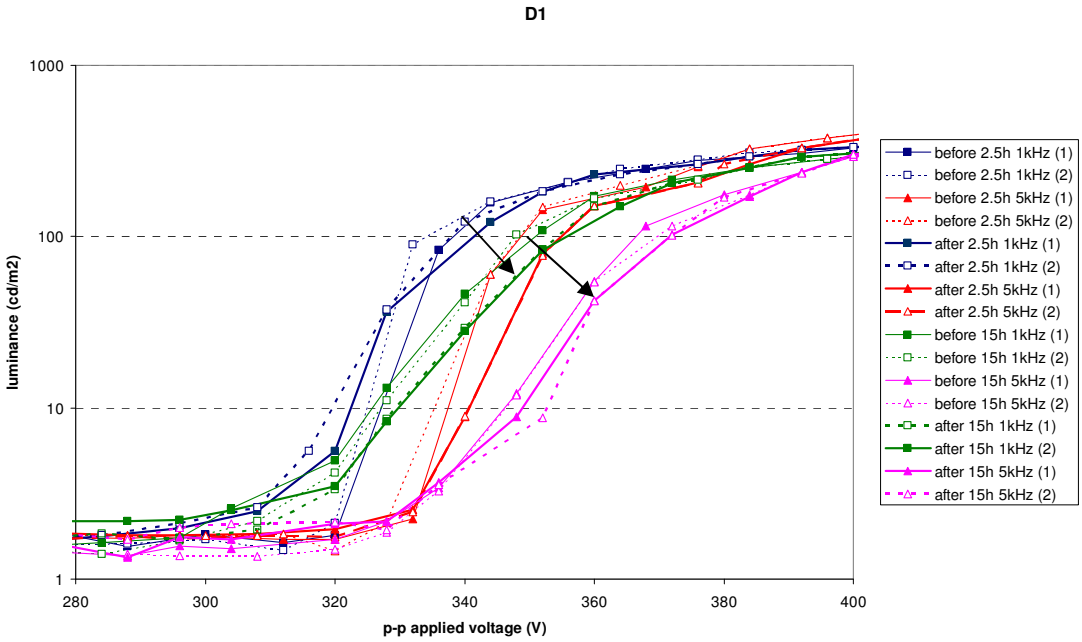

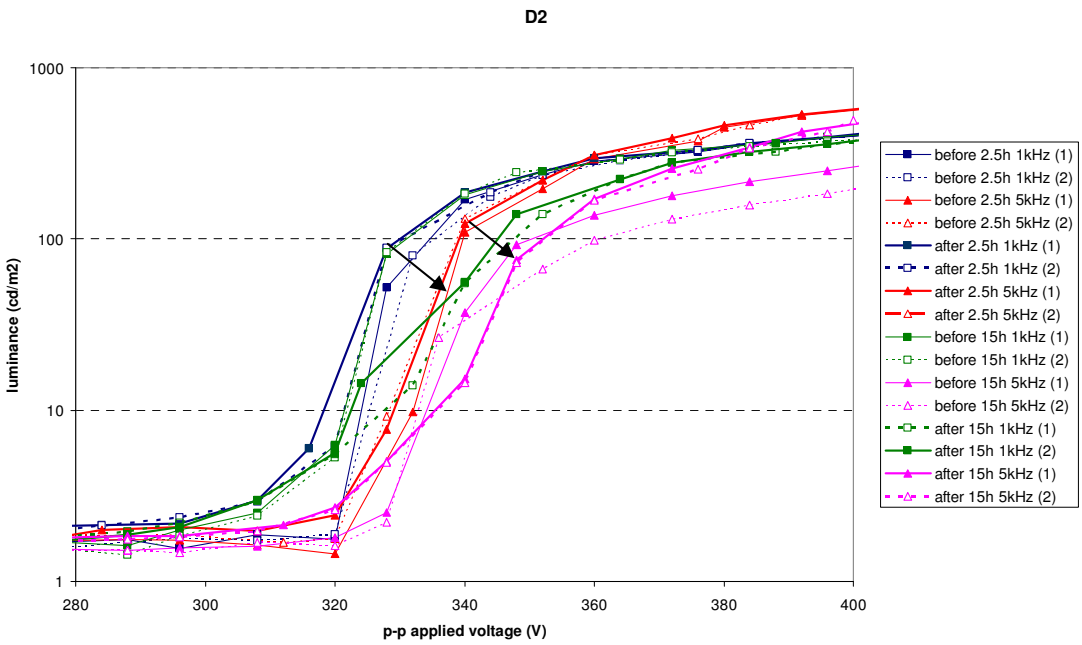

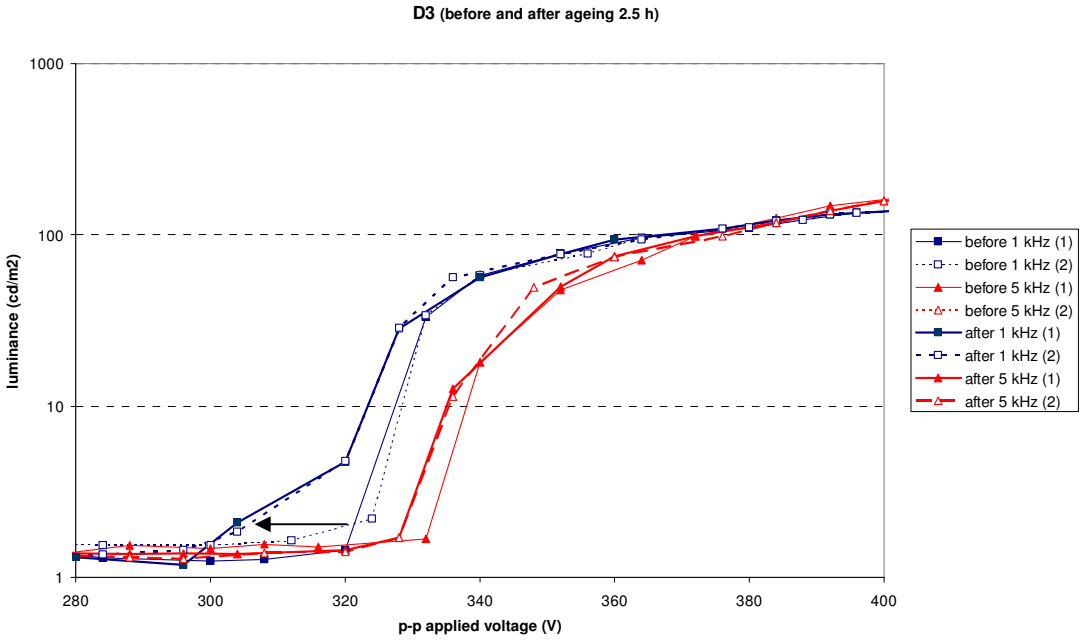
D3 (before and after ageing 2.5 h)
1000
100
10
1
luminance (cd/m2)
280
300
320
340
360
380
400
p-p applied voltage (V)
before 1 kHz (1)
before 1 kHz (2)
before 5 kHz (1)
before 5 kHz (2)
after 1 kHz (1)
after 1 kHz (2)
after 5 kHz (1)
after 5 kHz (2)

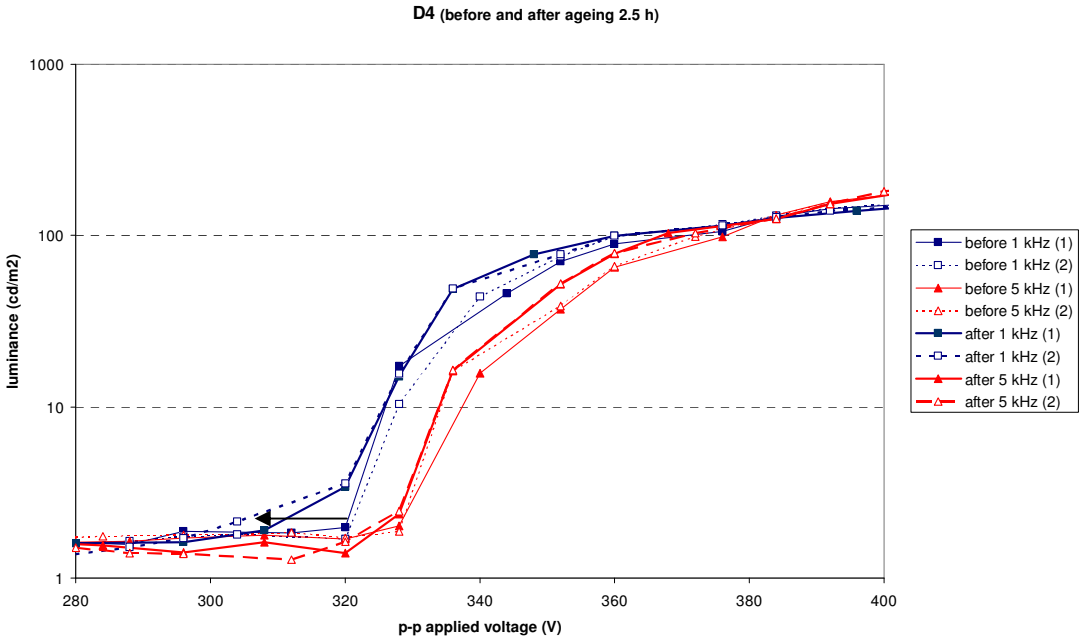
D4 (before and after ageing 2.5 h)
1000
100
10
1
luminance (cd/m2)
280
300
320
340
360
380
400
p-p applied voltage (V)
before 1 kHz (1)
before 1 kHz (2)
before 5 kHz (1)
before 5 kHz (2)
after 1 kHz (1)
after 1 kHz (2)
after 5 kHz (1)
after 5 kHz (2)

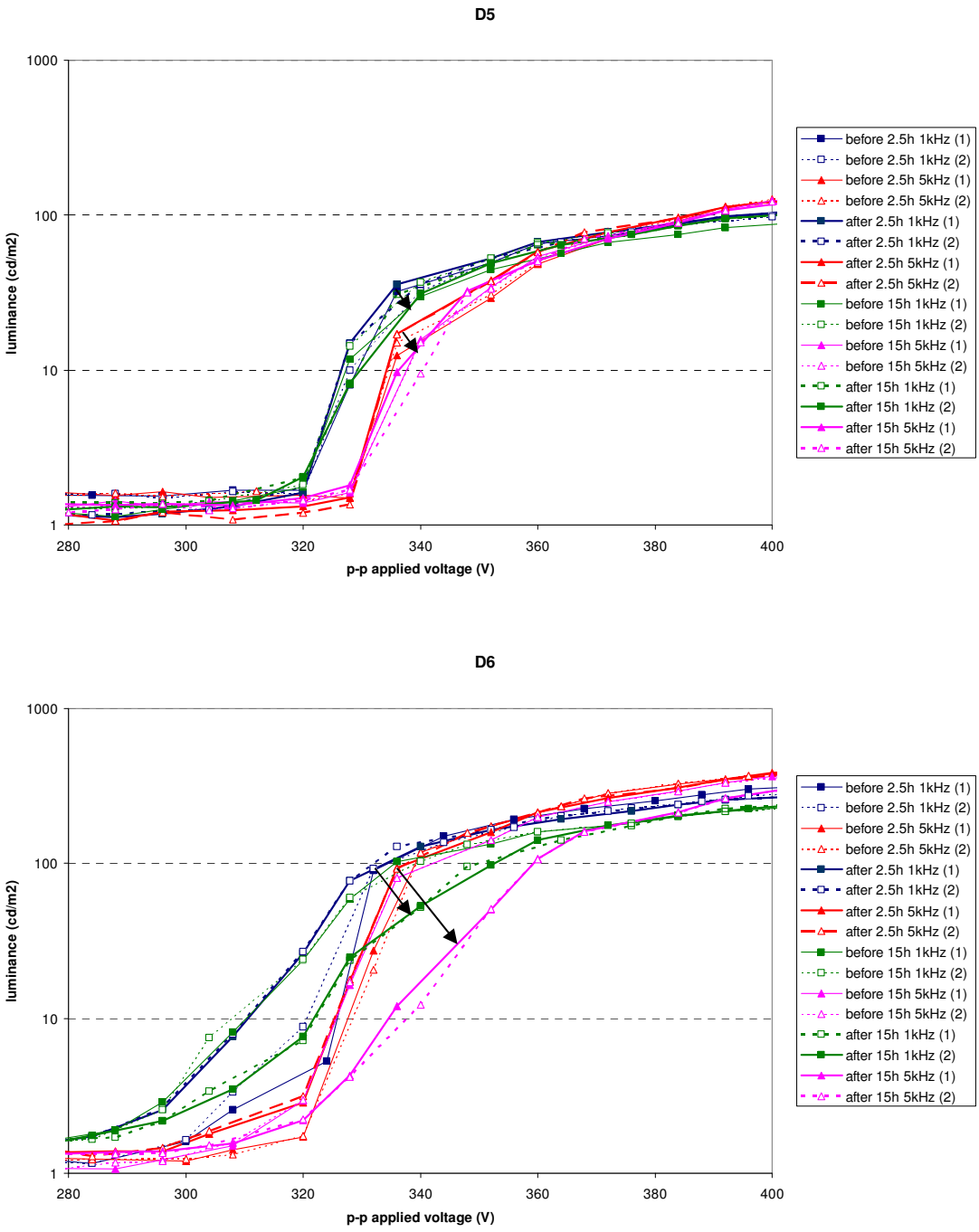

Figure 6-14: Luminance vs applied voltage of SRELD devices before and after agings of 2.5 and 15 hours for 1 and 5 kHz driving frequencies for chip number D_1, D_2, D_3, D_4, D_5 and D_6 (the arrows indicate the softening from virgin device to device that underwent 2.5 h and 15 h ageing consecutively, to note that D_3 and D_4 did not undergo 15 hours aging).

Turn on voltages and saturation luminance (obtained at 400 V peak to peak voltage) from the graphs shown in Figure 6-14 are summarised in Table 6-5 and Table 6-6.

			Chip number					
f	Ageing	V_{th} (V)	D_1	D_2	D_3	D_4	D_5	D_6
1 kHz	2.5 h	before	320	320	322	328	320	304
		after	308	320	304	306	320	296
		note	negative shifting and softening	softening	negative shifting	negative shifting and softening	slight hardening	negative shifting
	15 h	before	306	308	-	-	308	296
		after	310	308	-	-	308	296
		note	positive shifting	softening	-	-	slight softening	softening
5 kHz	2.5 h	before	330	320	330	328	328	320
		after	332	320	328	328	328	316
		note	softening	softening	negative shifting	softening	slight hardening hardening	slight softening
	15 h	before	336	336	-	-	328	316
		after	336	320	-	-	320	320
		note	softening	negative shifting and softening	-	-	negative shifting and softening	big softening

Table 6-4: Turn on voltage (or threshold voltage V_{th}) for 4 SRELD chips at 1 and 5 kHz driving voltage frequency, before and after 2.5 and 5 h ageing.

			Chip number					
f	Ageing	L_{400V} (cd/m^2)	D_1	D_2	D_3	D_4	D_5	D_6
1 kHz	2.5 h	before	345	422	142	152	100	288
		after	345	422	142	152	100	275
	15 h	before	302	357			92	225
		after	302	357			100	225
5 kHz	2.5 h	before	380	560	157	181	109	383
		after	384	560	157	181	109	383
	15 h	before	302	250			107	365
		after	302	490			107	280

Table 6-5: Luminance (at 400 V peak to peak voltage) for 4 SRELD chips at 1 and 5 kHz drive voltage, before and after 2.5 and 5 h ageing.

Figure 6-14 shows the effect of aging on the characteristics of the luminance vs. voltage (L-V). Generally, these L-V results indicate a greater device stability compared to those obtained previously from RF magnetron sputtering where there was a higher device degradation which might be due to the poor reproducibility caused by the dielectric used (Y_2O_3) [99].

Four types of L-V behaviours were observed with ageing for these results. Positive and negative shifts occurred when the threshold voltage shifted towards higher and lower voltages respectively. Moreover, softening and 'hardening' were also noticed at the 'shoulder' of the L-V curve.

These devices exhibit in preponderance L-Vs with negative threshold voltage shifting combined with softening. Other work has also shown that ALD prepared ZnS:Mn TFEL devices have a negative shift [38]. However, sputtered or even evaporated films do not reveal the same L-V shift, instead the turn-on voltage increases with time [100].

It is important to note that the device results from chip D_1 exhibit a positive threshold shifting which might be due to the fact that this chip was not virgin before performing this investigation, and therefore previous tests may have altered the electrical properties of this material.

Chip D_5 presents the best stability with almost no change in terms of saturation luminance and L-V shape after 2.5 and 15 h aging processes; it even suggests an improvement of performance with a sharper increase after threshold voltage ('hardening'). It was consequently concluded that using a PSK aperture stop was beneficial to the devices stability as well as a 2 µm pull-back reducing softening effects.

6.4 Conclusions

ACTFEL devices have been deposited onto Si and glass substrates using two different sputtering techniques. Equivalent structures have been compared in terms of device performance for these two different technologies. Devices deposited onto silicon wafers using HiTUS ZnS:Mn are seen to offer a brighter maximum luminance , which might be due to the use of reactive sputtering enhancing the stoichiometry – reducing sulphur vacancies, as well as sharper turn-on characteristics despite being deposited with no substrate heating. Additionally, HiTUS allows for the deposition of working EL devices with no substrate heating or post deposition annealing; an achievement not possible with RF magnetron sputtering. For temperatures of 200 °C, complete structures fabricated on glass entirely by HiTUS are seen to offer lower luminance than equivalent devices deposited using RF magnetron sputtering. This highlights the importance of the dielectric layer for the efficient generation of EL. The results presented thus

far suggest that if the Y_2O_3 layers deposited using HiTUS can be optimised, ambient EL devices with comparable luminance to equivalent devices deposited using RF magnetron sputtering at elevated substrate temperatures could be possible. SRELD devices have been tested using forming processes helping towards increasing their lifetime and reliability. These devices exhibited L-Vs with negative threshold voltage shifting which may stabilise after longer aging times or by increasing the ambient temperature.

In general, the experimental techniques developed for this PhD research have been demonstrated to be effective for evaluating devices and materials utilised in TFEL and LETFEL based investigations. This work is continuing and will focus on use of HiTUS deposition to capitalise on the high quality luminescent films obtained – at low temperatures. The laser annealing work presented in Chapter 5 will be explored further with use of HiTUS deposited films, and the potential for successive laser processing of these layers will be studied.

Chapter 7 Conclusions and future work

7.1 *Introduction*

The main aim of this research project was to investigate the optimisation of ZnS:Mn phosphor thin films for use in TFEL device applications. In order to achieve this aim, the phosphor growth was first studied using RF magnetron sputtering, and investigating the use of a co-sputtering deposition from standard source targets – in order to examine optimisation in a manner that would be reproducible. In addition, to specifically address issues encountered with batch to batch reproducibility, the use of luminescent probing of the films as a potential film quality/dopant level monitoring techniques was investigated. Finally, the use of excimer laser processing techniques was investigated in combination with the dopant optimisation. This included an evaluation of a novel successive layer laser processing method to potentially enhance the full emitting volume of the active phosphor thin films. TFEL devices were fabricated utlising the resultant films, and towards the latter phase of the research, these were used to compare to devices fabricated utilising alternative deposition techniques as part of collaborative R&D projects undertaken with industrial partners.

7.2 Achievements

This research work has presented successful results of a study of ZnS:Mn thin film phosphors used in TFEL and LETFEL devices, examining techniques for phosphor growth optimisation and post deposition processing in order to strengthen

development of novel TFEL devices. The main achievements of this study are summarised below.

7.2.1 Optimisation of phosphor thin films for PL efficiency and TFEL for EL efficiency

Thin films of phosphor have been successfully deposited by RF magnetron sputtering. ZnS:Mn films were simultaneously co-sputtered from ZnS and ZnS:Mn(1 wt.%) solid targets. The thin films have been deposited at different manganese concentrations by varying the relative RF power applied to each target. Equivalent films were deposited onto a layer of Y_2O_3 to fabricate electroluminescent test devices.

Luminescence has been characterised via photoluminescent excitation using a 337 nm pulsed N_2 laser, resulting in a PL optimum obtained at 0.38 Mn wt.% nominal concentration (given by $\frac{P_{ZnS:Mn}}{P_{ZnS:Mn}+P_{ZnS}}\times 1\%$) similar to the EL optimum obtained at ~0.36 Mn wt.%. Both values compare with literature data. The rapid rise in luminescent emission by both PL and EL as Mn concentrations is increased towards the optimum is related to the concomitant increase in available emitting centres – i.e. substitutional Mn ions. Beyond the optimum, the rapid fall off in luminescent emission is demonstrated to be correlated to the corresponding decrease in luminescent decay time, which can be considered to be due to an increase in non-radiative decay probability associated with Mn-Mn interactions.

7.2.2 Implementation of two monitoring techniques for dopant concentration

These techniques were investigated as potential methods for the control of the Mn concentration to ensure optimised batch to batch film deposition. The first method

studied relates to the identified relationship between ratio of red over yellow PL emissions and Mn concentration ($\frac{I_r}{I_y} \propto C_{Mn}$). The second method relates to the relationship between measured photoluminescent decay constant and dopant concentration ($\tau \propto C_{Mn}$). This latter resulted in the publication of a paper by the author based on the research [94]. The correlated Mn concentration vs decay constant and $\frac{I_r}{I_y}$ results were presented as potential non-destructive (in-situ) techniques for characterising this phosphor during deposition. These results clearly showed the influence of the manganese concentration on the decay constant and $\frac{I_r}{I_y}$. With increasing the concentration of Mn^{2+} ions in the host ZnS lattice, the after-glow period (when the excitation has ceased) decreases and $\frac{I_r}{I_y}$ increases. This also confirmed previous indications on the effect of higher Mn concentrations, and is indicative of the effect that is associated with Mn-Mn ion interactions leading to non-radiative decay probability increase.

7.2.3 Benefit of laser annealing combined with Mn concentration variation

Solid targets co-sputtered and powder ZnS:Mn thin films with different Mn concentrations were annealed with an excimer KrF laser varying fluence and number of pulses. PL was greatly enhanced (up to 13 times) compared the 'as deposited' films. The laser annealing effect was more effective on the films obtained from co-sputtering targets. From the trend of the results , it was suggested that a higher Mn concentration could be the optimum when combined with laser annealing. This would be consistent with an improvement in the host lattice being produced by the

laser treatment, thus allowing a higher proportion of the dopant ions to reside in active sites and thus contribute more effectively to the luminescence.

TFEL devices were also fabricated using three different Mn concentrations for the phosphor layer and were laser processed during fabrication. The results again demonstrated that laser annealing was more beneficial at higher Mn concentrations; this was further attributed to the redistribution of the Mn ions in the ZnS film reducing the concentration of shallow states which influence the structural and optical characteristics of these devices.

7.2.4 Successive layer laser processing for highly efficient luminescent material

As an attempt to modify the whole phosphor film and therefore improve EL efficiency, a series of experiments were undertaken to examine the feasibility, and effect, of using successive laser processing of 200nm layers deposited sequentially. Films of ZnS:Mn were deposited 200nm at a time, with growth interrupted to undertake laser processing. The results have shown dramatic improvements on phosphor thin films and have demonstrated a novel processing technique for enhanced TFEL devices. These phosphor thin films had potentially their full thickness with crystal structure modified.

7.2.5 Industrial collaboration for performance enhancement of TFEL devices

The project collaboration with PQL has demonstrated the benefits of using a novel sputtering technique called HiTUS on TFEL devices with potential application on plastic substrates [9, 10].

SRELD devices have been tested using forming processes helping towards increasing their lifetime and reliability. These devices exhibited L-Vs with negative threshold voltage shifting which may stabilise after longer aging times or by increasing the ambient temperature.

7.3 Future work

7.3.1 Calibration of dopant concentration monitoring technique

During this research project, the variation in 'nominal Mn concentration' was investigated, through direct comparison of the resultant thin films against the deposition parameters. It was not possible to determine he actual Mn concentration during the research. Hence, to calibrate the monitoring techniques identified, phosphor thin films with various Mn concentrations should be measured for decay constant and ratio of red over yellow PL emissions and then analysed for accurate determination of wt.% of Mn. This would result in two calibration curves of $\tau \propto C_{Mn}$ and $\frac{I_r}{I_y} \propto C_{Mn}$.

Samples were first analysed with Energy-dispersive X-ray spectroscopy (EDX) at Surrey University. However, results were inconclusive for the low concentrations and only two Mn concentrations were analysed.

- C_{Mn} (nominal) = 0.25 wt.% against C_{Mn} (EDX) = (0.16±0.07) wt.%
- C_{Mn} (nominal) = 0.50 wt.% against C_{Mn} (EDX) = (0.66±0.07) wt.%

These results can give rough estimations but need more investigation. Additional samples have been sent at the time of the writing with various Mn concentrations for X-ray photoelectron microscopy (XPS).

7.3.2 Fully optimised phosphor film for TFEL devices from combined effect of dopant concentration and laser annealing

The combination of dopant concentration variation and laser annealing conditions can be engineered to produce optimised performance; the results presented in this work highlighted how future optimisation work could be undertaken. The next step will be to further investigate this study with the fabrication of TFEL devices with Mn concentration closer to the optimum. It is anticipated that, from these results, TFEL devices with slightly higher Mn concentration than the optimum and with suitable laser processing parameters would produce enhanced electroluminescence.

7.3.3 Optimisation of laser treatment for successive deposited phosphor layers for TFEL devices

Results obtained for the laser treatment of successive layer annealing of Zn:Mn for TFEL devices were limited to samples that underwent an irradiation of 3 pulses. This study could be extended to 1 and 2 pulses for a more complete investigation. More importantly, from conclusions of this work, the fluences would need to be lower than those chosen previously to achieve optimised full phosphor thickness phase transformation and not modify the electrical properties of the underlying dielectric.

7.3.4 Investigation of combined laser energies for TFEL devices

An alternative technique is projected to also transform the material from the cubic to the hexagonal phase. It is known that the luminous efficiency of the hexagonal phase of ZnS:Mn is higher than that of the cubic phase of as-grown films. It is proposed to create a transformation of an upper layer of ZnS:Mn films with 193 nm radiation with an excimer laser. By comparison with the growth of single crystals, it is

intended to use this layer as a seed for further phase change at greater depths by annealing consecutively with 248 and 308 nm radiations.

This work would investigate the use a range of laser energies corresponding to 351 and 192 nm as well as 248 nm. Each wavelength has a different absorption coefficient decreasing from 192 to 351 nm. Hence, the effective penetration depth in the thin film will increase by varying the wavelength from 192 to 351 nm.

Both PL and EL measurements would be made at each wavelength and different power densities. Concomitantly, both destructive and non destructive examination will be made to identify possible/probable lattice transformations. These experiments would include high resolution edge-on, electron microscopy, spectroellipsometry and surface analysis.

Finally as a concluding remark, considerable progress has been made on the optimisation of these thin films and devices, and therefore by combining these results with potentially HiTUS deposition, future development of this technology presents some exciting opportunities, particularly for use in plastic and transparent light emitter devices.

LIST OF REFERENCES

[1] C. B. Thomas, R. Stevens and W. M. Cranton, "Laterally emitting TFEL for head-mounted displays," *1996 SID International Symposium. Digest of Technical Papers. First Edition,* pp. 365-369, 1996.

[2] E. A. Mastio, M. R. Craven, W. M. Cranton, C. B. Thomas, M. Robino and E. Fogarassy, "The effects of KrF pulsed laser and thermal annealing on the crystallinity and surface morphology of radiofrequency magnetron sputtered ZnS : Mn thin films deposited on Si," *Journal of Applied Physics,* vol. 86, pp. 2562-2570, Sep 1, 1999.

[3] E. A. Mastio, C. B. Thomas, W. M. Cranton and E. Fogarassy, "The effects of multiple KrF laser irradiations on the electroluminescence and photoluminescence of rf-sputtered ZnS:Mn-based electroluminescent thin film devices," *Applied Surface Science,* vol. 157, pp. 74, 2000.

[4] E. A. Mastio, W. M. Cranton and C. B. Thomas, "Lattice misfit versus performance of thin film electroluminescent structures," *Journal of Applied Physics,* vol. 89, pp. 1605-1611, Feb 1, 2001.

[5] E. A. Mastio, W. M. Cranton, C. B. Thomas, E. Fogarassy and S. de Unamuno, "Pulsed KrF laser annealing of RF sputtered ZnS:Mn thin films," *Applied Surface Science,* vol. 138-139, pp. 35, 1999.

[6] S. C. Liew, D. C. Koutsogeorgis, W. Cranton and C. B. Thomas, "Pulsed KrF laser annealing of blue emitting SrS : Cu,Ag thin films," *Electronics Letters,* vol. 38, pp. 1466-1468, Nov 7, 2002.

[7] Y. S. Kim and S. J. Yun, "Studies on polycrystalline ZnS thin films grown by atomic layer deposition for electroluminescent applications," *Appl. Surf. Sci.,* vol. 229, pp. 105-111, 5/15, 2004.

[8] J. Ihanus, M. P. Lankinen, M. Kemell, M. Ritala and M. Leskela, "Aging of electroluminescent ZnS:Mn thin films deposited by atomic layer deposition processes," *J. Appl. Phys.,* vol. 98, pp. 113526-1, 12/01, 2005.

[9] S. Wakeham, M. Thwaites, C. Tsakonas, W. M. Cranton, R. M. Ranson, G. Boutaud and D. Koutsogeorgis, "A new reactive sputtering technique for the low temperature deposition of transparent light emitting ZnS:Mn thin films," *Physica Status Solidi (a),* accepted for publication.

[10] S. Wakeham, M. Thwaites, W. Cranton, C. Tsakonas, D. Koutsogeorgis and G. Boutaud, *Journal of the Society for Information Display,* vol. Selected papers from Eurodisplay 2009, June 2010.

[11] K. Booth and S. Hill, *Essence of Opto-Electronics.* Englewood Cliffs, NJ: Prentice-Hall, 1998.

[12] L. S. Hung and C. H. Chen, "Recent progress of molecular organic electroluminescent materials and devices," *Materials Science and Engineering: R: Reports,* vol. 39, pp. 143-222, 12/1, 2002.

[13] P. W. M. Blom and M. J. M. De Jong, "Device operation of polymer light-emitting diodes," *Philips Journal of Research,* vol. 51, pp. 479-494, 1998.

[14] H. Becker, A. Busing, S. Heun, A. Falcou, O. Gelsen, E. Kluge, W. Kreuder, A. Parham, H. Schenk, J. Steiger, H. Spreitzer, P. Stocel, K. Treacher and H. Vestweber, "Light emitting polymer materials for full color displays," in *First International IEEE Conference on Polymers and Adhesives in Microelectronics and Photonics: Incorporating POLY,PEP and Adhesives in Electronics (POLYTRONIC 2001), October 21, 2001 - October 24,* 2001, pp. 336.

[15] J. K. Borchardt, "Developments in organic displays," *Materials Today,* vol. 7, pp. 42-46, 9, 2004.

[16] B. G. Streetman and S. Banerjee, *Solid State Electronics Device,.* Prentice Hall, 2000.

[17] J. Wilson and J. F. B. Hawkes, *Optoelectronics: An Introduction,.* Pearson Higher Education, 1998.

[18] D. Travis, *Effective Color Displays: Theory and Practice*, Academic Press, 1991.

[19] R. Ranson, "Photoluminescence & plasma display panels," in *DisplayMasters,* 2005.

[20] G. Destriau, "Recherches sur les Scintillations des Sulfures de Zinc aux Rayons α," *J. Chem. Phys.,* vol. 33, 1936.

[21] J. W. Allen, "Impact excitation and Auger quenching of luminescent centres in crystals, with special reference to ZnS:Mn," *Journal of Physics C (Solid State Physics),* vol. 19, pp. 6287, 1986.

[22] T. Inoguchi, M. Takeda, Y. Yakihara, Y. Nakata and Y. M., "Stable high-Brigtness Thin Film Electroluminescent Devices," *Proceedings of the S.I.D,* vol. 74, pp. 84-85, 1974.

[23] Y. A. Ono, *Electroluminescent Display,.* World Scientific, 1995.

[24] J. S. Kim, S. G. Lee, H. L. Park, J. Y. Park and S. D. Han, "Optical and electrical properties of ZnGa2O4/Mn2+ powder electroluminescent device," *Mater Lett,* vol. 58, pp. 1354-1357, 3, 2004.

[25] S. Urabe, US Patent 6924592 - phosphor powder and EL device, 2005.

[26] D. H. Shin and K. H. Bae, US Patent 7482747 - Flexible EL device, 2005.

[27] M. J. Russ and D. I. Kennedy, "The Effects of Double Insulating Layers on the Electroluminescence of Evaporated ZnS:Mn Films," *Journal of the Electrochemical Society,* vol. 114, pp. 1066-1072, 1967.

[28] W. M. Cranton and C. B. Thomas, "Material Processing For Thin Electroluminescent Displays," *Microdiplay 2001 SID,* pp. 102, 2001.

[29] D. H. Smith, "Modeling a.c. thin-film electroluminescent devices," *Journal of Luminescence,* vol. 23, pp. 209, 1981.

[30] R. Stevens, W. M. Cranton and C. B. Thomas, US Patent 5910706 - Laterally transmitting thin film electroluminescent device, 1999.

[31] R. Stevens, C. B. Thomas and W. M. Cranton, "Enhancing The Brightness Of Thin-Film Electroluminescent Displays By Improving The Emission Process," *Ieee Electron Device Letters,* vol. 15, pp. 97-99, Mar, 1994.

[32] R. Stevens, A. H. Abdullah and W. Cranton, "Ultra-high resolution emissive micro-mirror LETFEL displays for the injection of intelligent graticule information in avionic head-up display systems," in *Design and Engineering of Optical Systems,* 1996, pp. 735-46.

[33] A. H. Kitai, *Solid State Luminescence Theory, Materials and Devices.* London: Chapman & Hall, 1993.

[34] D. V. Morgan and K. Board, *An Introduction to Semiconductor Microtechnology,* John Wiley & Son Ltd, 1990.

[35] D. M. Mattox, *Handbook of Physical Vapor Deposition (PVD) Processing.* Noyes Publications, 1998.

[36] H. Xian, P. Benalloul, C. Barthou and J. Benoit, "Quantitative analyses and crystallographic studies of ZnS:Mn thin films prepared by r.f. magnetron reactive sputtering," *Thin Solid Films,* vol. 248, pp. 193-8, 08/15, 1994.

[37] T. Suntola and J. Hyvarinen, "Atomic layer epitaxy," in *Annual Review of Materials Science. Vol.15*Anonymous Palo Alto, CA, USA: Annual Reviews, 1985, pp. 177-95.

[38] J. Ihanus, M. P. Lankinen, M. Kemell, M. Ritala and M. Leskela, "Aging of electroluminescent ZnS:Mn thin films deposited by atomic layer deposition processes," *J. Appl. Phys.,* vol. 98, pp. 113526-1, 12/01, 2005.

[39] Y. A. Ono, "Different techniques employed in deposition of TFEL devices," *Acta Polytech Scand Appl Phys Ser,* pp. 41-48, 1990.

[40] C. B. Thomas, D. Sands, K. M. Brunson and H. S. Reehal, "Influence of the deposition temperature on the photoluminescence from thin film ZnS:Mn," *Journal of the Electrochemical Society,* vol. 136, pp. 1235, 1989.

[41] Y. Nakanishi, S. Mori, T. Nakamura, H. Tatsuoka, H. Kuwabara and Y. Hatanaka, "Effect of insulating layer structural properties for thin-film electroluminescent devices," *Materials Chemistry and Physics,* vol. 43, pp. 292, 1996.

[42] E. A. Mastio, *PhD. Thesis,* Nottingham Trent University, 1999.

[43] A. Fuh, R. P. Gallinger, P. Schuster, J. Adolph and O. Caporaletti, "The effects of post-deposition annealing on ZnS:Mn film crystalline structure and electroluminescent characteristics," *Thin Solid Films,* vol. 207, pp. 202, 1992.

[44] I. P. McClean, N. Konofaos and C. B. Thomas, "Conductance technique measurements of the density of states between Si and ZnS grown by molecular beam epitaxy," *Journal of Applied Physics,* vol. 74, pp. 397, 1993.

[45] D. Bauerle, *Laser Processing and Chemistry,* Springer, 3rd Ed., 2000.

[46] R. F. Wood and J. G. E. Jr, "Melting model of pulsed laser processing," in *Semiconductors and Semimetals. Vol.23: Pulsed Laser Processing of Semiconductors,* Anonymous Academic Press, 1984, pp. 165.

[47] S. de Unamuno and E. Fogarassy, "A thermal description of the melting of c- and a-silicon under pulsed excimer lasers," *Applied Surface Science,* vol. 36, pp. 1, 1989.

[48] S. C. Sandu, *PhD. Thesis,* Universite Claude Bernard-Lyon 1, 2003.

[49] J. M. Gallego, H. S. Reehal and C. B. Thomas, "DC Electroluminescence," *SID Proceedings,* vol. 135, pp. 135-139, 1983.

[50] H. S. Reehal, C. B. Thomas, J. M. Gallego, G. Hawkins and C. B. Edwards, "Pulsed UV laser irradiation of ZnS films on si and GaAs," in *Laser-Solid Interactions and Transient Thermal Processing of Materials,* 1983, pp. 677-82.

[51] D. C. Koutsogeorgis, E. A. Mastio, W. M. Cranton and C. B. Thomas, "Pulsed KrF laser annealing of ZnS:Mn laterally emitting thin film electroluminescent displays," *Thin Solid Films,* vol. 383, pp. 31, 2001.

[52] D. C. Koutsogeorgis, *PhD. Thesis,* Nottingham Trent University, 2004.

[53] D. C. Koutsogeorgis, *Private Communication,* 2006.

[54] F. X. Wagner, K. Dhese, P. H. Key, D. Sands, S. R. Jackson, R. Kirbitson and J. E. Nicholls, "Photo-luminescence of pulsed excimer laser annealed Sb-implanted CdTe," *Applied Surface Science,* vol. 86, pp. 364, 1995.

[55] D. Sands, F. X. Wagner and P. H. Key, "Evidence for a thermal mechanism in excimer laser ablation of thin film ZnS on Si," *Journal of Applied Physics,* vol. 85, pp. 3855-3859, 1999.

[56] W. M. Cranton, P. H. Key, D. Sands, C. B. Thomas and F. X. Wagner, "XeCl laser ablation of thin film ZnS," *Applied Surface Science,* vol. 96-98, pp. 501, 1996.

[57] D. Sands, *Private Communication,* 2007.

[58] W. M. Cranton, C. B. Thomas, K. Koutsogeorgis, E. Mastio, M. Craven, R. Stevens, R. Ranson, M. Sethu, J. Rudiger, S. Barros, A. Liew, C. Tsakonas and P. Theng, "Materials processing and device engineering for laterally emitting thin film ElectroluminescentMiniature displays," in *Proc. SID Microdisplays,* pp. 102, 2001.

[59] S. A. Campbell, *The Science and Engineering of Microelectronic Fabrication,* Oxford University Press*,* 2001.

[60] S. Miura, K. Okamoto, S. Sato, S. Andoh, H. Ohnishi and Y. Hamakawa, "GREEN COLOR ACTFEL WITH SPUTTERED ZnS:TbF3." in *Japan Display '83,* pp. 84-87, 1983.

[61] E. C. Freeman, D. H. Baird and J. R. Weaver, "Use of coactivators in rare-earth-activated ZnS for electroluminescent displays," in *Third International Display Research Conference (Japan Display '83),* 1984, pp. 183-5.

[62] M. I. Abdalla, J. L. Plumb and L. L. Hope, "LARGE-AREA AC THIN-FILM EL DISPLAYS," *SID International Symposium (Society for Information Display),* pp. 245, 1984.

[63] A. F. Cattel and A. G. Cullis, "Variation in the luminescent and structural properties of sputter-deposited ZnS:Mn thin films with post-deposition annealing," in Switzerland, pp. 172, 1982.

[64] R. Tueta and M. Braguier, "Fabrication and characterization of indium tin oxide thin films for electroluminescent applications," *Thin Solid Films,* vol. 80, pp. 143, 1980.

[65] Y. Shimizu and T. Matsudaira, "ITO films for EL panels," *Conference Record of the 1985 International Display Research Conference,* pp. 101, 1985.

[66] W. M. Cranton, D. M. Spink, R. Stevens and C. B. Thomas, "Growth and dielectric characterization of yttrium oxide thin films deposited on Si by r.f.-magnetron sputtering," *Thin Solid Films,* vol. 226, pp. 159, 1992, 1992.

[67] W. M. Cranton, *PhD. Thesis,* University of Bradford, 1995.

[68] M. Bass, *Handbook of Optics,* McGraw-Hill, 1994.

[69] J. M. Hurd and C. N. King, "Physical and electrical characterization of co-deposited Zns:Mn electroluminescent thin film structures," *Journal of Electronic Materials,* vol. 8, pp. 879-891, 1979.

[70] E. A. Mastio, E. Fogarassy, W. M. Cranton and C. B. Thomas, "Ablation study on pulsed KrF laser annealed electroluminescent ZnS:Mn/Y2O3 multilayers deposited on Si," *Applied Surface Science,* vol. 154-155, pp. 35, 2000.

[71] G. S. a. S. May S.E., *Fundamentals of Semiconductor Fabricatio,.* Wiley, 2004.

[72] D. K. Shroder, *Semiconductor Material and Device Characterizatio,* John Wiley & Sons, 1998.

[73] S. Tanaka, V. Shanker, M. Shiiki, H. Deguchi and H. Kobayashi, "Multicolor electroluminescence in alkaline-earth sulfide thin-film devices," *Proceedings of the S.I.D,* vol. 26, pp. 255, 1985.

[74] W. R. Runyan and T. J. Schaffner, *Semiconductor Measurements & Instrumentation.* McGraw-Hill, 1998.

[75] Veeco Metrology Group, *WYKO Surface Profilers Technical Reference Manual.* 1999.

[76] Veeco Metrology Group, *Wyko NT1100 Setup Guide.* 2002.

[77] H. Fukada, T. Miyata and T. Minami, "Thin-film EL devices using Eu-activated SnO2-based multi-component oxide phosphors," *IDW '06 - Proceedings of the 13th International Display Workshops,* vol. 1, pp. 413, 2006.

[78] W. Glass, A. Kale, N. Shepherd, M. Davidson, D. DeVito and P. H. Holloway, "Sputter deposited electroluminescent zinc sulfide thin films doped with rare earths," *Journal of Vacuum Science & Technology A (Vacuum, Surfaces, and Films),* vol. 25, pp. 492, 2007.

[79] Z. Ding, Z. Yu and W. Xue, "Research on blue emitting BaAl2S4: Eu phosphor layers of TFEL," *Proceedings of SPIE - the International Society for Optical Engineering,* vol. 6624, pp. China Ordnance Society; Beijing Institute of Technology, 2008.

[80] N. A. Vlasenko, S. A. Zynio and Y. V. Kopytko, "The effect on Mn concentration on ZnS:Mn electroluminescence decay," *Physica Status Solidi A,* vol. 29, pp. 671, 1975.

[81] A. J. Warren, C. B. Thomas and P. R. C. Stevens, "The effect of Mn concentration on the photoluminescence of ZnS:Mn," *Journal of Physics D (Applied Physics),* vol. 16, pp. 225, 1983.

[82] K. Takamichi, A. Nitta, K. Tanaka and M. Aozasa, "Mn^{2+} centers in ZnS:Mn thin-film EL device active layer," *Memoirs of the Faculty of Engineering, Osaka City University,* vol. 43, pp. 1, 2002.

[83] S. Schon, M. Chaichimansour, W. Park, E. W. Thomas, T. Yang, B. K. Wagner and C. J. Summers, "Improved photoluminescent properties of ZnS:Mn due to the δ-doping process," *Journal of the Society for Information Display,* vol. 6, pp. 67, 1998.

[84] V. Marrello and A. Onton, "DEPENDENCE OF ELECTROLUMINESCENCE EFFICIENCY AND MEMORY EFFECT ON Mn CONCENTRATION IN ZnS:Mn ACTEL DEVICES," *IEEE Transactions on Electron Devices,* vol. ED-27, pp. 1767, 1980.

[85] O. Goede and T. Dang Dinh, "Energy transfer processes in (Zn,Mn)S mixed crystals," *Physica Status Solidi B,* vol. 124, pp. 343, 1984.

[86] H. S. Bhatti, R. Sharma and N. K. Verma, "Fast photoluminescence decay processes of doped ZnS phosphors at low temperature," *Physica B: Condensed Matter,* vol. 382, pp. 38, 2006.

[87] V. Marrello and A. Onton, "Dependence of electroluminescence efficiency and memory effect on Mn concentration in ZnS:Mn ACTEL devices," *IEEE Trans. Electron Devices,* vol. ED-27, pp. 1767-70, 1980.

[88] K. Hirabayashi and H. Kozawaguchi, "ZnS:Mn electroluminescent device prepared by metal-organic chemical vapor deposition," *Japanese Journal of Applied Physics, Part 1 (Regular Papers & Short Notes),* vol. 25, pp. 711-13, 05, 1986.

[89] A. N. Krasnov, R. C. Bajcar and P. G. Hofstra, "Threshold voltage trends in ZnS:Mn-based alternating-current thin-film electroluminescent devices: Role of native defects," *J. Cryst. Growth,* vol. 194, pp. 53-60, 1998.

[90] B. Selle, "Decay of the luminescence of ZnS: Mn under excitation in the characteristic mn absorption region," *Physica Status Solidi,* vol. 5, pp. 649, 1964.

[91] R. Tornqvist, "Electroluminescence in ZnS:Mn thin film structures grown with atomic layer epitaxy," *Acta Polytechnica Scandinavica, Applied Physics Series,* pp. 2, 1983.

[92] W. M. Cranton, *Private Communication,* 2007.

[93] D. C. Koutsogeorgis, W. M. Cranton, R. M. Ranson and C. B. Thomas, "Performance enhancement of ZnS:Mn thin film electroluminescent devices by combination of laser and thermal annealing," *J. Alloys Compounds,* vol. 483, pp. 526-529, 8/26, 2009.

[94] G. Boutaud, W. M. Cranton, D. C. Koutsogeorgis, R. M. Ranson, C. Tsakonas and C. B. Thomas, "Growth optimisation of ZnS:Mn thin film phosphors for high

intensity miniature electroluminescent displays," *Materials Science and Engineering: B,* vol. 165, pp. 202-206, 12/15, 2009.

[95] J. -. Fornell, H. G. Grimmeiss, R. Mach and G. O. Muller, "The influence of manganese doping on the self-activated centre in ZnS," *Semiconductor Science and Technology,* vol. 3, pp. 511-13, 05, 1988.

[96] G. Y. Yeom, J. A. Thornton and M. J. Kushner, "Cylindrical magnetron discharges. II. The formation of DC bias in RF-driven discharge sources," *J. Appl. Phys.,* vol. 65, pp. 3825-32, 05/15, 1989.

[97] Y. Hoshi and R. Ohki, "Low energy rf sputtering system for the deposition of ITO thin films," *Electrochim. Acta,* vol. 44, pp. 3927-3932, 1999.

[98] W. M. Cranton, R. Stevens, K. Koutsogeorgis, R. Ranson, A. Needham, M. Thorne and A. Magon, "Laterally emitting thin film electroluminescent device engineering for sunlight readable vehicular displays," in *Society for Information Display, International Conference on Vehicles and Photons, Digest of Technical Papers,* Detroit, USA, 2007, pp. p 27.

[99] A. N. Krasnov, "Selection of dielectrics for alternating-current thin-film electroluminescent device," *Thin Solid Films,* vol. 347, pp. 1-13, 06/22, 1999.

[100] J. D. Davidson, J. F. Wager and S. Kobayashi, "Aging studies of evaporated ZnS:Mn alternating-current thin-film electroluminescent devices," *J. Appl. Phys.,* vol. 71, pp. 4040-8, 04/15, 1992.

[101] J. M. Gallego, H. S. Reehal and C. B. Thomas, "DC electroluminescence in novel n-p Si/ZnS:Mn heterostructures," in *Conference Record of 1982 International Display Research Conference,* pp. 30-3, 1982.

APPENDICES

A.1 *Charge reservoir EL devices*

A.1.1 Introduction

As an attempt of increasing EL structure efficiency, a project on 'charge reservoir' EL devices was investigated. The following band diagram on Figure A-1 shows the representation of such a device, its structure is the same as traditional EL devices but with the incorporation of ITO layers and very thin layers of yttrium oxide.

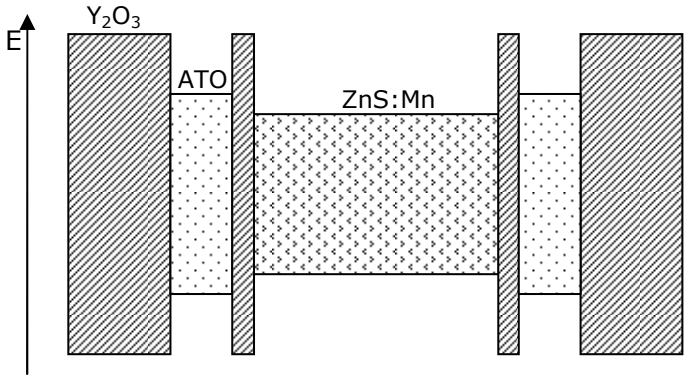

[79]

Figure A-1: Energy band diagram of a 'charge reservoir' EL device

This new device is based on new configuration where the charge is initiated in two conductive thin films sandwiched between the thick dielectric layers and the phosphor layer, on either side of the phosphor layer, and not only from the interface states of the dielectric/phosphor interfaces. In this new configuration, thin conductive ITO layer act as the charge reservoir layers. Thin dielectric barrier layers (10nm of yttrium oxide) should be deposited between the conductive layers and the phosphor layer to prevent indium diffusion into the phosphor layer.

Different parameters (thickness, conductivity, surface roughness, but mainly electroluminescence) were studied to determine the reliability of such potential EL devices. A series of aims for growth plans were first established as explained thereafter:

1. Preliminary aim: To make sure that the following typical structure works:

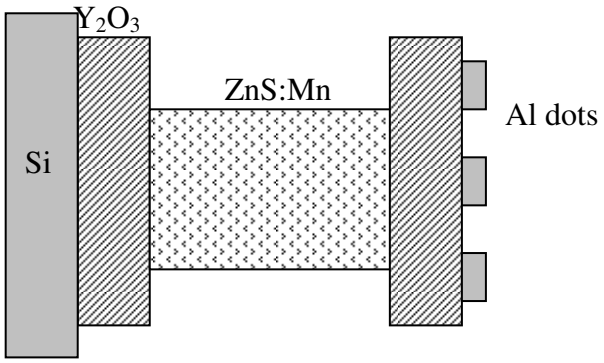

   If it is successful, the Al dots can then be substituted (or/and compared) with ITO dots. This simpler but quicker process of EL device could be replacing patterning of aluminium for a parallel study on optimisation of manganese concentration for electroluminescence (see Chapter 4).

2. Overall aim: To develop the following working device the two similar injection layers in both ends.

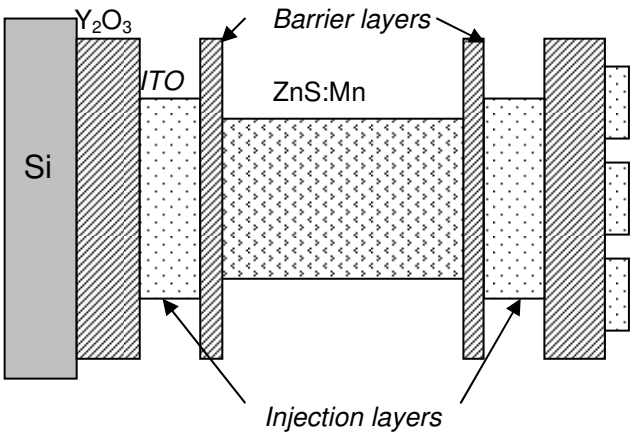

To achieve this objective, mainly BVs (ac/dc), IVs and possibly the CVs of the required device need to be investigated by varying the following ITO resistivity, ITO thickness, ITO surface roughness and the thickness of the Y_2O_3 barrier layer. Also the thickness of ZnS and the incorporation of YO barrier layer might also need to be investigated. In the long run the ITO injection layer and the Y_2O_3 barrier layer might be substituted with other materials.

- ITO parameters:

  The ITO resistivity would control the number of available carriers and also surface roughness. The ITO resistivity depends on oxygen partial pressure and the ITO surface roughness is mainly controlled by the growth temperature, i.e. the higher the growth temperature the smoother is the ITO surface. Also surface roughness secondarily depends on oxygen partial pressure.

  Varying the thickness of ITO might not be so important but only for structural purposes i.e any eventual consequences on the layers above it. However, varying the ITO thickness changes the amount of electrons that are available to tunnel through the barrier. But this amount might also depend on the frequency of the driving voltage.

- Y_2O_3 thickness:

  The thicker the Y_2O_3 barrier layers the higher the threshold voltage will be, therefore these layers need to be as small as possible.

3. First aim: To investigate the following device:

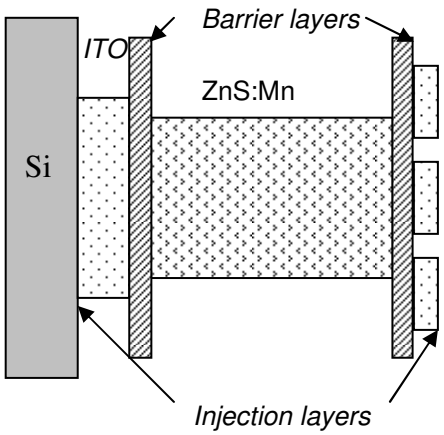

This device resembles the original EL devices that had the structure MIM (or metal/insulator/metal). These devices suffer from current runaway meaning that the current through the device cannot be controlled and a slight change in the voltage would cause exponential increase of current that would break down the device eventually [101]. However, in spite of the limitations of the device it might be possible to see if there is a production of EL that would substantiate the geometry of the proposed device. The half device would be characterised in terms of the studies that are intended for the whole proposed device: BVs, ac IVs, dc IVs, CVs. AFM and XRD might also be used for each layer to investigate how the ITO injection layer affects the subsequent layers.

A.1.2 Results and discussions

Some full such devices had been made but with no conclusive results were observed. However, some encouraging and positive results in electroluminescence with the incorporation of the bottom buffer ITO layer had been noticed. Alternatively, as a progressive approach and to save on time, the following device fabrication, as shown

in Figure 6-16, had been proposed to be investigated first in order to investigate the optimum thickness of the barrier layer for electron injection into the phosphor layer:

1. Silicon wafer/ Y_2O_3 layer/ZnS:Mn followed by typical 500°C annealing to activate the phosphor,
2. with or without a barrier layer (for direct comparison) of Y_2O_3 with different layer thicknesses
3. ITO charge reservoir layer deposition done thorough out a contact mask with 2 mm apertures to isolate each charge reservoir device.
4. Top dielectric layer deposition identical as bottom layer of Y_2O_3
5. Top electrode layer deposition done thorough out a contact mask with 1 mm apertures

No post annealing is required for the whole device as it was observed that annealing the device with ITO charge reservoir present shorts out the device, i.e. no light output and very low voltage across the device, possibly due to the fact that indium infuses in the Y_2O_3.

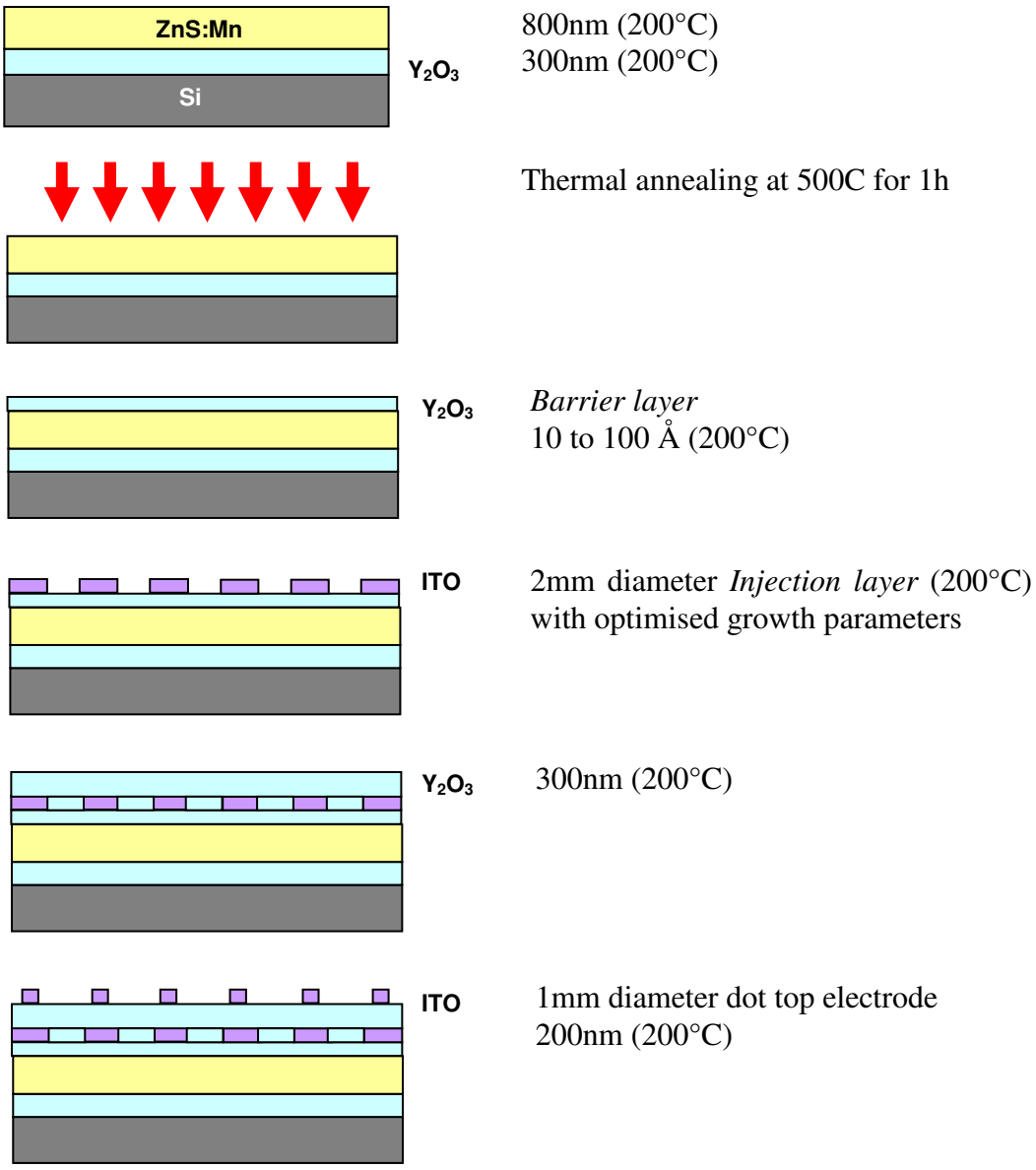

Figure A-2: Schematic diagram of 'half charge reservoir' EL device fabrication process

After optimising the injection layer growth parameters, half charge reservoir EL devices were fabricated varying the barrier layer as well as typical EL devices with similar growth conditions. All EL measurements were carried out using a sinusoidal waveform voltage at a frequency of 500 Hz with voltage increments of 8 V peak to peak and 5s duration. Results obtained for half charge reservoir EL devices with varying barrier layer thickness are shown in Figure A-3.

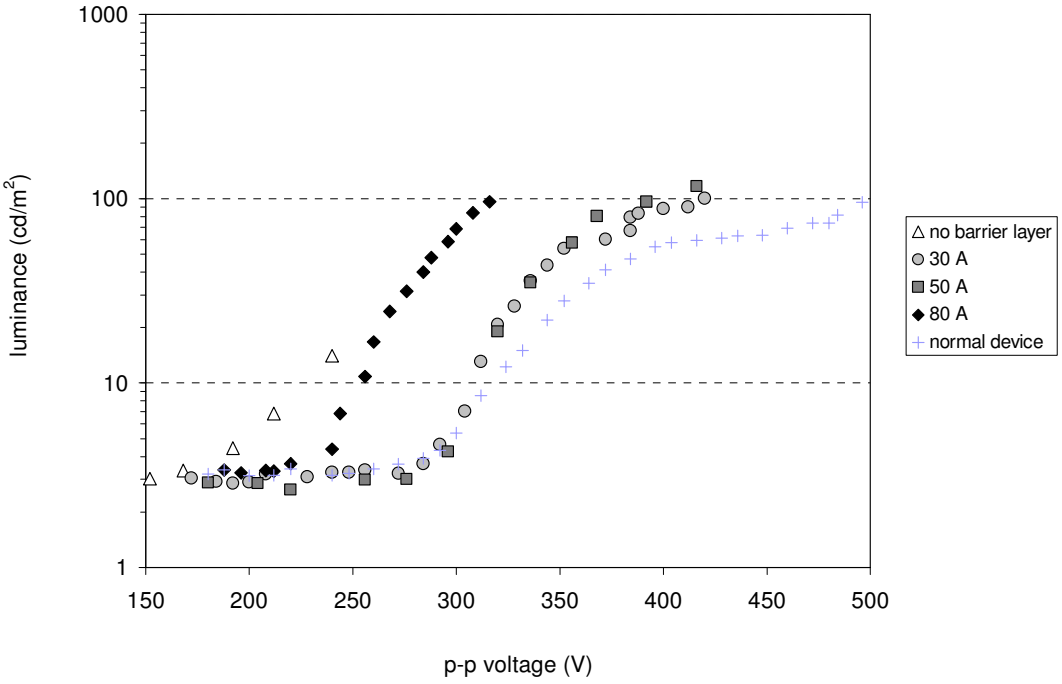

Figure A-3: Effect of varying barrier layer thickness in 'half charge reservoir' EL devices on luminance vs drive voltage (all devices have the top injection layer except 'normal EL device')

The EL structure with the inclusion of an injection layer without a barrier layer short lived, breaking down below 250 V (peak to peak) with very low luminance (less than 15 cd/m^2) due to destructive breakdown initiated due to current runway process. The addition of the barrier layer improved the performance of this new type of devices. However, from a barrier layer thickness of 100 Å and above, devices failed systematically. Lowest threshold voltages were obtained with a barrier layer of 80 Å. However, these results are quite speculative. This study needs a more complete investigation.

A.2 *Seme Lab project*

A.2.1 Experimental

Some work was also undertaken for Thin Films Services which was recently created by the Displays Research Group at NTU. Growth, laser processing and characterisation of ZnS:Mn thin films deposited on glass substrate were achieved.

Glass substrates were put in a furnace for temperature testing. They resisted a temperature of 600°C (melting at 630°C) which is well above the 500°C necessary for pre-baking and thermal annealing. These glass substrates were cleaned using heated diluted Decon 90 with deionised water in a sonicate bath. They were dipped into deionised water, rinsed with isopropanol and blown dry with nitrogen.

800nm ZnS:Mn thin films were deposited using co-sputtering of solid targets of ZnS and ZnS:Mn (at 50 and 30W from optimum found).

A.2.2 Results

Laser annealing was then performed with a KrF laser (248nm wavelength and 20ns pulse duration) on these samples placed in a pressure cell. Number of pulses and fluence were varied with atmospheric pressure and with a 150 psi pressure.

These results are shown on Figure A-4.

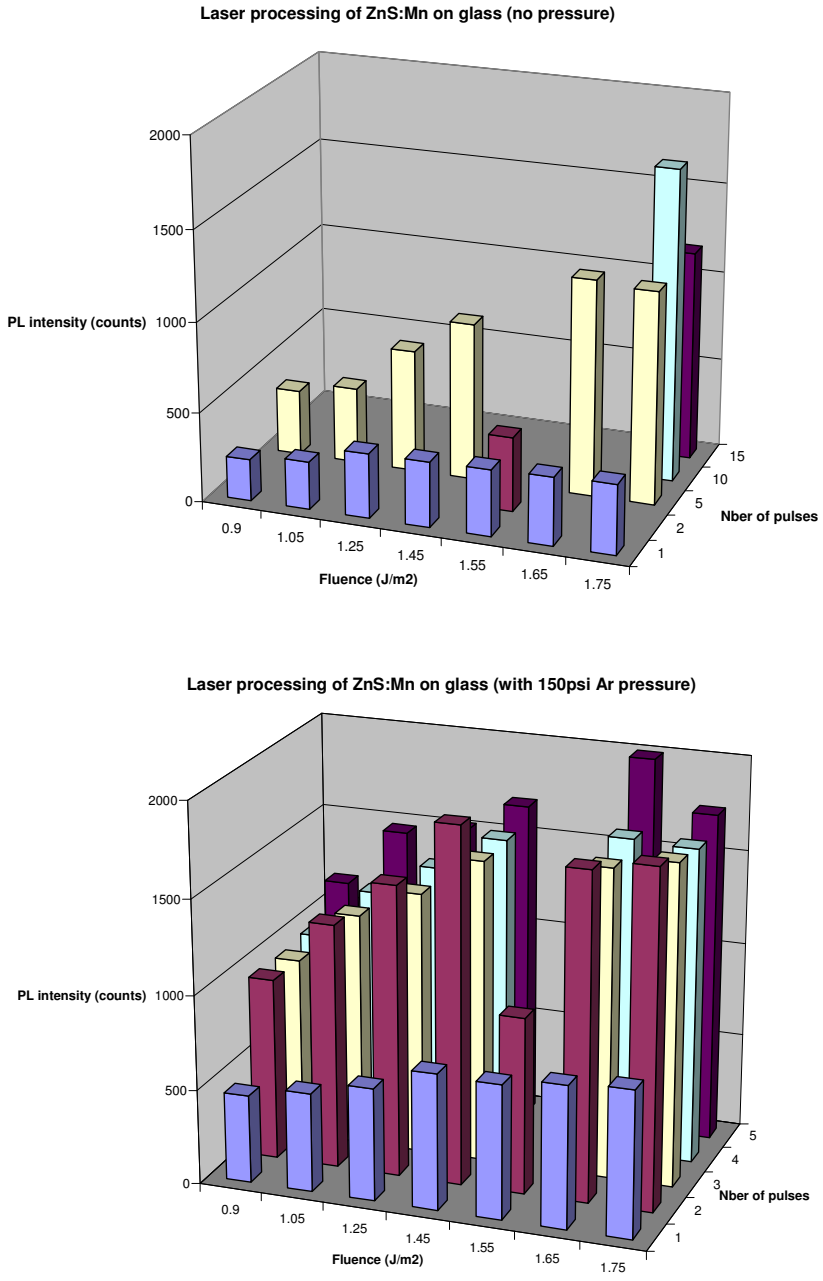

Figure A-4: Laser processing of ZnS:Mn on glass substrate at atmospheric pressure and 150psi argon pressure.

As expected, laser processing of ZnS:Mn thin films deposited on glass is a lot more efficient if applied under a 150psi argon pressure. This is also improved by using high fluences. Finally, the critical number of pulses for the best PL was obtained at 2 (at least twice the PL achieved from 1 pulse).

A.3 *Publication*

Article title: Growth optimisation of ZnS:Mn thin film phosphors for high intensity miniature electroluminescent displays

Reference: MSB12129

Journal title: Materials Science & Engineering B

Corresponding author: Mr. G. Boutaud

First author: Mr. G. Boutaud

PDF offprint dispatch: 21-11-2009